Grant FA8655-04-1-3073

Microscopic optical characterization of ZnO bulk crystals, free standing III-Nitride substrates and III-V structures for non-linear optics

By

J.Jiménez,

Co-workers : J. Mass, M. Avella, A.Martín, O. Martínez

Física de la Materia Condensada, ETSII,

47011 Valladolid, Spain

Report due, Final report 21/09/04 – 20/09/08

REPORT DOCUMENTATION PAGE	Form Approved OMB No. 0704-0188

Public reporting burden for this collection of information is estimated to average 1 hour per response, including the time for reviewing instructions, searching existing data sources, gathering and maintaining the data needed, and completing and reviewing the collection of information. Send comments regarding this burden estimate or any other aspect of this collection of information, including suggestions for reducing the burden, to Department of Defense, Washington Headquarters Services, Directorate for Information Operations and Reports (0704-0188), 1215 Jefferson Davis Highway, Suite 1204, Arlington, VA 22202-4302. Respondents should be aware that notwithstanding any other provision of law, no person shall be subject to any penalty for failing to comply with a collection of information if it does not display a currently valid OMB control number.
PLEASE DO NOT RETURN YOUR FORM TO THE ABOVE ADDRESS.

1. REPORT DATE *(DD-MM-YYYY)*	2. REPORT TYPE	3. DATES COVERED *(From – To)*
01-10-2008	Final Report	20 September 2004 - 20-Sep-07

4. TITLE AND SUBTITLE

Microscopic optical characterization of ZnO bulk crystals, free standing III-Nitride substrates and III-V structures for non-linear optics

5a. CONTRACT NUMBER
FA8655-04-1-3073

5b. GRANT NUMBER

5c. PROGRAM ELEMENT NUMBER

6. AUTHOR(S)

Professor Juan I Jimenez Lopez

5d. PROJECT NUMBER

5d. TASK NUMBER

5e. WORK UNIT NUMBER

7. PERFORMING ORGANIZATION NAME(S) AND ADDRESS(ES)
Universidad de Valladolid
Valladolid 47011
Spain

8. PERFORMING ORGANIZATION REPORT NUMBER

N/A

9. SPONSORING/MONITORING AGENCY NAME(S) AND ADDRESS(ES)

EOARD
Unit 4515 BOX 14
APO AE 09421

10. SPONSOR/MONITOR'S ACRONYM(S)

11. SPONSOR/MONITOR'S REPORT NUMBER(S)
Grant 04-3073

12. DISTRIBUTION/AVAILABILITY STATEMENT

Approved for public release; distribution is unlimited.

13. SUPPLEMENTARY NOTES

14. ABSTRACT

This report results from a contract tasking Universidad de Valladolid as follows: Objective 1: To study the influence of the growth parameters on the defects and inhomogeneities of ZnO crystals grown by Hydrothermal technique. This technique has the advantage of large bulk crystal production, but presents the possibility of unintentional impurity introduction. Furthermore, the incorporation of impurities is not uniform. This objective will be achieved by the way of:
Analysis of the distribution of defects and impurities in the different growth sectors and faces (Zn, and O terminated) using SRCL.
Study of the distribution of the excitonic luminescence and the green and orange bands using SRCL.
Spectral CL images to understand the incorporation of impurities and native defects in terms of homogeneity.
Identification of unintentional impurities introduced during growth.
Influence of the growth conditions, nutrient, solvent (KOH, LiOH…) and saturation temperature, on the incorporation of impuriteis and native defects.
Study of the role of Hydrogen.
Study of the luminescence in damaged surfaces by varying the voltage of the e- beam excitation to reach different depths of analysis.
Study of the surface quality using simultaneous UV microRaman spectroscopy and microphotoluminescence.

Objective 2: To study the defects and inhomogeneities of free standing III-Nitride crystals (AlN and GaN) to be used as substrates for III-nitride layer deposition. To investigate these free standing layers as substrates of high quality epitaxial GaN and AlGaN layers necessary for lasers and high power devices. This requires low defect density and homogeneous large wafers to allow the fabrication of reliable devices and to reduce the costs.
To achieve such an objective we will study the CL spectra of both GaN and AlN.
Identification of the main impurities and point defects in the layers.
Study of the homogeneity in at both long range, wafer homogeneity using Raman and UV excited PL.
Study the homogeneity at short range, micrometric and submicrometric scales, using spectral imaging cathodoluminescence. In particular, one should study the existence of the cell like pattern revealed by CL in nitrides and how does it appear in free standing materials, in order to understand the distribution of the extended defects in these substrates.

Objective 3 is the strain analysis in other crystals and structures provided by David Bliss's group. Special attention will be paid to antiphase domain structures based on GaAs, which are very promising devices for infrared frequency converters. A critical point in these structures is the strain distribution, because the strain field can affect the dielectric index resulting in optical losses.

This objective will be achieved by mapping the strain field of these structures using spectral imaging CL, both in top view and cross section. This last view allows the study of the domain walls, which are also critical to optical losses.
The study will be complemented with microRaman spectroscopy and mapping.

Schedule of reports/deliveries.
Periodic reports will be delivered every 6 months.
Short (half a page) progress reports will be delivered every three months.
Mid term and final reports will be also delivered summarizing the main achievements

15. SUBJECT TERMS
EOARD, Semiconductor Growth, Semiconductor materials, optical materials

16. SECURITY CLASSIFICATION OF:			17. LIMITATION OF ABSTRACT	18, NUMBER OF PAGES	19a. NAME OF RESPONSIBLE PERSON
a. REPORT UNCLAS	**b. ABSTRACT** UNCLAS	**c. THIS PAGE** UNCLAS	UL	93	A. GAVRIELIDES
					19b. TELEPHONE NUMBER *(Include area code)* +44 (0)1895 616205

Standard Form 298 (Rev. 8/98)
Prescribed by ANSI Std. Z39-18

1. Introduction.

The research carried out during the four years of the project, was focused on two different topics: i) the characterization of **hydrothermal (HTT) ZnO crystals**, and ii) the characterization of **orientation patterned OP-GaAs crystals** for non-linear optics. Therefore, this report addresses the two topics and summarizes the main results obtained all along these years. Also, some data on sapphire crystals are added.

The samples were supplied by AFRL in Hascom, MA, and were studied by Cathodoluminescence (CL). This experimental technique allows sub-micrometric spatial resolution, suitable for the analysis of the specific problems concerning these samples.

The study of ZnO crystals was carried out by spectrally resolved cathodoluminescence (CL), aiming to understand the main issues concerning the luminescence emission of HTT crystals and their relation to the crystal growth conditions. The study of these crystals was focused on diverse aspects: influence of the growth sectors, surface, extended defects and the identification of the different luminescence bands. The results conferred a special relevance to the analysis of the visible luminescence, and the band peaking around 3.3 eV. The study of the different growth sectors allows get insight into the complexity of the visible luminescence emission in ZnO; while the analysis of mechanically damaged samples provides new insights about the origin of the 3.3 eV band.

The study of the OP-GaAs crystals was focused on the analysis of the main aspects relevant to the optical losses that are crucial for the use of these crystals as mid IR tunable coherent light sources using a pumping laser. Optical losses are due to light scattering and absorption phenomena, which are mostly related to the domain walls, decorated extended defects, and residual impurities and intrinsic defects. The relation of these effects with the growth parameters and the dimensions of the structures is the key to improve the transmission of the anti-phase domain structures. In the case of sapphire, a study of the depth distribution of the different luminescence bands and the and the profiles of the dopant elements, detected by SIMS, was carried out.

First, we will provide a short introduction to the cathodoluminescence (CL) technique used for this research; then, we will present separately the results accomplished for each of the materials studied. III-Nitrides were also considered in the workplan, however, the

samples have not yet the optimal conditions; therefore, this study is not included in this report.

2. Cathodoluminescence

This is a powerful technique to study wide band gap semiconductors and inhomogneous materials as OP-GaAs crystals. It consists of the study of the luminescence emission as a consequence of the excitation with an electron beam. The excitation with an electron beam gives a big versatility to this technique as compared to photoluminescence. It allows mapping with high spatial resolution the luminescence distribution by using the scanning capability of the e-beam in an scanning electron microscope (SEM), which also allows to correlate the morphology to the luminescence emission. It allows a larger range of energy excitations and therefore the penetration probe depth can be conveniently controlled; this is a great advantage respect to photoluminescence, where the excitation with above band gap light allows probing only a few nms beneath the surface of the sample under study. This aspect will be very relevant in the case of the ZnO crystals, where a strong depth dependence of the luminescence intensity was found, which accounts for the complexity of the surface of ZnO substrates; the substrate surface being a crucial issue for the homoepitaxial growth of ZnO layers.

The CL study was carried out with a XiClone system from Gatan attached to a JEOL 820 SEM. The temperature of the samples was varied between 80 K and room temperature. The CL detection is done with a multichannel CCD detector allowing the acquisition of the full spectrum for each pixel of a selected region of interest. Any monochromatic image can be reproduced, which is very useful to understand the nature of the defects, but also to understand the influence of the growth sectors for the incorporation of impurities and native defects in the case of ZnO, and the distribution of defects and or impurities in the OP GaAs crystals. On the other hand, the spectrum of any point of the scanned area is available. Finally, using Gaussian fitting routines applied to the full image, one can map the spectral parameters of the selected regions of interest; this provides an added value to these measurements as compared to conventional CL or photoluminescence.

3. ZnO crystals

3.1 ZnO crystals growth sectors

Several samples cut from HTT crystals grown at AFRL Hanscom were studied. These samples are normally cut from the c+ growth sector. The crystals were sliced obtaining samples, with basal planes with O termination (c-) and Zn termination (c+). Also, off-seed samples were cut in order to study other face orientations; in particular, prismatic faces (1010) (m planes), which are non polar, and pyramid faces (1011) (p planes) that are either Zn-rich, p^- planes, or O-rich, p^+ planes. The growth rate, the incorporation of defects and impurities, and, therefore, the optical properties depend on the growth sectors. The m-plane growth is expected to be the best material with the lowest number of defects and the lowest incorporation of impurities.

The main impurities present in these crystals are: Li, usually 1-10 ppm, K and Na, usually not above 1-2 ppm, also, Al, Fe, Si, and C can be present from 1-10 ppm. This is valid for material grown on the zinc face of the seed. Material grown on the oxygen face of the seed (oxygen sector) is green in color and has a much higher concentration of impurities (5x-10x), therefore it is not interesting for the purpose of this study, since a material with such a high concentration of impurities cannot be used for optoelectronic applications.

The geometry of the triangular off-seed samples exposed several facets, Fig.1. The samples were yellowish to the naked eye, with colorless borders about 1.5 mms wide.

Mechano chemical polishing is a crucial issue of ZnO, since it is a soft material. The O-face appears as the surface of choice, since the surface finish after polishing was free of defects, while a dense array of subsurface damage lines were revealed in the Zn-face by panchromatic CL images, Fig.2.
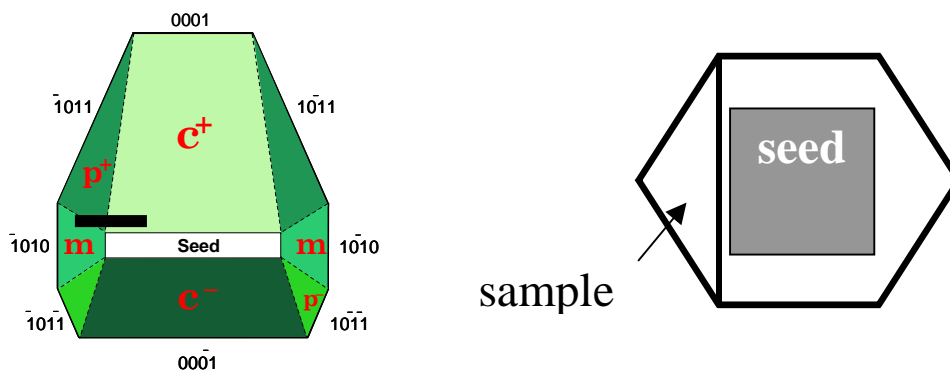

Fig.1. *Sample geometry*

Other samples, presented opposite aspect, colorless basal planes and yellowish borders, which suggests that the incorporation of impurities depends not only on the growth sector, but also on the growth conditions. This does not modify the observation of higher subsurface damage in Zn side.
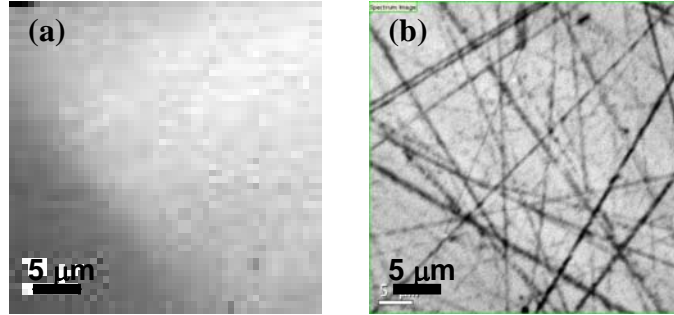

Fig.2 *panchromatic CL images of the O-face (a) and the Zn-face (b), showing subsurface damage in the Zn-face*

3.2.Panchromatic CL images. Non radiative recombination centers (NRRCs)

The different facets were analyzed by panchromatic CL images, Fig.3. A marked brightness contrast between the different sectors was observed in both samples faces. The colorless borders can be separated in two different regions according to their CL emission, corresponding to the m and p faces respectively. The brightest face was the m sector, which confirms the higher quality of this face in terms of crystal purity. The lowest luminescence intensity was observed for the basal plane (c sector). This behavior is observed for both up and down faces. The panchromatic CL contrast is
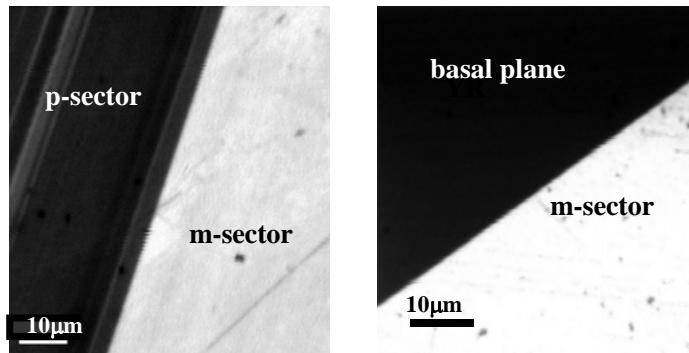
Figure 3. *Panchromatic CL images showing the boundaries between the different growth sectors.*

mainly governed by the competition between radiative and non radiative recombinations, or the ratio between the concentrations of radiative and non radiative recombination centers. This is a crucial issue concerning ZnO, because the nature of the non radiative recombination centers is still not well understood. It has been claimed that dislocations are the dominant NRRCs; however, HTT crystals present a very low dislocation density, 10^2 cm^{-2}. In fact, the CL images show a rather homogeneous distribution for each growth sector, which confirms that the role of dislocations in the luminescence contrast is only determinant at a local scale. This result clearly suggests that defects related to either native point defects or impurities are at the origin of the NRRCs. The second point concerns the formation of such centers, that are formed with higher concentration in the basal planes (c sector) and they are much less efficiently formed in the m sector. Note that the fact that the panchromatic CL is the image of the global light emitted by the sample permits to establish the relevance of the non radiative recombination in the CL contrast, since the reduction of the luminescence intensity in dark regions affects both the excitonic and the deep level related bands. This suggests that the incorporation of non radiative recombination centers depends on the growth plane, and apparently the higher NRRCs concentration occurs in the faster growing direction, which corresponds to the c-axis direction (basal planes).

3.3. CL spectrum

The luminescence spectrum of ZnO crystals consists of three main spectral regions, the near band gap emission (NBE) with energies above 3.31 eV, the bands with energies below 3.31 eV, usually associated with donor acceptor pair (DAP) transitions and/or phonon replicas of the different excitonic bands, and the visible luminescence in the green–red spectral range. Typical spectra obtained in the different growth sectors are shown in Fig.4.
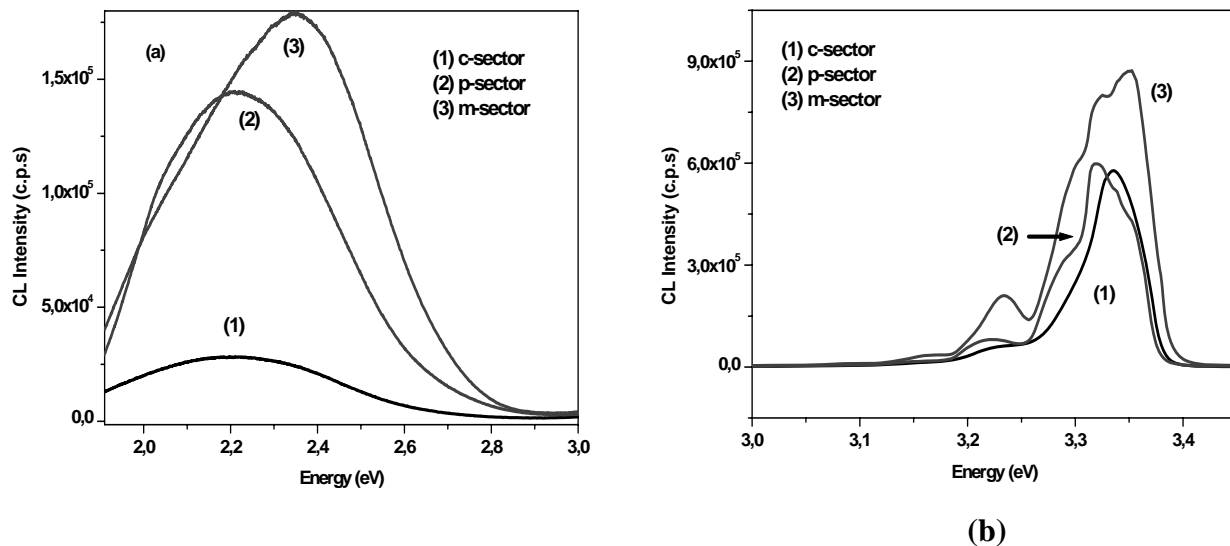
Figure 4. *CL spectra at different growth sectors. (a) visible range, (b) UV range.*

The first difference between the facets concerns the luminescence emission intensity in the NBE spectral range. The highest intensity is observed in the m growth sector, while the emission intensities in c and p growth sectors are similar.

The NBE spectrum consists of several close lying free and bound excitonic transitions. At 80K the bound excitons are not yet thermally freeze and the NBE spectrum appears as a complex band convolution of several closely spaced bands, due to several bound excitonic transitions, which makes difficult the analysis of the luminescence spectra, because the spectral resolution of our spectrometer does not allow to resolve the different excitonic bands at 80 K.

Differences between the O-face and the Zn-face are observed. The main difference is the high energy side of the NBE band, which is shifted to the red in the Zn terminated face. Also shifts between the different sectors of a face are observed. Raman measurements showed that this effect cannot be associated with local lattice stresses induced by polishing, since there was not difference in the Raman frequencies of the phonon modes measured in both faces. It has been claimed that the free excitons are not observed in the Zn-terminated faces, due to intrinsic surface states of the Zn-terminated surfaces (R.E. Sherriff, D.C. Reynolds, D.C. Look, B.Jogai, J.E. Hoelscher, T.C. Collins, G.Cantwell, W.C. Harsch; *J.Appl. Phys.* 88, 3454 (2000)) that produce self absorption of the most energetic photons of the luminescence spectrum; however, both faces of the samples present Zn (c+ and p+) and O (c- and p-)-terminated planes; therefore, it seems reasonable to assign some role to the surface preparation in the formation of the surface states. The surface states should be responsible for the band tailing absorbing the photons with the higher energy in the luminescence spectrum. A

similar effect was observed in ion implanted ZnO (V.A. Coleman, H.H.Tan, C.Jagadish, S.O. Kucheyev, M.R. Phillips, J.Zou; *Mater. Res. Soc. Symp.* Proc. Vol. 289, B8.7.1 (2005)) and undoped ZnO crystals. The optical absorption edge was also observed to shift to the red with increasing oxygen concentration (M.R. Phillips, M.Wagner, O.Gelhausen, V.Coleman, J.B. Brady, C. Jagadish, E. Malguth, A. Hoffmann, E.M. Goldys, J.J. Rusell; *E.MRS Fall meeting, Symp. F*, (Warsaw, Poland, 2004)); it suggests that the shift towards the red of the luminescence threshold energy would be related to surface oxygen excess.

The NBE spectrum at 80 K presents a band composed of several subbands in the 3.32 - 3.37 eV spectral window, the relative weight of the different bands depends on the samples and the growth sectors. The main contribution, around 3.35 eV arises from the so-called I4 band. Among the donors responsible for this emission, hydrogen is the most commonly accepted one, it was shown that in these samples non negligible amounts of hydrogen under the form of OH^- can exist (L.E. Halliburton, L.Wang, L.Bai, N.Y.Garces, N.C. Giles, M.J. Callahan, B.Wang; *J.Appl. Phys.* 96, 7168 (2004)).

The emission at 3.33 eV, usually labeled as the I_9 excitonic band has been associated with either Al impurities (donor bound exciton) or alkali impurities, Li and Na, (acceptor bound excitons) (E.Tomzig, R.Helbig; *J. Luminescence* 14, 403 (1970), B.K. Meyer, H.Alves, D.M. Hofmann, W.Kriegseis, D. Forster, F. Bertram, J. Christen, A. Hoffmann, M. Strasburg, M. Dworzak, U. Haboeck, A. V. Rodina; *Phys. Stat. Sol. (b)* 241, 231 (2004)), all of them have a relevant presence in these crystals. The dominant presence of this band in the polar growth sector suggests that these sectors incorporate the impurity responsible for this band with higher efficiency than hydrogen, which balances the NBE luminescence emission towards the 3.33 eV band. It was pointed out that the incorporation of H_2O and OH^- is reduced in the presence of Li (E.D. Kolb, R.A.Laudise; *J. Am. Ceram. Soc*. 49, 302 (1966)), which suggests that Li could be at the origin of the 3.33 eV luminescence emission, since the intensity of the bands at 3.35 eV and 3.33 eV seems to be anticorrelated for the different growth sectors.

The contribution of the luminescence emission related to I4 excitons is dominant in the prismatic sectors, while the I9 excitonic transition is enhanced in the basal and pyramid sectors. Therefore, one can argue that hydrogen incorporaton is easier in the m sector, while the pyramid and basal incorporate less hydrogen in relation to the other impurities.

The spectral region below 3.32 eV, consists of several bands separated each other by ≈70 meV, which is roughly the energy of the LO phonon (72 meV) in ZnO. There is a main band at ≈3.31 eV and several phonon replicas at 3.24, 3.17 and 3.1 eV. The nature of the 3.31 eV band is a matter of controversy. It has been associated with a donor-acceptor pair (DAP) transition (T.B. Hur, G.S.Jeen, Y.H.Hwang, H.K.Kim; *J. Appl. Phys*. 94, 5787 (2003)), which the nature of the defects involved is not known. It is also identified as the first phonon replica of the free exciton transition, FX-1LO band (B.K. Meyer, H.Alves, D.M. Hofmann, W.Kriegseis, D. Forster, F. Bertram, J. Christen, A. Hoffmann, M. Strasburg, M. Dworzak, U. Haboeck, A. V. Rodina; *Phys. Stat. Sol. (b)* 241, 231 (2004)). Also, a band related to structural defects was reported at such an energy (B.K. Meyer, H.Alves, D.M. Hofmann, W.Kriegseis, D. Forster, F. Bertram, J. Christen, A. Hoffmann, M. Strasburg, M. Dworzak, U. Haboeck, A. V. Rodina; *Phys. Stat. Sol. (b)* 241, 231 (2004)). Further investigation is required to elucidate the nature of this band and its relation to impurities or crystal defects. The enhancement of the first phonon replica of the free excitonic band has been reported to occur in crystals with symmetry breakdown, this is due to the fact that Frohlich exciton scattering by one LO phonon is forbidden in perfect crystals; however, this scattering is allowed when symmetry is breakdown which can occur in surfaces damaged by polishing (D.A.Lucca, D.W.Hamby, M.J. Klopfstein, G. Cantwell; Phys. Stat. Sol. (b) 229, 845 (2002)). Aiming to studying the nature of this band, we did mechanical damage by Vickers indentation and we studied the crystal areas surrounding the indentation. This study will be presented later on in this report.

3.4. Visible luminescence

The visible luminescence presents large differences between the growth sectors and crystals. The visible luminescence consists of a broad band extending from below 500 nm to beyond 700 nm. This broad band is composed of at least three sub-bands called green luminescence (GL), yellow luminescence (YL) and red luminescence (RL). The visible luminescence is very relevant for the use of ZnO as a phosphor, but also in an opposite sense for future optoelectronic UV devices. The visible luminescence is in competition with excitonic emission; therefore it should be reduced in order to improve the performance of blue-UV optoelectronic devices. On the other hand, the deep levels can compensate the shallow levels, making difficult to reach doping levels necessary for

p-n junctions or contact layers. Therefore, a comprehensive understanding of the visible luminescence is necessary to control the presence the deep levels, which is a step forward to the development of UV optoelectronic devices based on ZnO.

The relative importance of the visible sub-bands depends on the growth sector. The green band is dominant in the m sector, the yellow luminescence is dominant in the p sector and the basal plane shows a tendency to increase the contribution of the red band, though the dominant band remains to be the yellow band. The intensity of the visible luminescence is almost equivalent in the p and m sector and much weaker in the basal planes, see the CL contrast in the visible spectral range, Fig.5, and compare it to the contrast observed for the NBE emission, Fig. 3.
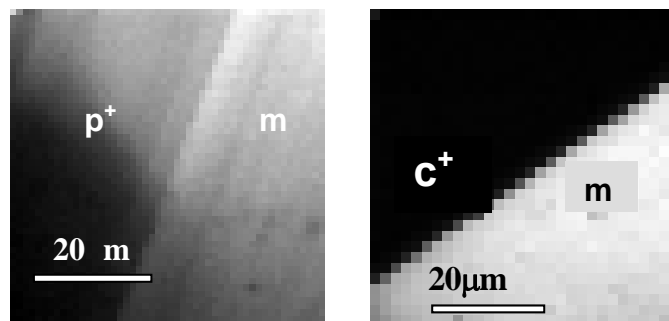
Figure 5. Monochromatic images (visible luminescence) of the boundaries between the growth sectors, showing weak contrast between pa and ma and strong contrast between m and c sectors.

It should be noted that the visible luminescence intensity strongly depends on the samples, which outlines the importance of the growth processes in the formation of the deep levels.

The green band is present in any type of ZnO; its origin is a matter of controversy, thought is usually associated with the presence of oxygen defects, either oxygen vacancies (V_O), which are deep donors (F.Leiter, H.Alves, D.Pfisterer, N.G. Romanov, D.M. Hoffmann, B.K. Meyer; Phys.Stat.Solidi. b 340-342, 201 (2003)), or oxygen antisites (O_{Zn}), which are deep acceptors (B.Lin, Z.Fu, Y.Jia; *Appl.Phys. Lett*.79, 943 (2001)). The orange and red bands have been associated with deep levels related to impurities, in particular, Li (T. Sekiguchi, S. Miyashita, K.Obara, T.Shishido, N.Sakagami; *J.Cryst. Growth* 214-215, 72 (2000)) and Fe (T.Monteiro, C.Boemare, M.J.Soares, E. Rita, E. Alves, J.Appl.Phys. **93** 8995 (2003)); also, Cu has been claimed to give visible luminescence (N.Y.Garces, L.Wang, L.Bai, N.C. Giles, L.E. Halliburton,

G. Cantwell; *Appl. Phys.Lett.* 81, 622 (2002)); however, the SIMS analysis of the samples studied did not reveal the presence of Cu. On the other hand, the visible luminescence associated with Cu is structured, presenting several phonon replicas, which are not observed in these samples. Therefore, the luminescence arising from Cu, if any, is overshadowed by more intense emissions related to intrinsic defects.
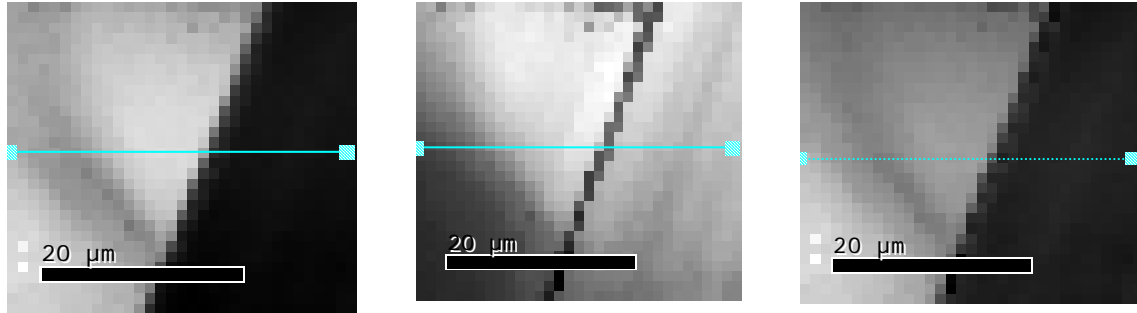

Fig.6. Spectral images (yellow luminescence). a) peak wavelength, b)integrated intensity, c) FWHM

CL spectral imaging of the visible bands reveals different spectral parameters for the visible bands in different growths sectors, Fig.6. The distribution of the spectral parameters of the three sub-bands suggests that the deep centers responsible for the visible luminescence are complex in nature and do not have the same structure in the different growth sectors. Fig.7 shows the profiles along a line, perpendicular to the boundary line between p and m sectors, of peak wavelength and FWHM for GL and YL. The peak energies of both bands are higher in the m-sector, also the FWHM of the peaks is different in both sectors. These data suggest tat the defects responsible for both emissions differ from one sector to other, which points to complex defects rather than point defects.

As mentioned above, the GL has been related to oxygen deficiency, while the YL has been related to excess O. The presence of both bands simultaneously in all samples renders not suitable such a hypothesis about simultaneous rich and poor oxygen contents. Therefore, one should consider defects with stoichiometric compatibility, e.g. oxygen vacancies and zinc interstitials, or zinc vacancies and oxygen antisites, or oxygen interstitials. Li has been also associated with YL; however, high quality Tokyo Denpa samples, grown by the hydrothermal method, showed a very weak visible luminescence; furthermore, it was structured, suggesting that it was due to residual copper impurities, evidencing the very low intrinsic defects concentration in this

sample. This rules out the role of Li as the deep level responsible for the yellow luminescence, because Li is always present in hydrothermal crystals. In this sense, the influence of Li could be indirect, and it would be related to the suppression of zinc vacancies, when it is substituting Zn in the ZnO lattice, which confers a relevant role to V_{Zn}s in the visible luminescence.
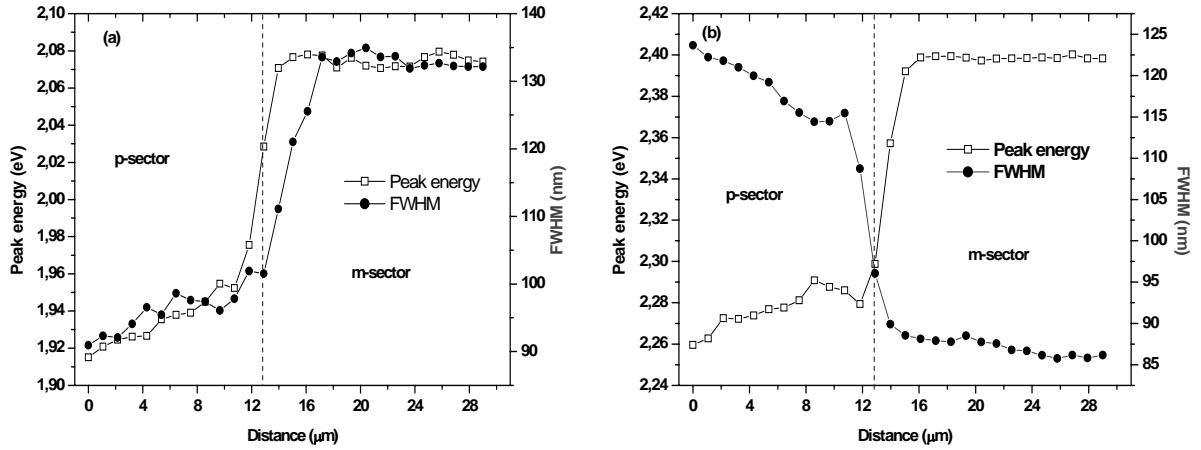
Figure 7. *Peak energy and FWHM profiles along a line crossing transversely the m-sector/p-sector boundary yellow (a) and green (b) bands.*

The temperature dependence of the visible CL emission was studied between 80 and 300K. The spectra obtained in such temperature range are shown in Fig.8, where one observes a very interesting balance between the two bands, One observes that for increasing temperature the YL is progressively quenched, and practically disappears above 200 K; then, the visible band is dominated by the green emission. In the normalized spectra of Fig.8 one observes how above 200K only the green band is observed.
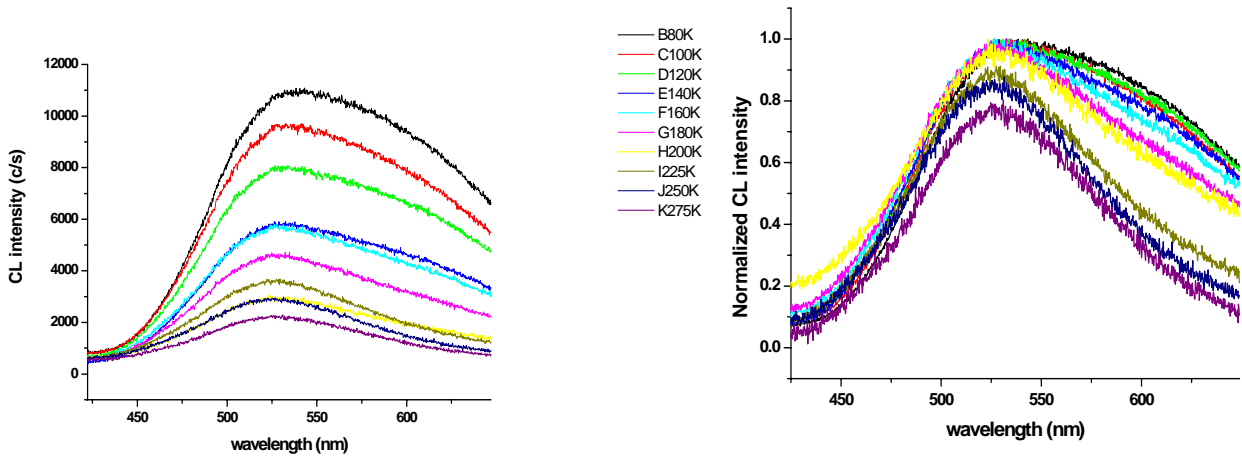
Fig.8, *CL spectra in the visible range for different temperatures ranging fro 80 K to room temperature. The spectra on the right are normalized showing better the effect of the YL quenching discussed in the text*

If one represents the peak wavelength as function of the temperature, one observes the evolution shown in Fig.9, the YL band shifts to the blue at 200 K, while the GL band does not shift. This behaviour suggests that the YL is due to DAP transition, while the GL band is due to the recombination of a free carrier in a deep level.

The bahaviour of the luminescence emission observed in Fig.8 might point out that the deep level responsible for both emissions could be common to both GL and YL. According to this the YL should be due to a DAP (Donor acceptor pair) transition, while the GL would be related to a free to bound transtion, either a free electron (hole) with a hole (electron) trapped in a deep level. This could be described by the scheme of Figs. 10 and 11, the thermal ionization of the shallow level in the DAP should result in only one luminescence band.
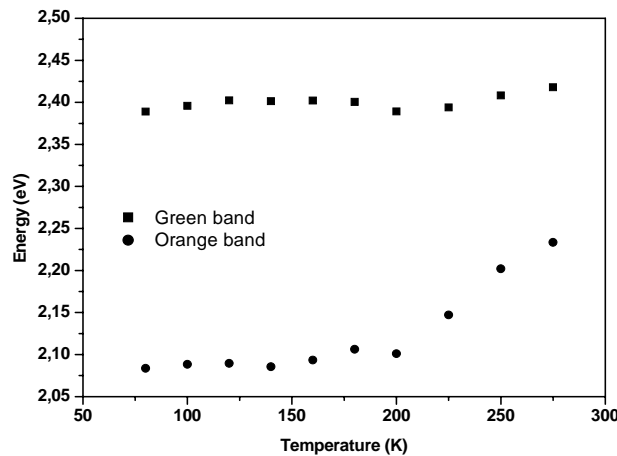
Fig.9. *Temperature dependence of the peak wavelength of YL and GL bands*
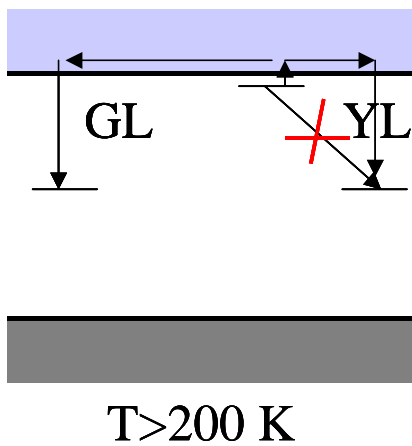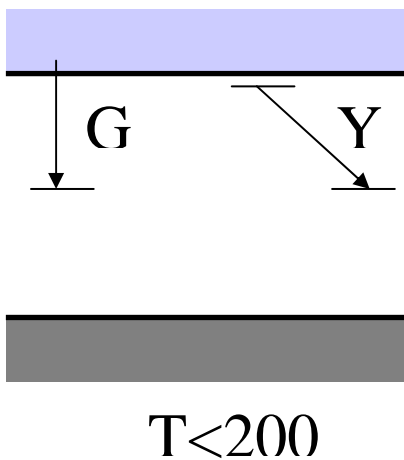
Fig.10. *Level scheme accounting for visible luminescence at low temperature*

Fig.11. *Level scheme accounting for visible luminescence at high temperature*

For increasing temperature the shallow donor (acceptor) of the DAP pair giving the YL is thermally ionized and the recombination of the free electron (hole) with the trapped hole (electron) is the only remaining recombination path, therefore, only GL would be observed, Fig. 11. According to this, the balance between YL and GL should be governed by the concentration of the shallow levels participating in the DAP transition. This could agree with the depth dependence of the visible luminescence, as well as the dependence of the YL/GL intensity ratio with the excitation parameters in the CL measurements. In particular, the dependence of the visible luminescence with the acceleration voltage of the electron beam shows a marked depth profile for both green and yellow luminescence emissions. Both emissions follow a depth distribution, which suggests that they can be related to transitions involving one or more common defects. This behavior of the balance between the two bands is mainly observed in the prismatic face of the crystals, while it was more ambiguous in other facets and other crystals.
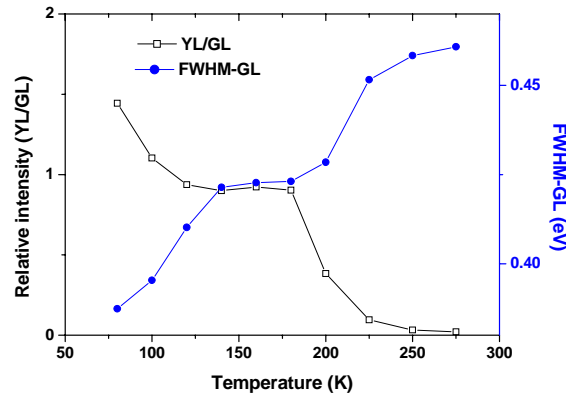
Fig.12. *Plot of the relative intensity of the YL, (YL/GL), and the FWHM of the GL band as a function of temperature*

The study of the spectral parameters of both transitions suggests another interpretation. In Fig. 4 we represent the peak wavelengths of GL and YL as a function of temperature. Using a Gaussian fitting routine the broad band was separated in two peaks, one of them was the GL, the other one is YL up to 200K; above such temperature, this band is a residual band shifted to the red, which cannot be related to the YL, but it seems rather a red band that emerges once the YL is shifted to the blue by ionization of the shallower level of the DAP pair. The relative intensity of both bands as a function of temperature is shown in Fig. 12. One observes that the green band becomes relatively more intense for increasing temperature and that a singularity is observed around 200K. The other

curve in the figure is the FWHM of the GL band, which is observed to increase with T, showing a fair anticorrelation with the relative intensity, and a singularity in the same thermal range. This behavior is due to the fact that when the shallow level participating in the DAP recombination responsible of the YL is thermally ionized the YL band shifts to the high energy merging with the GL band, which is broadened as a consequence of the close overlapping of both bands. Therefore, one can conclude that the deep levels responsible for YL and GL are different. The differences observed between the different samples and growth sectors, should obey the ratio between the concentrations of both defects and the structure of the defects themselves, which can adopt slightly different configurations depending on the growth conditions and the growth sector.

CL measurements in different samples show differences in the shape of the visible luminescence. Several spectra are shown in Fig. 13. Note that the visible band of the Tokyo Denpa sample (not shown in this Figure)is very weak and is structured, which suggests that it is due to Cu impurities and that the intrinsic defects responsible for the broad unstructured visible band are absent or they have a very low concentration, accounting for the excellent quality of such sample.
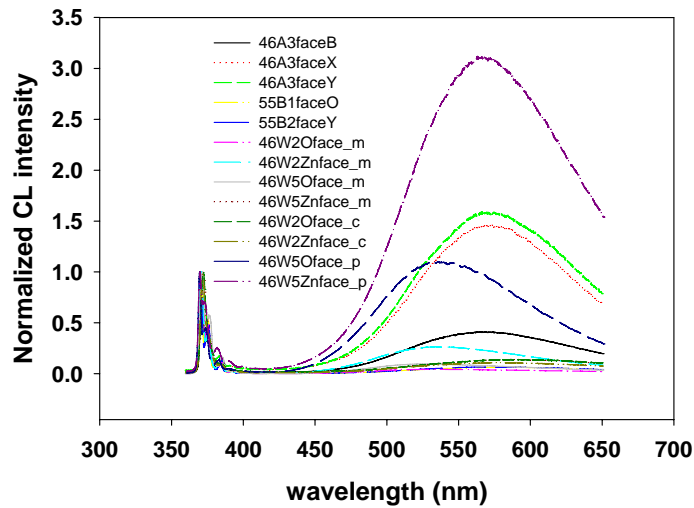
Fig.13. *CL spectra of different samples and facets, normalized to the NBE band*

3.5 *Depth dependence*

A very important observation concerns the dependence of the visible luminescence with the properties of the e-beam, which we have already mentioned. The excitation e-beam is characterized by the acceleration voltage and the beam current. The acceleration voltage determines the penetration of the e-beam, while the beam current for a given acceleration voltage represents the excitation intensity.

A marked evolution of the spectra with the acceleration voltage is observed. The visible luminescence is progressively enhanced by increasing the e-beam kV. The CL spectra were obtained for different kV varying the beam current in order to keep constant the e-h pair generation rate. The spectra obtained at different kV for the p and m growth sectors are shown in Fig.14, evidencing depth distribution of the visible luminescence bands.
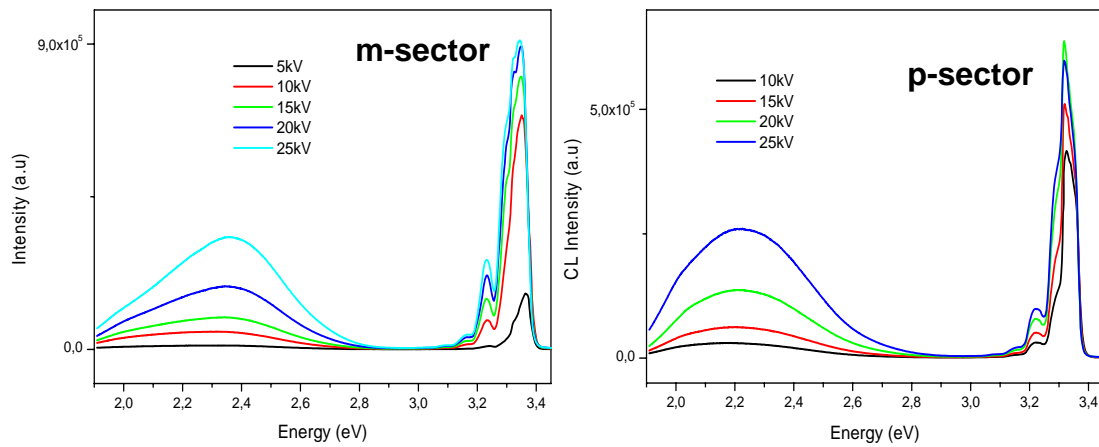
Fig.14. *CL spectra obtained at different e-beam kV, showing enhancement of the visible luminescence for increasing kV.*

This behavior is observed for all the growth sectors and all the samples measured, which suggests changes in the distribution of the deep centers from the sample surface to a depth around 2 μms, according to the e-beam penetration estimation using the Kanaya- Okayama fomula (K.Kanaya, S. Okayama; *J.Phys. D* 5, 43 (1972)). The fact that the same effect is observed in both basal planes of the samples rules out the existence of impurity concentration gradients as a cause of the in depth distribution of the visible luminescence. On the other hand, the UV luminescence does not follow the same in depth dependence, which suggests that the in depth distribution of the visible luminescence is not merely due to non radiative recombination centers generated by the surface polishing, or the surface reactivity. In fact, the influence of the surface is mostly

appreciated for low acceleration voltages, for which the ratio between the visible luminescence and the excitonic luminescence is small. This ratio increases with increasing acceleration voltage. In order to estimate the role of the surface, both faces were compared, without significant differences between them. Also as grown crystals were studied and the results were similar, therefore, one has to assume that the surface of the crystal is very reactive, suggesting that the deep centers are *passivated* close to the surface. Since one cannot expect the same distribution of impurities in surfaces cut from opposite facets of the crystals and treated in a different way, one should also assume that the deep levels should involve intrinsic defects. Fig.15 shows the dependence of the intensity of the different bands with the acceleration voltage, for constant generation rate, the e-beam current was corrected to keep constant the excitation flow.
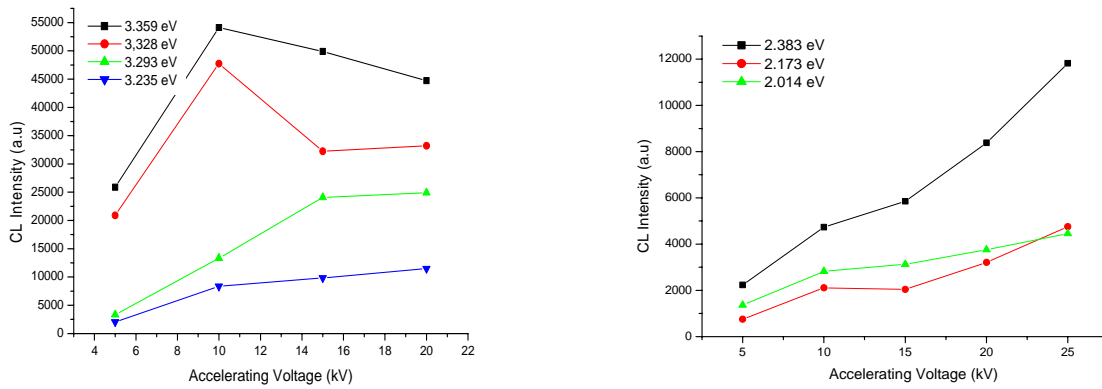
Fig.15. *Evolution of the CL intensity with the acceleration voltage (Depth penetration) for the different luminescence bands*

Mechanisms related to the exposition of the surface to the atmosphere could modify the depth distribution of some defects. In this sense it is interesting to note that the largest in depth variation corresponds to the green band, which is associated with native defects without the participation of impurities. Therefore, oxygen seems to play a major role in the distribution of the deep levels responsible for the visible luminescence near the surface. Recent theoretical calculations have addressed a relatively easy diffusion of some native defects (A. Janotti, C.Van de Walle; J. Cryst. Growth 287, 58 (2006)). The activation energy for Zn interstitials was estimated to be as low as 0.5 eV. Additional

effort is necessary to understand the role of the native defects in the luminescence emission.

3.6. Near band gap emission at 3.31 eV

As already described in the literature and in previous reports the Near band gap luminescence emission consists of several excitonic, free to bound and DAP transitions. Also, it has been claimed that there is a band related to structural defects. In particular, a band peaking at 3.31 eV in the CL spectra at 80 K is observed, Fig.16. The nature of this band is a matter of controversy and has been related to different causes. In particular, it has been associated with DAP transitions, a phonon replica of the free exciton transition, an eA° transition and a band related to a structural defect. In all the spectra acquired in the different samples studied it was present; however, significant differences from sample to sample were observed, see several spectra from different samples in Fig. 16. The intensity of this band is strongly dependent on the sample. It is worth noting that it is very intense in the Tokyo Denpa sample, where it was found to be the dominant band in the NBE spectral window. The relative intensity of this band respect to the bound excitonic band depends on the sample and the growth sectors. In general it is enhanced in samples with improved quality, as it was the case of Tokyo Denpa sample. The Tokyo Denpa sample was characterized by a very low concentration of defects other than the impurities responsible for the bound excitons. Both radiative and non-radiative deep recombination centers were present in a low concentration, as deduced from the characteristics of the very intense NBE emission, and the very weak
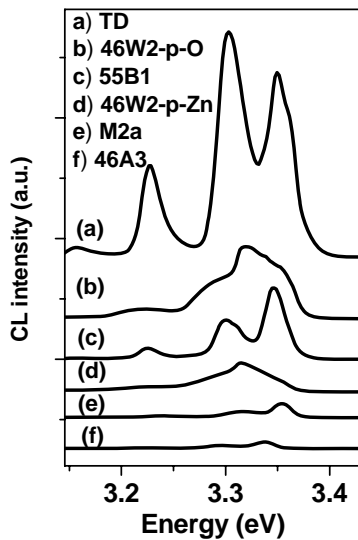
Fig.16. *Spectra obtained with different samples and facets, see the high intensity of the NBG range in Tokyo Denpa sample with the strong band around 3.30 eV. See also the big differences in the relative intensity of this band among the different samples.*

visible emission compared to the spectra obtained for other samples

The presence of the 3.31 eV band has been related to the damage introduced by polishing, according to this, one should expect a higher relative intensity of this peak when the acceleration voltage of the e-beam is decreased, because at lower KV one proofs the regions closest to the surface, where the polishing damage must be more important. The subsurface damage was estimated to extend around 200 nm from the surface (D.W.Hamby, D.A.Lucca, M.J. Klopfstein; J. Appl. Phys. 97, 043504 (2005)) However, there is not a significant increase of the relative intensity of the 3.31 eV band for decreasing kV of the e-beam. This means that subsurface damage is not responsible for such emission, or the subsurface damage is moderated under mechano-chemical polishing as suggested by Hamby et al. (D.W.Hamby, D.A.Lucca, M.J. Klopfstein; J. Appl. Phys. 97, 043504 (2005)), contrarily to what happens for mechanical polishing. On the other hand, the high intensity of this band in TD sample, which had a high crystalline quality does not support the relation between this band and crystal defects. In order to understand the role of freshly created defects on the luminescence emission of ZnO crystals and, in particular, on this band, Vickers indentations were performed and they were studied by cathodoluminescence. Microindentation is a way to achieve plastic deformation in a controlled way. Previous reports on the indentation of ZnO using both microindenters and nanoindenters focused on the description of the slip system responsible for the dislocation rosette around the indentation (J.E.Bradby, S.O.Kucheyev, J.S.Williams, C.Jagadish, M.V.Swain, P.Munroe, M.R.Phillips; Appl. Phys. Lett. 80, 4537 (2002); Z.Takkouk, N.Brihi, K.Guergouri, Y.Marfaing; Phys.B 366, 185 (2005)).
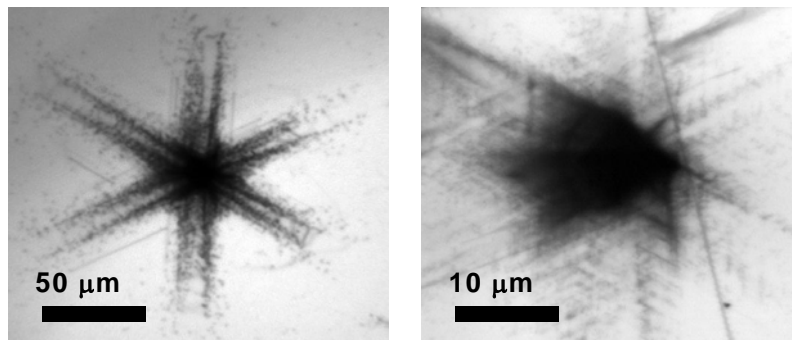
Fig.17 *Panchromatic CL images of indentations with 50mN (left) and 90 mN (right)*

Vickers indentations were applied to the samples with different loads. The plastic deformation induced slip along basal and pyramidal planes, which is revealed as a rosette of dislocations in the panchromatic CL images. As an example, see different rosettes performed with different loads in Fig.17. The rosette has a structure reflecting the hexagonal symmetry of the (0001) planes. It consists of a central core with dark contrast due to the generation of non radiative recombination centers associated with the heavy damage induced by the plastic deformation, and six double arms parallel to the [11-20] axes, also with dark contrast. These arms correspond to consecutive slip planes and each of them has dislocations with different atoms, either Zn or O, in their core. For increasing loads, the arms progressively disappear as the central damaged region increases in size, as a consequence of the superposition of several slip systems. However, we will not study here the slip systems, but the influence that the interaction between the dislocations and the crystal matrix has on the luminescence spectrum.

If one looks at the spectra of Fig. 16 one observes that the maximum intensity of the 3.31 eV band (labeled P1) corresponds to the TD sample, which is the one with the highest overall luminescence intensity. This suggests that this band might be due to the first phonon replica of the free exciton. The intensity ratio of the P1 band with respect to the bound excitonic band (BX band) is decreased in other samples with lower BX luminescence efficiency.

An indentation and the corresponding CL images are shown in Fig. 18.

Panchromatic image

SEM image
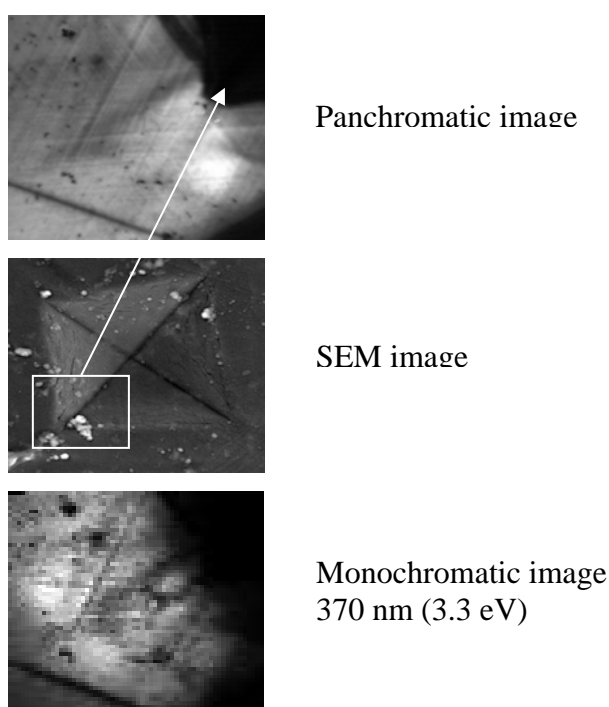
Fig.18. *Indentation of the prismatic sector of the O face of an AFRL sample*

Monochromatic image
370 nm (3.3 eV)
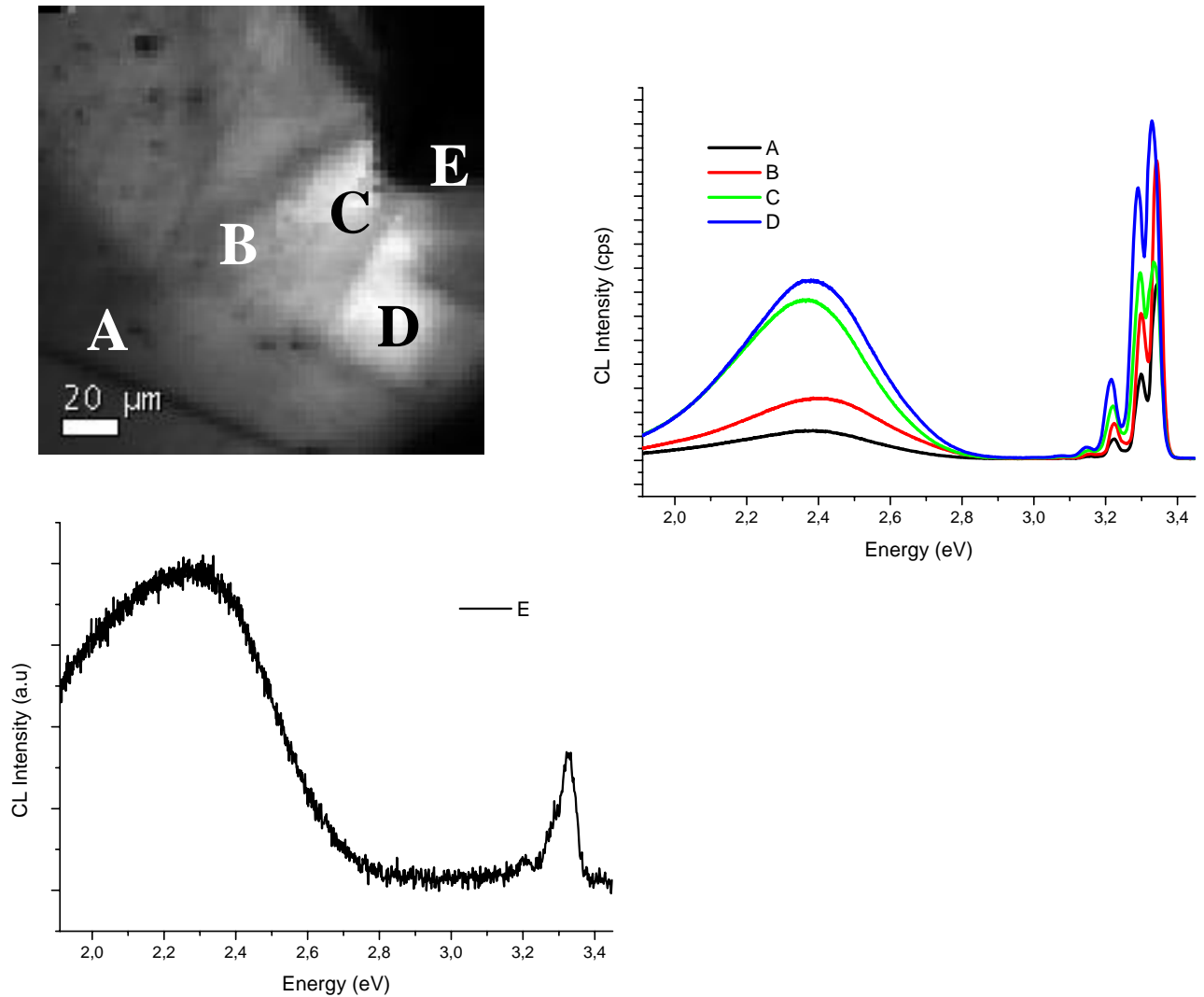
Fig.19. *CL image, and local spectra obtained at the points indicated in the image.*

Inside the indentation there is a strong generation of non-radiative recombination centers that reduce drastically the CL emission, the print looking dark in the CL image. Around the indentation the CL images reveal the formation of defects, which appear as fluctuations of the CL intensity in both panchromatic and monochromatic CL.

Now, the question is: what is the influence of these freshly created defects on the CL spectrum?. Local spectra were obtained in order to observe the influence of structural damage on the CL spectrum, Fig. 19.

One observes in the regions close to the indentation, points C and D, an enhancement of the 3.31 eV band and the visible luminescence respect to the bound excitonic band, which was already reported by other authors (V.A.Coleman, J.E.Bradby, C.Jagadish, M.R.Phillips; Appl. Phys. Lett. 89, 082102 (2006)). Note that inside the indentation,

point E, the luminescence emission is drastically reduced due to the strong generation of non radiative recombination centers by the plastic deformation; however, the visible luminescence is strongly enhanced respect to the BX transition.

In order to study this effect, we studied Vickers indentations in different crystals. Fig.20 shows the SEM image of the Vickers indentation in sample 46W2
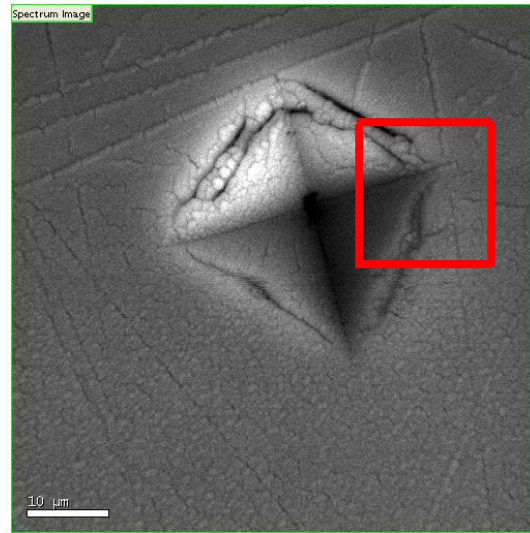
Fig.20: *SEM image of a Vickers indentation in sample 46W2. The red frame is the region scanned in CL, see the pile up around the indentation, which is normally observed for large load indentations.*

The spectral image of the framed region of Fig.20 was acquired; Fig.21, and several local spectra were selected to show the differences between the probed regions in terms of the luminescence emission. See how a crack is generated at the vertex of the square and propagates inside the sample.
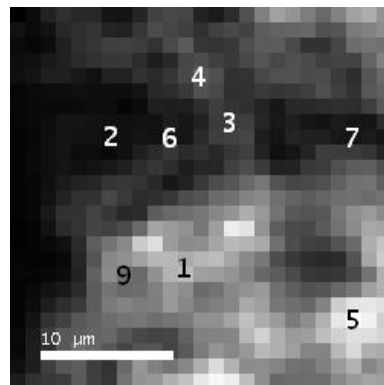
Fig.21. *CL image of the framed region in Fig.20.*

The spectra corresponding to the numbered positions in the image of Fig.21 are
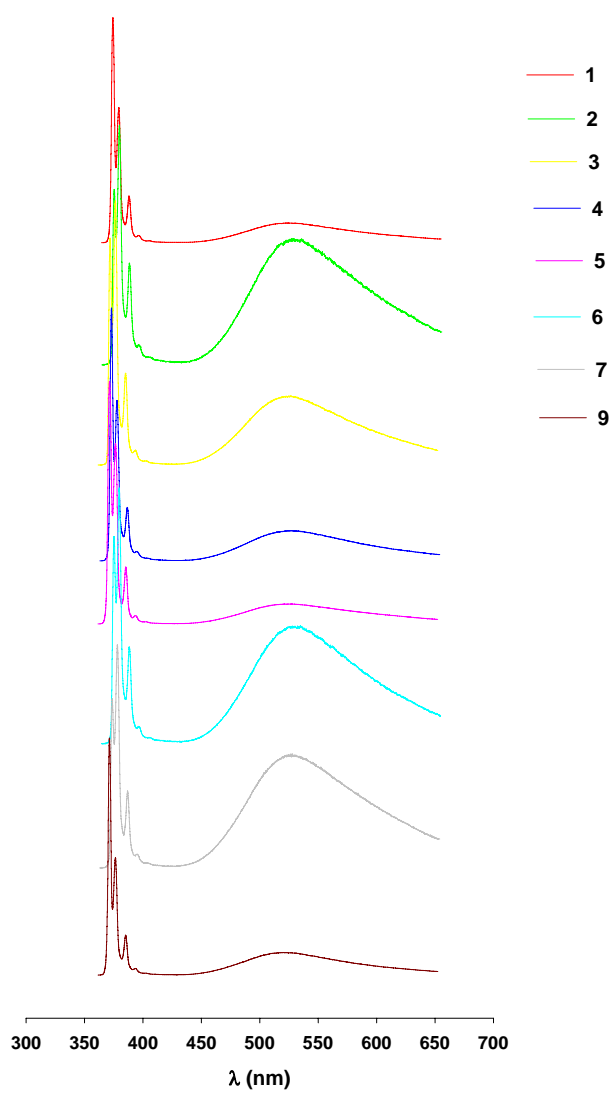
Fig.22a. *Full spectra obtained at the points numbered in Fig. 21*

represented in Fig.22a.
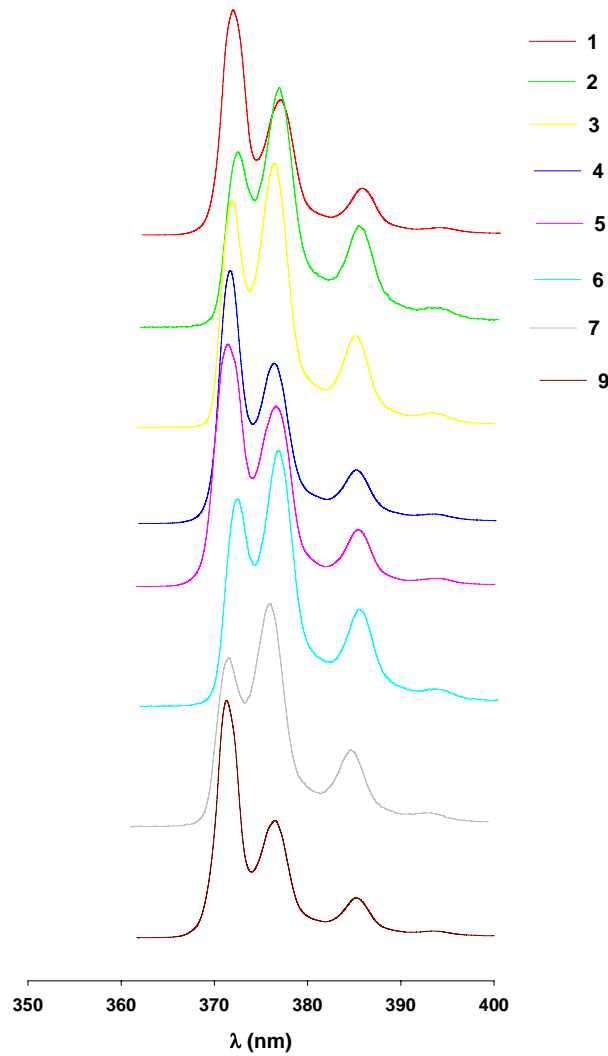
Fig.22b. *Near band gap range of the spectra of Fig. 11a*

The spectra are normalized to the maximum intensity. Fig 22b is the UV spectral region expanded for better observation. In these spectra one observes that the relative intensity of the BX band at 369 nm and the band at 376 nm (3.30 eV) (P1) depends on the spatial position. This relation also applies to the visible luminescence. In general, one can observe that in the regions with the higher concentration of defects, darker regions in fig.21, the relative intensity of these bands is significantly enhanced respect to the BX band. The intensity of the P1 band can be even reversed respect to the BX band. The overall CL intensity is reduced in damaged areas, which means that non radiative recombination centers are the dominating defects created by the indentation; however,

simultaneously, defects responsible for the 3.3.eV band (P1) and the visible band are created. Fig. 23 shows the monochromatic images obtained from the integrated intensities of the different luminescence bands.
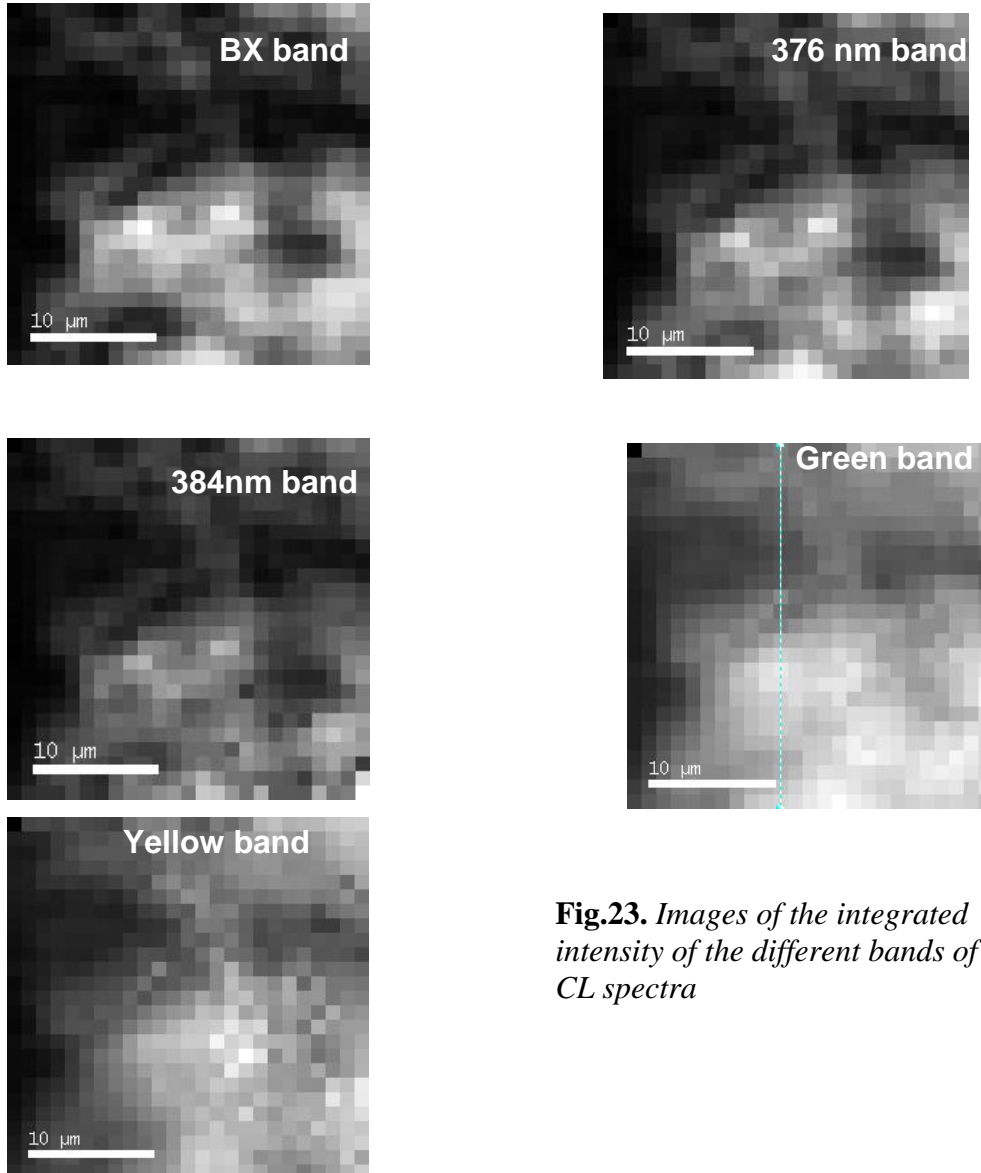
Fig.23. *Images of the integrated intensity of the different bands of the CL spectra*

All the images of Fig. 23 present a similar contrast, which reflects the distribution of non radiative recombination centers. However, underlying this contrast there is another contrast that is revealed by the relative intensities of the different bands respect to te BX band. These images are shown in Fig. 24.

Fig.24.*a) Monochromatic image at 370 nm (BX band), b) relative intensity of the 375 nm band respect to the 370 nm band, c) relative intensity of the visible band respect to the 370 nm band, d) absolute intensity of the 375 nm band*
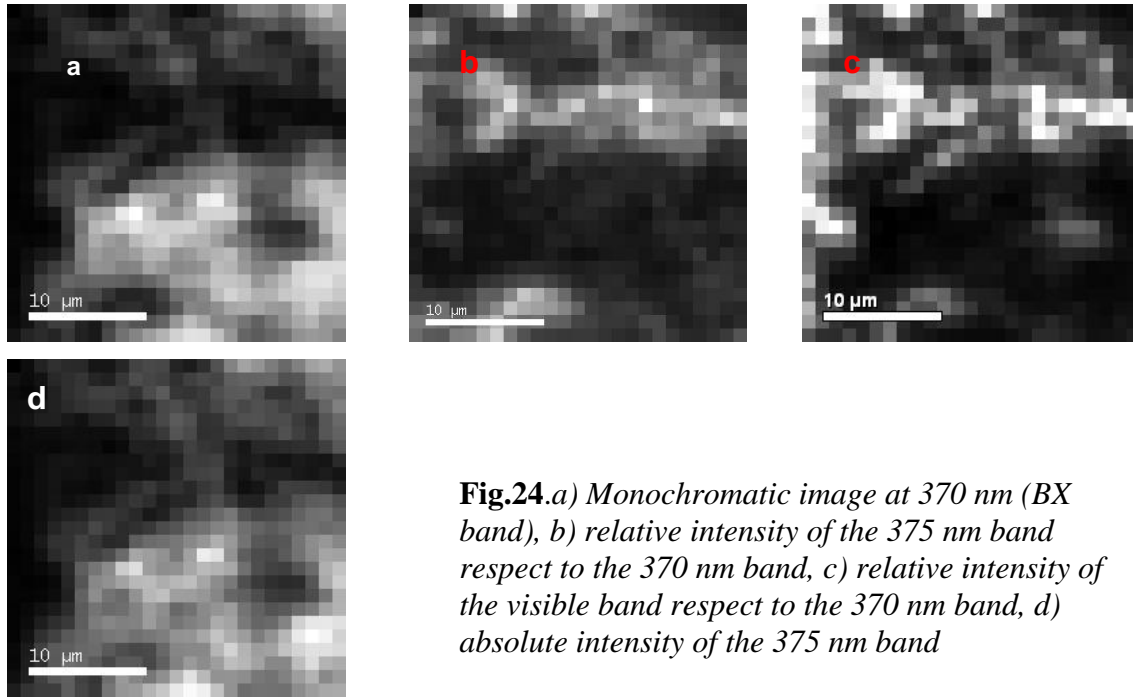
The relative intensities of the 376 nm band and the visible luminescence show a reverse contrast respect to the absolute intensity of the BX band and the absolute intensities of the other bands, see Fig. 24. This means that the levels responsible for those emissions are generated simultaneously to the non-radiative recombination defects in the regions where the overall luminescence appears darker.

In order to quantify the change in the contrast of the different images we should analyze the scan profiles along the vertical line of Fig. 23d, see Fig. 25

Fig.25. *Intensity profiles of the different bands obtained along the vertical scanning line indicated in Fig. 12d. The intensities are normalized to the maximum intensity of each band, therefore all of them have a maximum value of the unity.*
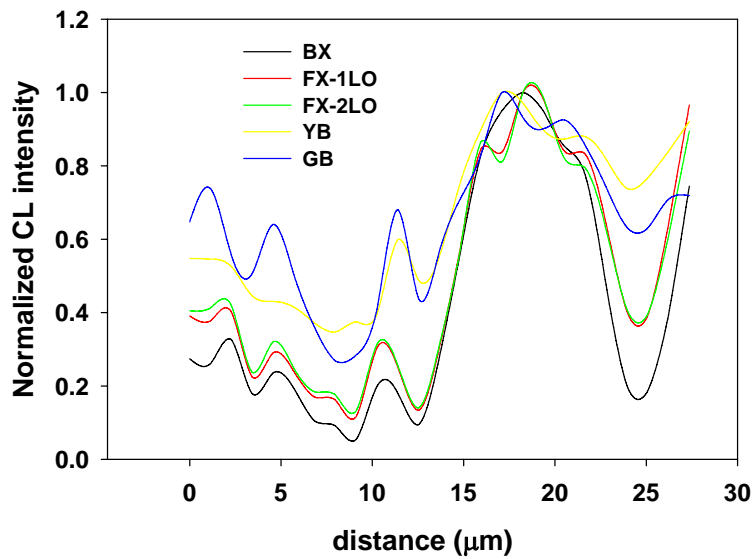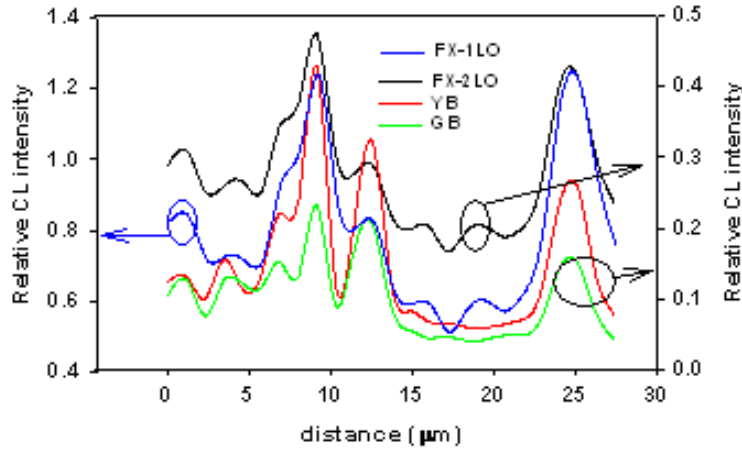
g.**Fig.26.** *Relative intensities of the FX-1LO; FX-2LO,*
B *and YB across the line of Fig12.d*

In this profile we observe that all the extrinsic band s follow the same profile distribution, which is governed by the distribution of the non radiative recombination centers created by plastic deformation. The relative intensities of the bands respect to the BX band are shown in Fig. 26, where one observes the underlying contrast generated by the plastic deformation. the bands at 376 nm and 384 nm are labeled FX-1LO and FX-2LO, because the 1LO and 2LO phonon replicas of the free exciton must be located at those wavelengths.

A marked contrast appears in Fig.26, exactly anticorrelated to the intensity distribution of Fig.25; this means that the regions with a high concentration of defects (non radiative recombination) present a relative enhancement of the, 376 nm(FX-1LO), 384nm (FX-2LO), GL and YL bands.

The strong relative enhancement of the two visible bands in regions with defects suggests that the visible bands are related to intrinsic defects, which can be created by mechanical deformation during the indentation. Also the enhancement of the 376 nm band and its phonon replica points to a defect related band.

In order to support this observation other indentations were studied. See Fig.27, where the typical rosette induced by indentation on the (0001) plane of wurtzite crystals for a low load is shown. The slip lines are observed as the arms propagating from the print.

A clear relative enhancement of the band at 3.31 eV is observed in defect regions. Taking into account these results one can argue that the band at 3.31 ev is rather probably related to structural defects, however, in undamaged regions it is rather

probably a phonon replica of the free excitonic band. The study of the indentations in Tokyo Denpa crystals will support this interpretation of the 3.31 eV (376nm) band.
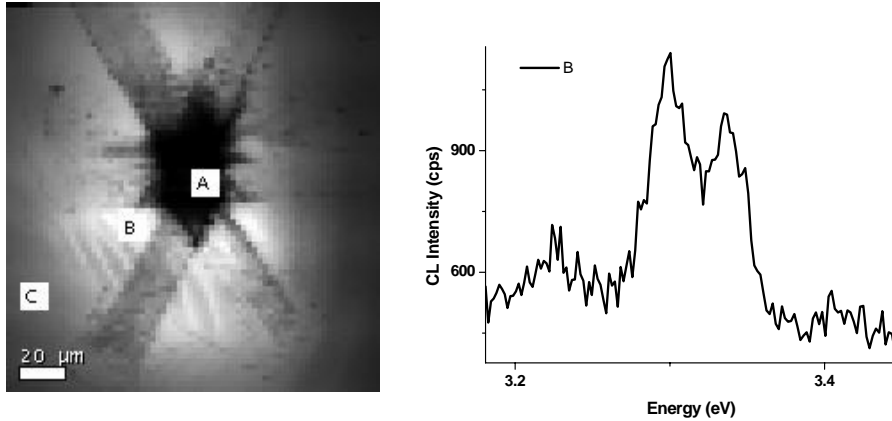
Fig.27. *CL image of an structural defect and local spectrum showing the enhancement of the 3.31 eV band in defective regions*.

The Tokyo Denpa crystal is characterized by a high crystalline quality, that results in a very strong excitonic emission, and very low visible luminescence intensity; furthermore, the visible luminescence is structured, which suggests that it is due to residual Cu impurities, rather than native defects, accounting for a very low concentration of intrinsic defects in this sample. The spectrum in defect free regions presents a very strong band at 3.31 eV (376 nm), even more intense than the bound excitonic band, which can hardly be accounted for by a defect related band, Fig.28, but it seems more reliable to associate it with a phonon replica of the free exciton. All over the crystal, for which the polishing damage is very weak one observes such a behaviour, which is clearly opposed to the observations done for the other samples. The spectrum changes dramatically when fresh defects are created by Vickers indentation.

Fig. 29, shows the CL image of a dislocation rosette formed by Vickers indentation, showing the core and the double arms propagating away. A CL spectral analysis was carried out on this indentation. Local spectra were obtained at regions with different levels of damage, which is put in situation by the panchromatic CL image.
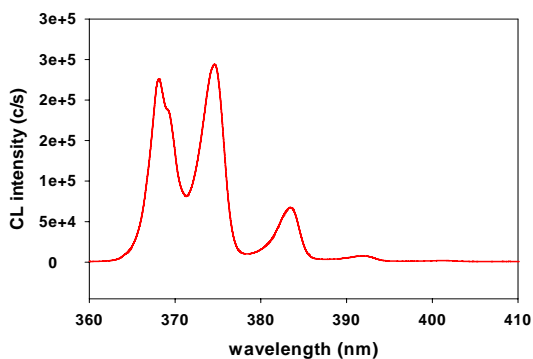
Fig.28. *Spectrum of Tokyo Denpa sample in a defect free region. showing a very strong NBE emission and a very weak visible emission*
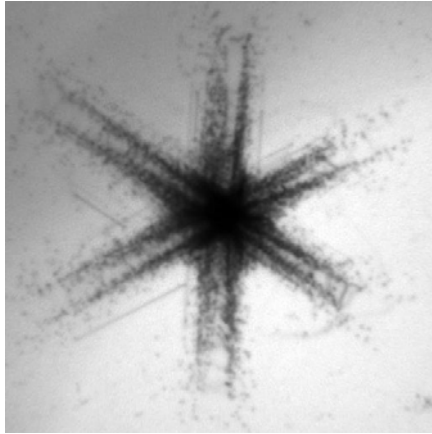
Fig.29. *CL image of an indentation in Tokio Denpa sample, showing the dislocation rosette and the double arms propagating away the indentation*

The rosette generated by the indentation on (0001) follows the slip planes of the scheme of Fig.30. he crystallographic directions of the double arms are indicated.
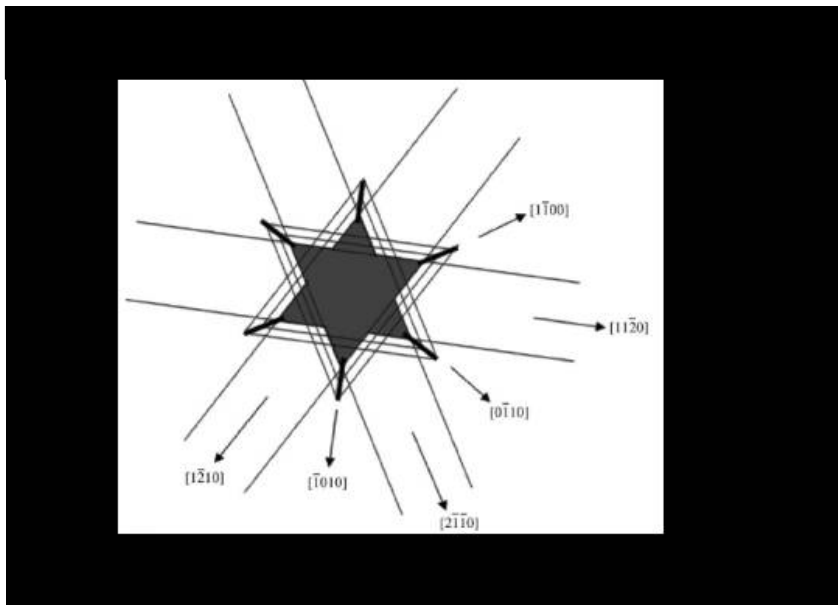
Fig.30. *Scheme of slip lines in (0001) ZnO*
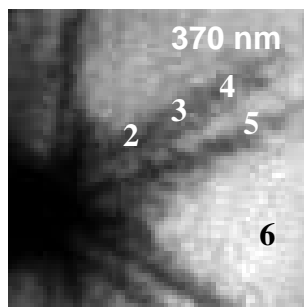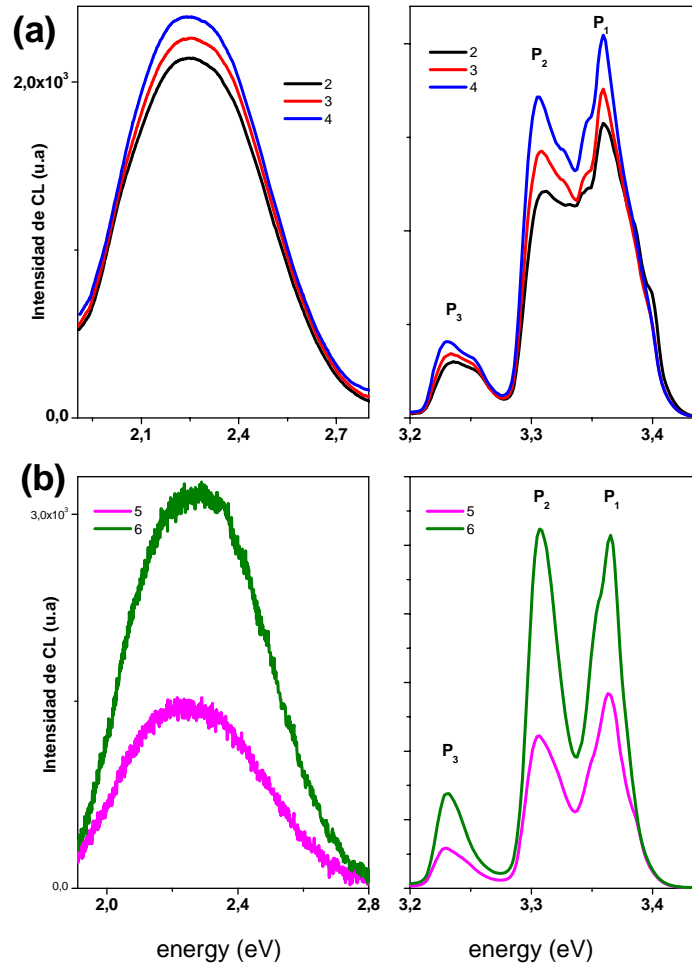

Fig.31. *Monochromatic CL image*

Fig.32. *Spectra obtained at the points marked in the image of Fig.20. See the splitting off of peaks P1 and P2 in the defect regions, spectra 2, 3, 4, and 5 in a minor extent*

The monochromatic image (BX band) is shown in Fig.31. The spectra at the points indicated in Fig.31 are shown in Fig.32. Note that contrarily to the behavior observed in other samples, in this case the CL band at 3.3 eV (376 nm), band P1, is quenched in the defect regions. If one looks at the defects areas, that band is not only quenched, but it is also split out. This means that this band in regions free of defects is a phonon replica of the free exciton, it is strong because of the high crystal quality. In the presence of defects it is quenched, reducing its intensity. Simultaneously a defect related band appears, see the high energy shoulder in the defect regions, points 2, 3, 4 and 5. It is important to note that this additional band presents a strong phonon replica, which appears as a split off of the P2 band, which suggests that the additional band observed in the high energy side of the P1 band could be related to an acceptor level, for which

phonon coupling is more intense than for donors in ZnO (K.Thonke, Th.Gruber, N.Teofilov, R.Schonfelder, A.Waag, R.Sauer; Phys.B 308-310, 945 (2001)).

An attentive observation of the CL spectra obtained in damaged areas of sample TD shows that the P_1 band is split into two close overlapping sub-bands, while in the non-damaged regions it appears as a single band, Fig.33.
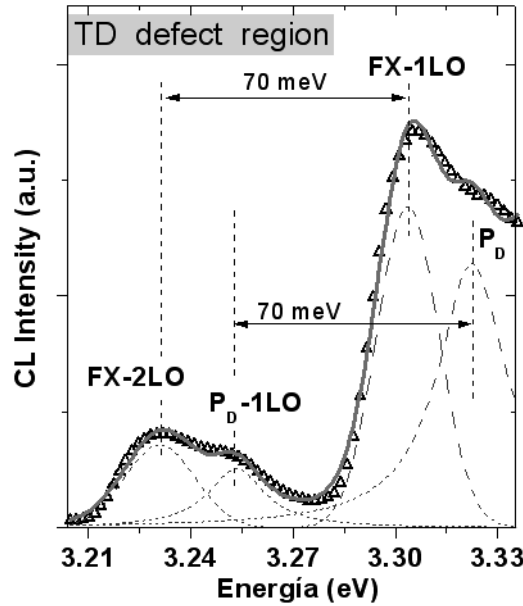
Fig.33. *CL spectrum in a damaged region showing splitting of the P1 and P2 bands*

These two sub-bands would be the first LO- phonon replica of the free exciton (the so-called FX(A)-1LO band peaking at $\approx$3.29 eV), and a band related to defects induced by the mechanical damage (so-called P_D peaking at $\approx$3.31 eV). These bands coexist
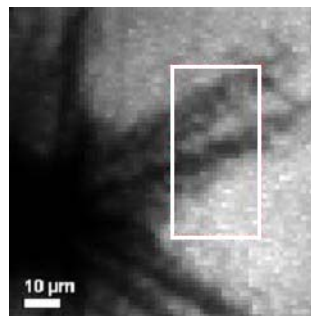
Fig.34.*CL image showing the region studied incide the frame*

depending on the crystal growth conditions and the surface treatment. The balance between the intensities of the two bands should determine the intensity and lineshape of

the convoluted P_1 band when the two bands cannot be spectrally separated. The phonon replica band would be the dominant one in defect free areas, while the defect-related band (P_D) should be prevalent in defect-rich regions.

Using a Gaussian fitting routine, the distribution of the two bands was imaged inside the region framed in Fig. 34. This control area is outside the Vickers print but includes the dark radial arms. The monochromatic CL images of BX, P_D and FX(A)-1LO bands show a similar contrast that is governed by the distribution of the NRRCs. However, if one extracts the images of the relative intensities of the P_D and FX(A)-1LO bands with respect to the BX band, one observes an underlying contrast emerging the distribution of both bands, Fig.35.
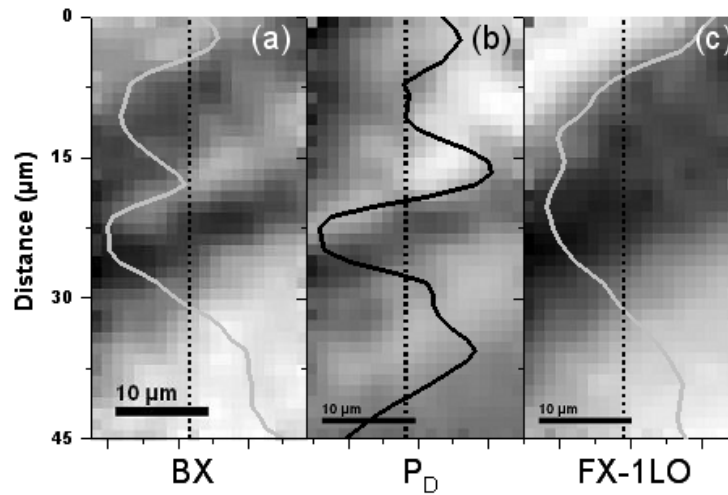
Fig.35. *CL images of the BX band intensity and the relative intensities of P_D and FX-1LO bands. Also the intensity profiles are superposed to the images*

The FX(A)-1LO band is quenched, both along the dark arms and in the regions around them, increasing its intensity out of the regions under the influence of the indentation. The quenching of this band is the consequence of the high concentration of defects in such region, which reduces the excitonic recombination, and in particular the free excitonic transitions and their replicas. The P_D band shows an opposite contrast; it decreases in regions far from the dark arms and increases around the dark arms; it is also quenched inside the dark arms. In Fig. 35 the profiles of the intensity of the BX band, and the relative intensities of the P_D and FX(A)-1LO bands along a vertical scan line are superposed to the images. The distribution of the P_D band suggests that the defects responsible for this band are point defects rather than extended defects: Point defects are generated by the interaction between the crystal and the propagating

dislocations. In the regions close to dislocations those defects can be captured by the dislocation strain field, the result is a reduction of these defects in the dark arms area; however, in the regions surrounding the dark arms, those defects are not removed and the P_D band is enhanced.

The defect related band, P_D, presents strong phonon replicas, Fig.33, which suggests an acceptor like character (K.Thonke, Th.Gruber, N.Teofilov, R.Schonfelder, A.Waag, R.Sauer; Phys.B 308-310, 945 (2001)), tentatively being due to the recombination of an exciton bound to a deep acceptor level. The formation of vacancy and interstitial defects is highly probable under indentation. According to these results, vacancy defect complexes are the main candidates to be the defects formed around the indentation. Because interstitial defects are highly mobile can be easily captured by the dislocation strain field (P.Erhart, K.Albe; Appl. Phys. Lett. 88, 201918 (2006)). A recent work established a relation between the V_{Zn}, and an excitonic band around 3.33 eV in ZnO films grown on sapphire substrates (A.Zubiaga, J.A.García, F.Plazaola, F.Tuomisto, K. Saarinen, J.Zúñiga Pérez, V. Muñoz SanJosé; J. Appl. Phys. 99, 053516 (2006)).

The point defects responsible for the P_D band should be created around the crystal defects. The P_1 band intensity increases when the acceleration voltage of the e-beam is increased. The probe depth of the e-beam in CL measurements depends on the acceleration voltage of the excitation e-beam (K.Kanaya, S. Okayama; J.Phys.D 5, 43
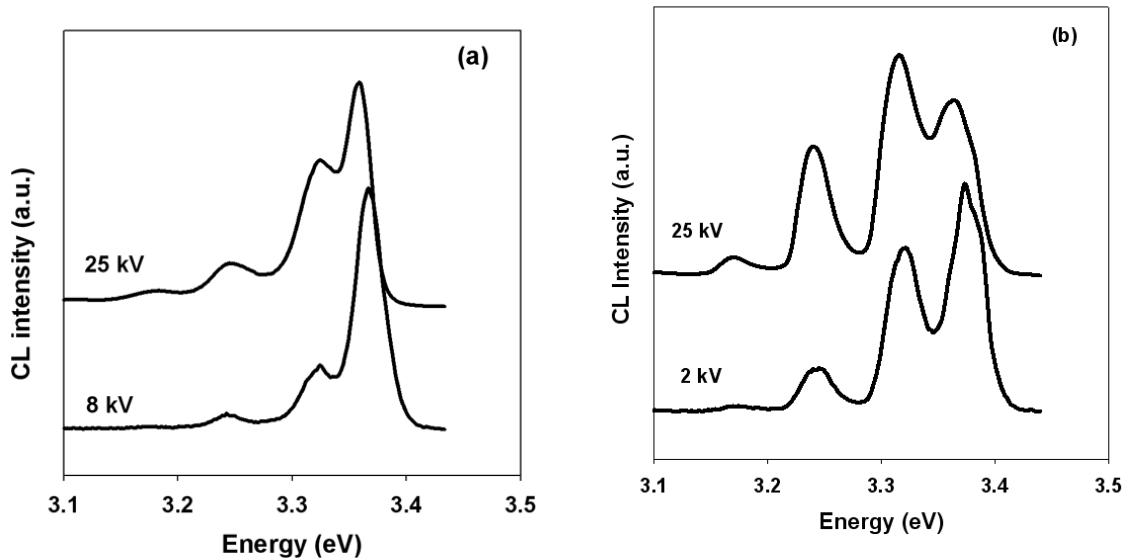
Fig.36. *CL spectra obtained in defect free regions for different e-beam acceleration voltages showing the influence of the surface finishing in the CL spectrum, a) AFRL sample, b) TD sample.*

(1972)). At high voltage, the probed volume is far from the surface, therefore is not under the influence of the damage induced by polishing. One should expect that the higher crystal quality inside the bulk crystal shall increase the intensity of the FX-1LO band. Fig.36 shows the spectra obtained in AFRL and TD samples at low and high voltage.

The surface finish of the AFRL sample is poorer than that of the TD sample. The spectra of the AFRL sample to be well observed needs an acceleration voltage threshold of 8 kV (penetration depth around 0.5 μm) versus the 2 kV (≈ 100 nm depth) for which the spectrum is well revealed in TD sample. At low voltage, the poor quality of the AFRL surface results in a low CL intensity, and the weak P_1 band; which, certainly is mostly contributed by the P_D band. The TD sample presents a much higher P_1 band, which is contributed by the FX-1LO transition, due to the high quality surface. Increasing the e-beam voltage to 25 kV (≈3 μm depth), the P1 band is increased for both samples due to the lower defect concentration in the inner part of the crystal with the concomitant increase of the FX-1LO transition.
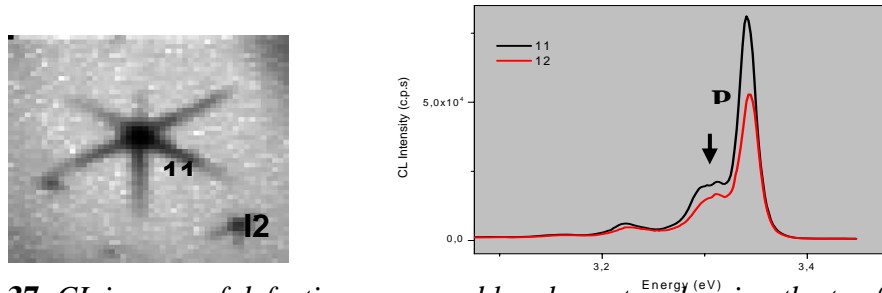
Fig.37. *CL images of defective zones and local spectra showing the twofold band at 3.3 eV*
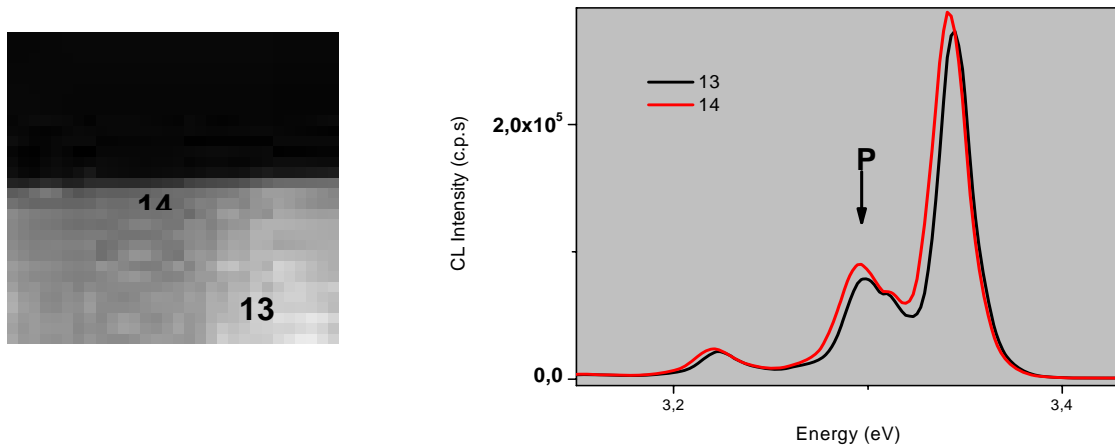
Fig.38. *CL images of a boundary between two sectors and local spectra showing the twofold band at 3.3 eV. AFRL sample*

Some small rosettes were observed in the surface of the samples, probably created by mechanical damage during polishing, Fig.37. Also the boundaries between two growth sectors presented such a behavior, see Fig. 38.

The images of the relative intensities of the different bands in the rosette of Fig.37 are shown in Fig. 39. Showing the relative increase of the different bands in the damaged regions. This rosette corresponds to an unintentional mechanical damage.
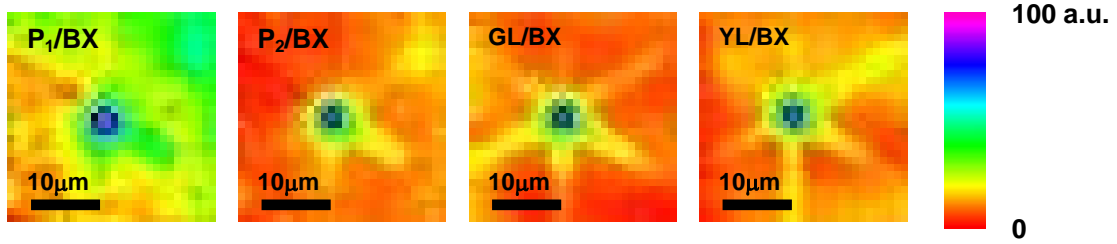
Fig.39. *Iimages of the relative intensities of the P1, P2, GL and YL bands*

A relation between the intensity of the 3.3 eV band and the visible luminescence was found in the defect regions, see Fig.40, where the intensity of the 3.3 eV band
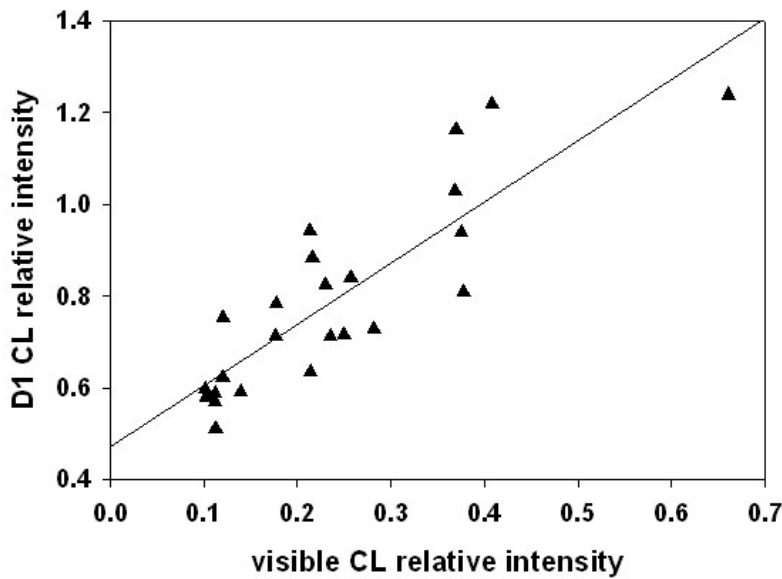
Fig.40.*Intensity of the P1 band normalized to the BX band vs the normalized visible luminescence intensity. The data are obtained over a large number of spectra obtained in different zones of the sample.*

normalized to the bound excitonic, BX, band vs the intensity of the visible band normalized to the BX band is represented. The data are obtained from a large number of points around the defective region; one observes a nearly linear relation between both, which suggests some relation between the defects responsible for both bands. Recently,

a luminescence band, close to the 3.3 eV band, has been associated with oxygen vacancies(H.Shibata et al; Phys.Stat.Sol.(c) 3, 1026 (2006))., though this not consistent with the probable acceptor like character of the P_D band

Also, we have observed that the 3.3 eV band is enhanced at the boundary between two growth sectors, where point defects are expected to be formed: see Fig.41 where the relative intensities of the yellow luminescence band, and the 3.3 eV (P1) and 3. 23 eV
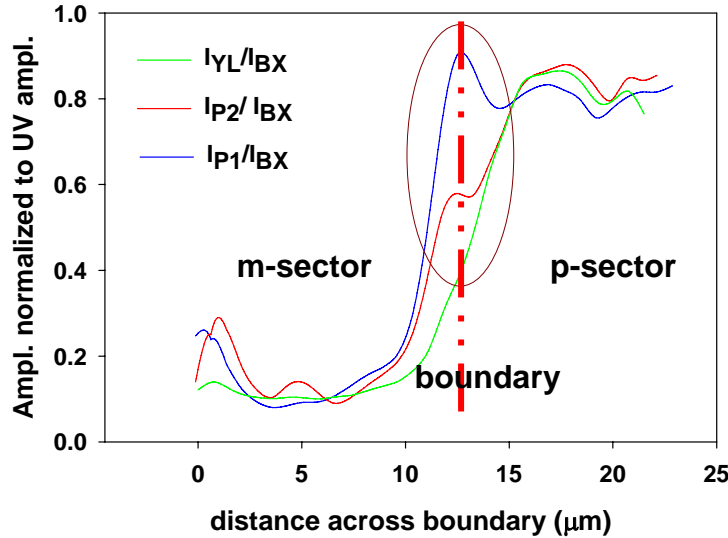

Fig.41.- *Profile of the relative intensities of the P1, P2 and YL bands across a line crossing the boundary between m and p growth sectors.*

(P2) bands are represented along a line crossing the border between two planes, prismatic and pyramidal respectively. Note the enhancement of the P1 band at the boundary.

Several indications about the existence of a defect related band around 3.31 eV energy (376 nm) have been presented. High quality crystals present a strong phonon replica band, which is quenched in the presence of defects, being replaced by a defect related band. In poorer quality crystals the phonon replica is already partially quenched in "absence of defects", when defects are introduced the defect related band close to the phonon replica band is enhanced. In this sense the phonon replica band can be used as a witness of the crystal quality, however, care must be taken because of the presence of the defect related band.

These results suggest that the quality of the substrates, including intrinsic quality, determined by the crystal growth conditions and purity, and the extrinsic one, determined y the surface treatments, can be determined by the relative intensity of the

P1 (3.3 eV) band (phonon replica of the free exciton plus the defect related band) respect to te bound exciton emission intensity. In Fig. 42 we represent this intensity ratio versus the bound exciton (BX) band intensity for different samples, different faces and different regions with different levels of damage. One observes a nice correlation between the intensity ratio P1(3.3 eV)/BX and the bound exciton band intensity (BX), showing a bathup curve. For high BX emission, the D1 band is dominated by the 1LO phonon replica of the free exciton, which is enhanced in high quality material. For decreasing BX intensity, the quality of the substrate decreases and the weight of the defect related band at 3.31 eV (P_D) increases respect to the phonon replica band (FX-1LO), enhancing the overall intensity of the P1 band. This behaviour is fully confirmed by the plot of Fig. 42; the right side of the plot corresponds to high quality substrates, while the left side corresponds to poor quality substrates. In other words a high qualiy substrate is characterized by a high overall luminesence emission, and a high P1/BX ratio. While a poor quality substrate is characterized by a low overall luminesecnce emission and a relatively high P1/BX intensity ratio.
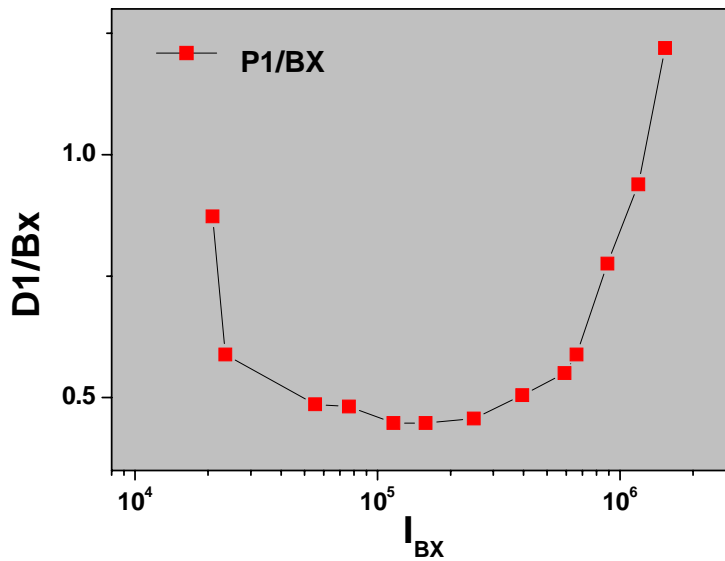
Fig.42: *P1/BX intensity ratio vs BX intensity. Couples of data were obtained over different samples and faces, and regions with different levels of structural damage. See the bathup curve accounting for the quality of the different substrates according to the damage level*

3.7. Electron irradiated crystals

The luminescence spectrum of ZnO crystals consists of three main spectral regions, the near band gap emission (NBE) with energies above 3.31 eV, the bands with energies below 3.31 eV, usually associated with donor acceptor pair (DAP) transitions and/or phonon replicas of the different excitonic bands, and the visible luminescence in the green–red spectral range. In the previous reports we have described these spectra types.

The NBE spectrum consists of several close lying free and bound excitonic transitions. At 80K the bound excitons are not yet thermally freeze and the NBE spectrum appears as a complex band convolution of several closely spaced bands, due to several bound excitonic transitions, which makes difficult the analysis of the luminescence spectra, because the spectral resolution of our spectrometer does not allow to resolve the different excitonic bands at 80 K.

Differences between the O-face and the Zn-face are observed. The main difference is the high energy side of the NBE band, which is shifted to the red in the Zn terminated face. It has been claimed that the free excitons are not observed in the Zn-terminated faces, due to intrinsic surface states of the Zn-terminated surfaces (R.E. Sherriff, D.C. Reynolds, D.C. Look, B.Jogai, J.E. Hoelscher, T.C. Collins, G.Cantwell, W.C. Harsch; *J.Appl. Phys*. 88, 3454 (2000)) that produce self absorption of the most energetic photons of the luminescence spectrum. The surface states should be responsible for the band tailing absorbing the photons with the higher energy in the luminescence spectrum. A similar effect was observed in ion implanted ZnO (V.A. Coleman, H.H.Tan, C.Jagadish, S.O. Kucheyev, M.R. Phillips, J.Zou; *Mater. Res. Soc. Symp. Proc.* Vol. 289, B8.7.1 (2005)) and undoped ZnO crystals. The optical absorption edge was also observed to shift to the red with increasing oxygen concentration (M.R. Phillips, M.Wagner, O.Gelhausen, V.Coleman, J.B. Brady, C. Jagadish, E. Malguth, A. Hoffmann, E.M. Goldys, J.J. Rusell; *E.MRS Fall meeting, Symp. F*, (Warsaw, Poland, 2004)); it suggests that the shift towards the red of the luminescence threshold energy would be related to surface oxygen excess. In fact, all that suggests the relevant role played by the ZnO surface, which was already discussed in the previous reports.

The NBE spectrum at 80 K presents a band composed of several subbands in the 3.32 - 3.37 eV spectral window, the relative weight of the different bands depends on the samples and the growth sectors. The main contribution, around 3.35 eV arises from the so-called I4 band. Among the donors responsible for this emission, hydrogen is the most commonly accepted one, and it appears under the form of OH^- (L.E. Halliburton,

L.Wang, L.Bai, N.Y.Garces, N.C. Giles, M.J. Callahan, B.Wang; *J.Appl. Phys.* 96, 7168 (2004)).

The emission at 3.33 eV, usually labeled as the I_9 excitonic band has been associated with either Al impurities (donor bound exciton) or alkali impurities, Li and Na, (acceptor bound excitons) (E.Tomzig, R.Helbig; *J. Luminescence* 14, 403 (1970), B.K. Meyer, H.Alves, D.M. Hofmann, W.Kriegseis, D. Forster, F. Bertram, J. Christen, A. Hoffmann, M. Strasburg, M. Dworzak, U. Haboeck, A. V. Rodina; *Phys. Stat. Sol. (b)* 241, 231 (2004)), all of them have a relevant presence in these crystals. It was pointed out that the incorporation of H_2O and OH^- is reduced in the presence of Li (E.D. Kolb, R.A.Laudise; *J. Am. Ceram. Soc.* 49, 302 (1966)), which suggests that Li could be at the origin of the 3.33 eV luminescence emission, since the intensity of the bands at 3.35 eV and 3.33 eV seems to be anticorrelated for the different growth sectors.

CL spectroscopy (V.Coleman, J.E.Bradby, C.Jagadish, M.R.Phillips; Appl. Phys. Lett. 89, 082102 (2006)), scanning capacitance microscopy (W.R.Liu et al; J.Cryst. Growth 297, 294 (2006)) have revealed the presence of acceptor like states, which are responsible for luminescence emissions around 3.33 (H.Alves et al; Opt. Mater.23, 33 (2003)), 3.31 (M.Schirra et al.; Physica B 401-402, 362 (2007), J. Mass, M. Avella, J. Jiménez, M. Callahan, D. Bliss;. Buguo Wang; J. Mater. Res. 22, 3526 (2007)), and 3.1 eV (R.Radoi et al, Nanotechnology 14, 794 (2003).

The spectral region below 3.32 eV, consists of several bands separated each other by $\approx$70 meV, which is roughly the energy of the LO phonon (72 meV) in ZnO. There is a main band at $\approx$3.31 eV and several phonon replicas at 3.24, 3.17 and 3.1 eV. The nature of the 3.31 eV band is a matter of controversy. It has been associated with a donor-acceptor pair (DAP) transition (T.B. Hur, G.S.Jeen, Y.H.Hwang, H.K.Kim; *J. Appl. Phys.* 94, 5787 (2003)), which the nature of the defects involved is not known. It is also identified as the first phonon replica of the free exciton transition, FX-1LO band (B.K. Meyer, H.Alves, D.M. Hofmann, W.Kriegseis, D. Forster, F. Bertram, J. Christen, A. Hoffmann, M. Strasburg, M. Dworzak, U. Haboeck, A. V. Rodina; *Phys. Stat. Sol. (b)* 241, 231 (2004)). Also, a band related to structural defects was reported around such energy (B.K. Meyer, H.Alves, D.M. Hofmann, W.Kriegseis, D. Forster, F. Bertram, J. Christen, A. Hoffmann, M. Strasburg, M. Dworzak, U. Haboeck, A. V. Rodina; *Phys. Stat. Sol. (b)* 241, 231 (2004), M.Schirra et al.; Physica B 401-402, 362 (2007), Y.Ohno et al; Appl. Phys. Lett. 92, 011922 (2008)). In our previous work we showed that a band around 3.32 eV can be a defect related band; it was enhanced and differentiated from

the phonon replica of the free exciton (FX-1LO) in the regions surrounding dislocations generated by Vickers indentation.(Cathodoluminescence study of ZnO wafers cut from hydrothermal crystals; J. Mass, M. Avella, J. Jiménez, A. Rodríguez, T. Rodríguez, M. Callahan, D. Bliss, Buguo Wang ; J. Cryst. Growth 310, 1000 (2008), Cathodoluminescence study of defects created by Vickers indentation in hydrothermal ZnO crystals; J. Mass, M. Avella, J. Jiménez, M. Callahan, D. Bliss;. Buguo Wang; J. Mater. Res. 22, 3526 (2007)).

A band corresponding to the one observed close to dislocations in the indented samples, around 3.32 eV (≈373 nm), was reported in e-irradiated material (M.A.Hernández-Fenollosa, L.C.Damonte, B.Marí; Superlatt. and Microstr. 38, 336 (2005)).

Therefore, we will make a comparative study between irradiated induced luminescence and the luminescence induced by plastic deformation. Note that polishing can result in mechanical damage, equivalent to low load nanoindentations, which makes that the surface of the ZnO can be critical to the PL response in terms of the 3.32 eV band..

The visible bands have been also reported to undergoing changes under the effect of both e-irradiation and plastic deformation (L.S.Vlasenko, G.D.Watkins; Phys.Rev.B 71, 125210 (2005), V.Coleman, J.E.Bradby, C.Jagadish, M.R.Phillips; Appl. Phys. Lett. 89, 082102 (2006)). However, we will focus our study on the 3.32 eV band.

We studied two samples irradiated with electrons with energy and doses high enough to produce defects. Irradiations were carried out at room temperature, and post irradiation Hall effect measurements revealed a p-type conversion, which evidences the generation of acceptor levels, shallow enough to supply holes to the valence band at room temperature. Therefore, we will focus in the NBE spectral range.

Two samples were studied, labeled TDC1 and TD2G3. The PL spectra and the main spectral parameters are shown in Figs 43 and 44 respectively.
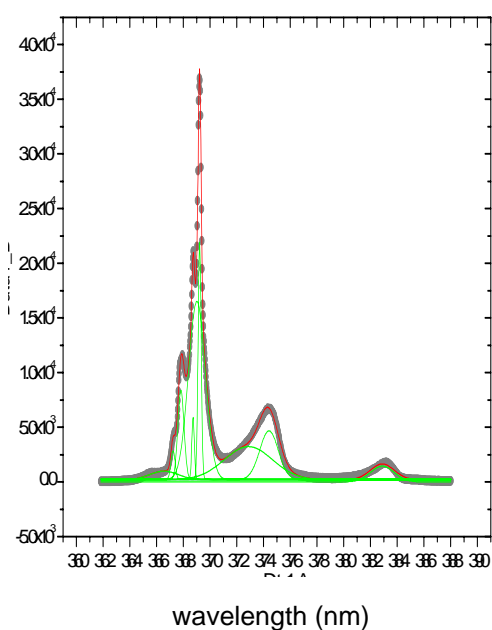
	Peak position (nm)	FWHM (nm)
1	366.5	2.4
2	367.2	0.37
3	367.8	0.54
4	368.7	0.22
5	369.2	0.27
6	369.0	1.48
7	372.8	4.223
8	374.4	1.63
9	382.8	2.08

Fig.43. *PL spectrum of sample TDC, and table with the main spectral parameters*
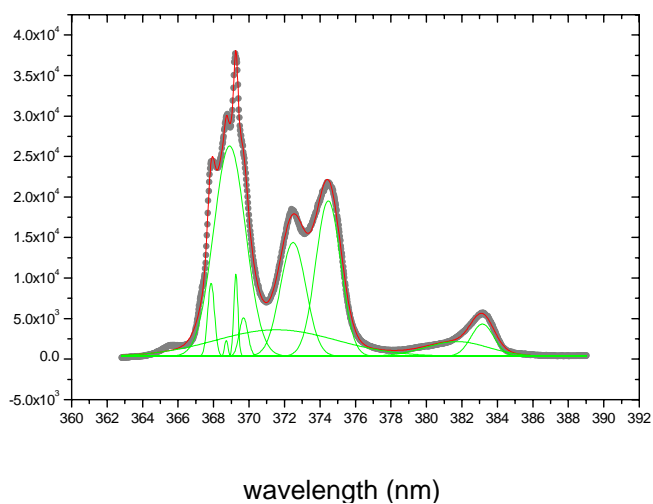
	Peak position (nm)	FWHM (nm)
1	367.8	0.45
2	368.7	0.22
3	369.2	0.27
4	369.7	0.57
5	368.9	2.11
6	372.5	1.71
7	374.4	1.65
8	381.7	4.14
9	383.1	1.51

Fig.44. *PL spectrum of sample TD2G3 and spectral parameters*

The main difference between the two samples concerns the spectral region above 370 nm. In particular sample TD2G3 exhibits a band a 372.5 nm, which is not well resolved in sample TD2C1. This band presents a phonon replica and is blue shifted 17 meV respect to the FX-1LO band. This band has been already reported in e-irradiated ZnO. A similar band was observed around the dislocations induced by Vickers indentation in similar ZnO crystals (J. Mass, M. Avella, J. Jiménez, M. Callahan, D. Bliss;. Buguo Wang; J. Mater. Res. 22, 3526 (2007)). Fig.33.

The separation between the two bands, P_D and FX-1LO, of Fig.33, was 19 meV, which fits very well to the separation observed in the PL spectrum.

The PL spectra of the two irradiated samples and a reference sample are shown in Fig. 44.
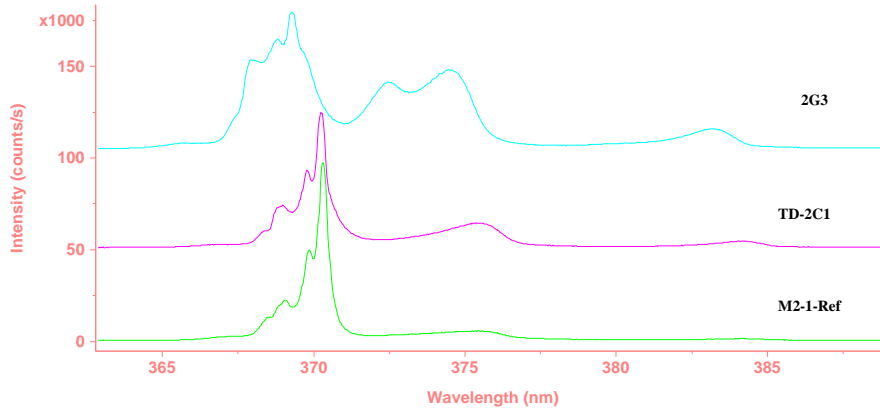
Fig.44. *PL spectra of the two irradiated samples and a reference sample*

The PL spectra of the three samples are similar, with the main difference of the defect related band and the FX-1LO band. The spectrum is shifted to the blue in sample TD2G3, which suggests that the irradiated faces (either Zn, or O faces) are not the same for both samples (by instance we have not this information).

Panchromatic CL images of the two irradiated samples revealed a strong subsurface damage. See Figs. 45 and 46.
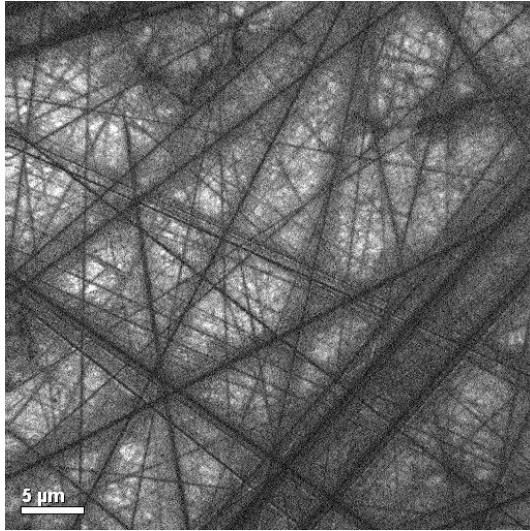
Fig.45. *Panchromatic CL image of sample TD2C1, irradiated face*
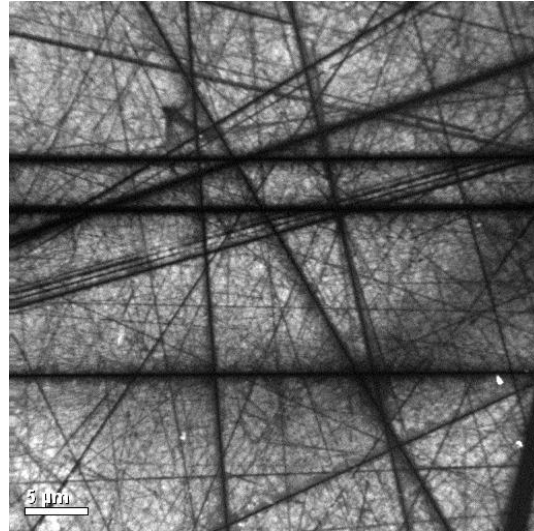
Fig.46. *Panchromatic CL image of sample TD2G3, irradiated face*

CL images and the spectra obtained at different points of sample TD2G3 are shown in Figs. 47 and 48. The defect related band is only observed around the polishing damaged regions corresponding to the dark lines revealed by CL.
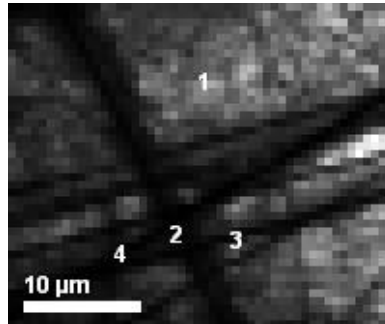
Fig.47. *CL image of sample TD2G3, the numbers correpond to the points where the spectra of Figure 7 were acquired.*
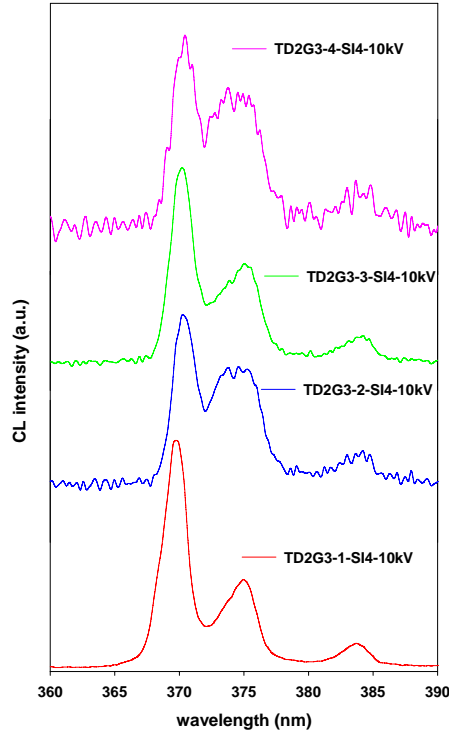
Fig.48. *CL spectra obtained obtained at the points indicated in Fig.6. (10kV)*

Note that the spectra do not show the band at 3.32 eV so clear as it was observed in the PL spectrum; however, it is enhanced in the regions close to scratches, points 2, 3, and 4; while it appears much less clear in point 1, which is far from the scratched area. Increasing the acceleration voltage of the excitation electrons, one observes a lower contribution of the defect related band respect to the spectra acquired at lower acceleration voltage shown in Fig.48, see Figs. 49, and 50.
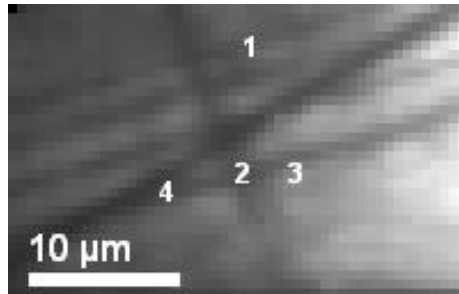
Fig.49. *CL image of the same region as the one in Fig.6, but obtained at 20 kV*
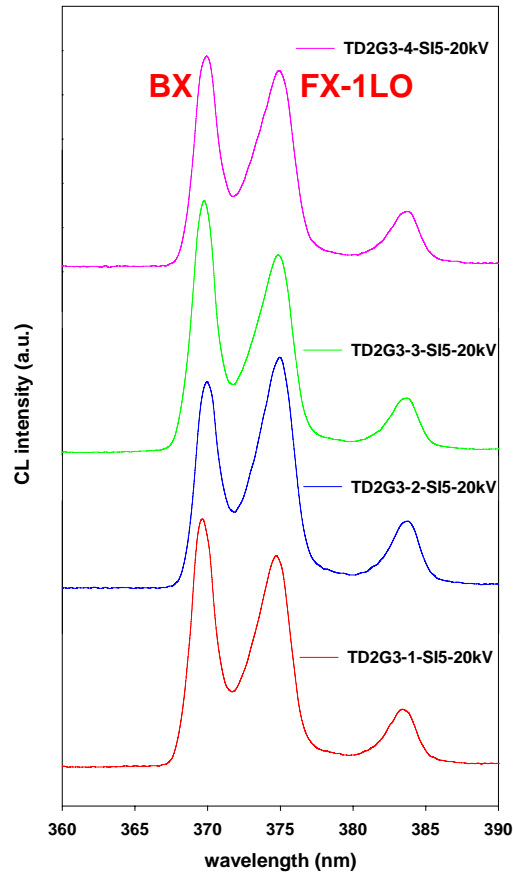
Fig.50. *CL spectra obtained at the points indicated in the image of Fig.8 (20kV)*

By increasing the acceleration voltage the probe depth is enhanced and therefore the influence of the subsurface defects is significantly reduced, see the smooth CL image, Fig. 49, and the similarity between all the spectra, which acquire the typical shape observed in TD samples, with a strong contribution of the FX-1LO band, which can be as intense as the bound excitonic bands (BX). Therefore the luminescence spectr are strongly influenced by the surface preparation. In particular the PL spectra are acquired very close to the surface, the probe depth of the 325 nm laser light is a few nms, One cannot probe a so shallow region with CL, because if the surface is not very smooth it charges and the CL spectra cannot be acquired at very low acceleration voltages to establish a correlation with PL.

A similar effect is observed for sample TD2C1, though it was more difficult to observe. Nevertheless some spectra present a clear evidence of the e- irradiation induced band, see Figs. 51 and 52.
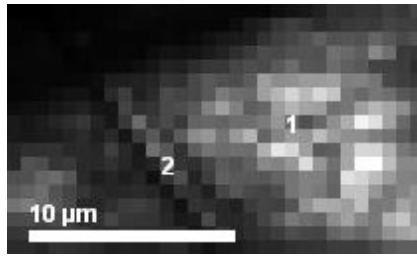
Fig.51. *CL image at 10 kV, sample TD2C1*
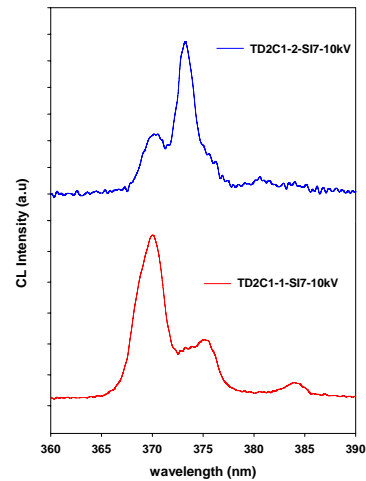
Fig.52.*CL spectra at the points numbered in Fig.10*

Why the difference between CL and PL spectra?. This is a critical issue, since it is probably due to the presence of extended defects close to the surface. In PL measurements the excitation light penetrates a few nms, and therefore the probe depth is very small, close to the surface, where damage induced by polishing is always present. In CL measurements, the penetration is higher, almost 1 μm for standard conditions (10kV) of our spectra. This means, that the probed region is far from the surface and therefore we are not probing the same region than in PL. However the defect band (3.32 eV) is enhanced around the scratches. This observation can be explained as follows.

The primary defects produced by electron irradiation are vacancies and interstitials. The atomic displacement rate can be estimated from the Macinley-Feshbach formula (F.Agulló-López et al; Point defects in materials; (Academic Press, New York 1988), using the displacement energy, E_d. The E_d values for ZnO, 41.4 eV for O and 18.5 eV for Zn, were estimated by Van Vechten (J.A.an Vechten; Hanbook on semiconductors; ed. by T.S.Moss and S.P.Keller (North Holland, Amsterdam 1988) ch.1). According to this, the displacement rate is higher for Zn, therefore, Zn sublattice defects are expected in a higher concentration respect to O sublattice defects. Tuomisto et al (Tuomisto et al., Phys.Rev. Lett. 91, 205502 (2003)) estimated a very low displacement rate of 0.03 cm^{-1}, which means that the defects should recombine at very low temperature as suggested by Y.V.Gorelkinskii, G.D. Watkins; Phys. Rev.B 69, 115212 (2004)). Frenkel pairs are

formed as primary defects, but due to the high mobility of the interstitials they recombine at relatively low temperature, therefore the concentration of defects at room temperature must be very low.

The presence of crystal defects prevents the recombination of the Frenkel pairs, because the interstitials are trapped by the crystal defects stabilizing the vacancies that are stable at room temperature. This is reason why the defects induced by e- irradiation are observed in PL, because at the top surface extended defects exist and capture the interstitials.

In the case of CL, the defect band is only observed in the neighborhood of the scratches, because the interstitials are captured at the dislocations induced around them. This is quite similar to the observations reported for plastically deformed material. When the acceleration voltage increases, the penetration depth is beyond 2 μm, and the 3.32 eV band is scarcely observed, because of the high recombination rate of Frenkel pairs, far away the crystal defect areas.

Therefore, the additional band observed under electron irradiation at 3.32 eV seems to be similar to the one induced by plastic deformation. It is probably associated with V_{Zn} defects. A relation between V_{Zn} and a luminescence band at 3.346 eV was recently reported (A.Zubiaga et al; J. Appl. Phys. 99, 05316 (2006)); note that this measurement was carried out at 10K, therefore it can be related to our band at 3.32 eV, which was measured at 80 K.

Further work on e- irradiated plastically deformed areas is under consideration.

3.8. *MgZnO alloys*

Concerning the MgZnO alloys the main results obtained are summarized as follows: Mg is effectively incorporated into the crystals as observed by the blue shift of the excitonic luminescence, Fig. 53; the incorporated amount is difficult to estimate, but lies within the solubility limit in equilibrium conditions (4%)
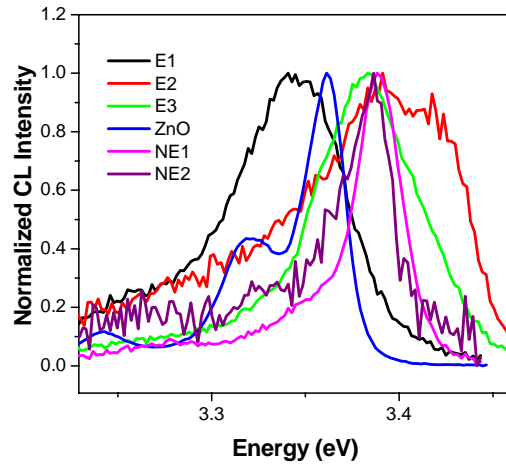
Fig.53. *Normalized spectra in the UV spectral range showing the blueshift corresponding to the incorporation of Mg.*

The spectral parameters obtained for the CL spectra of Fig.43 are summarized in table I.

sample	E(eV)	I (c/s)	Γ (eV)	E(eV)	I (c/s)
ZnO etched	3.36	1.63	0.029	2.19	0.49
E-1	3.34	0.15	0.079	2.17	0.489
E-2	3.42	0.06	0.109	2.19	0.42
E-3	3.38	0.23	0.073	2.22	0.54
non-etched					
NE-1	3.39	0.31	0.032	2.17	0.49
NE-2	3.38	0.03	0.044	2.13	0.45

TableI. *Spectral parameters of the spectra of Fig.1, UV and visible bands*

Samples E and NE, mean etched and non etched respectively. The NE sample presents a sharp peak, with a full width at half maximum (FWHM) about half the FWHM of sample E, and only twice the FWHM of the reference sample. Note that these spectra were taken with an acceleration voltage of 20 kV, which gives a probe depth around 2 μm, which reduces the possible interference of the ZnO layer deposited on the top

surface, and which is expected to remain in NE sample, while it is expected to be removed in E sample.

Sample E exhibits a different behaviour; for example, in facet 2 it presents a double peak with a high energy component peaking at 3.42 eV, and the low energy one peaking at 3.38 eV. A similar trend, though less marked, appears in E-3. This behaviour suggests clustering or layered distribution of Mg cations in the ZnO lattice in this sample. The third facet of sample E, E-1, exhibits a broad band shifted to the low energy, there is not blue shift respect to the ZnO reference sample, but the weak high energy tail appears as evidence of Mg alloying, which suggests that not all the Mg was incorporated in substitutional position, but the broad band suggests that disordering was also introduced in the ZnO lattice. The irregular shape of the samples prevented the identification of the facets. New samples with improved geometry are being studied

At the present status the samples are very inhomogeneous; which is consistent with the defect incorporation facet dependence in HTT ZnO. Also the distribution of Mg seems to change close to the surface but this also seems to depend on the sample and the facets. See Fig. 54 where the peak energy is represented vs the acceleration voltage, remember that the probe depth increases with the acceleration voltage.
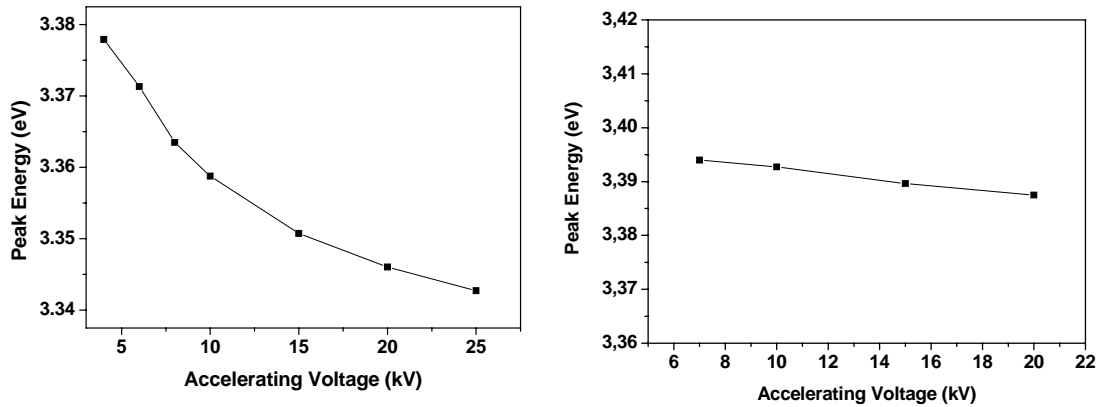
Fig.54. *UV peak energy vs the acceleration voltage of the e-beam (probe depth), facets E-1 (left) and NE-1 (right).*

The data of Fig. 54 suggests a certain accumulation of Mg close to the surface, it is more marked in the etched surface. Further studies are required to understand this behaviour, which is certainly related to the solubility of Mg

Parallel studies of Raman spectroscopy of ZnO crystals have been carried out in cooperation with Dr. Artús from CSIC Barcelona Spain.

4. OP GaAs crystals

4.1. Introduction.

Orientation patterned (OP)-GaAs crystals are very promising for tunable coherent light sources in the mid infrared. Material characteristics concerning the propagation losses, the crystal dimensions and the available periods must be taken into account to implement crystals for specific wavelength ranges and operating modes (CW or pulsed). The study of the OP crystals, aiming to analyze the main factors that can contribute to the optical losses, is a crucial step toward the use of these crystals in many promising applications, as remote gas sensing, infrared countermeasures….

The main emphasis of this study is paid to the interfaces, in particular the domain walls, and the substrate domain interfaces. Also attention is paid to the extended defects and the identification of residual free carriers, which are one of the main sources of losses. The discontinuities associated with the domain walls and/ or extended defects can play a major role in the optical losses, since they act as light scattering centers and also the strain fields around them induce refraction index changes with the corresponding consequences in the light transmission losses.

4.2. Panchromatic images

Panchromatic images give an overview of the cleaved face (011) and (0-11) for <00-1> and <001> oriented domains respectively, Fig.1. The substrate (0-11) is located at the bottom in the panchomatic image. The bottom images are monochromatic images at the labeled wavelengths, corresponding to the maxima of the main spectral features, one is the intrinsic emission and the other corresponds to a defect related band, related to defect complexes. The spectrum in the layer is very different from the spectrum of the substrate. First, the main luminescence band (band to band) is very narrow, which suggests a good crystalline quality and a low residual impurity concentration; second, it is shifted to the high energy respect to the substrate, which is probably due to a lower concentration of defects, or to differences in the residual stress between the layer and the substrate. On the other hand, the CL spectrum in the layer shows an asymmetric broadening towards the high energies, which can be due to either free carriers in the substrate or valence band splitting due to residual stress.
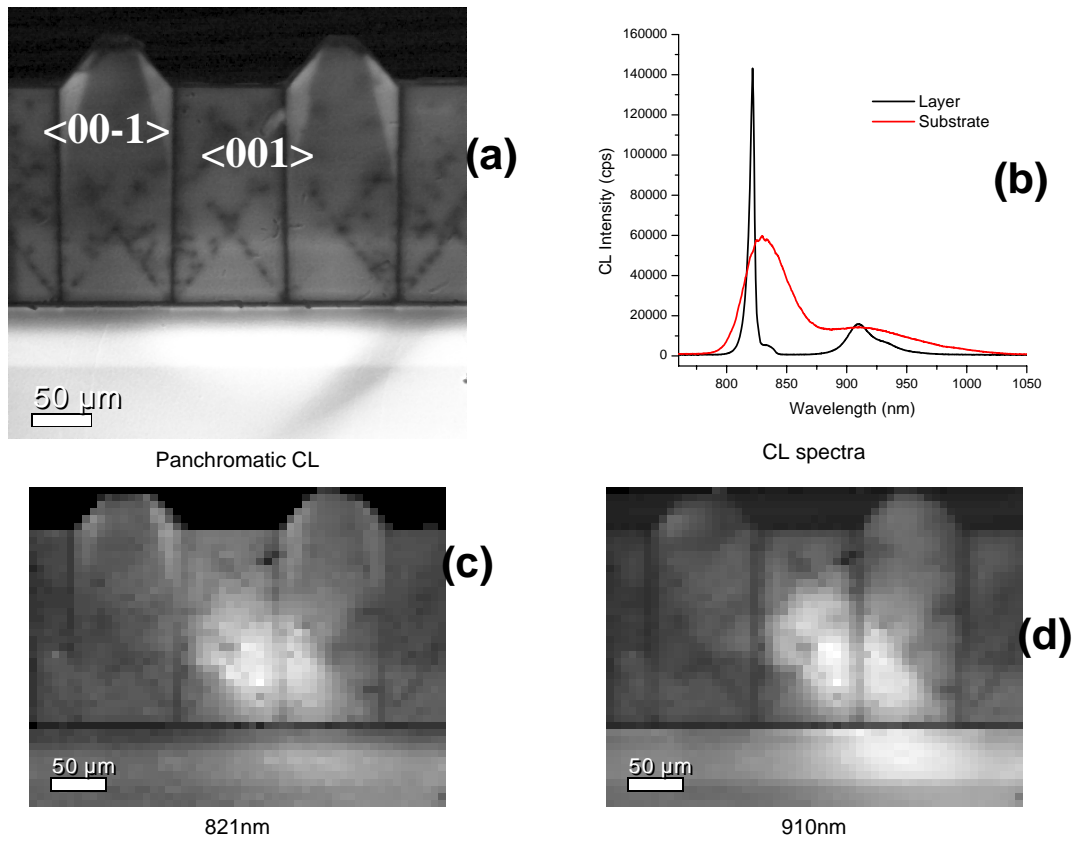
Fig.1. *Panchromatic CL image(a), CL spectra(b), monochromatic images, 821 nm (c), 910 nm(d)*

The top image is the panchromatic image, the two lower images are monochromatic images obtained at the energies of the intrinsic and defect related luminescence bands. One observes the two oriented domains, <001> and <00-1>. The domain walls appear as dark lines due to the non-radiative recombination at the interface, antibonds are non radiative recombination centers. Also, one observes cross-hatched dark lines and bright areas at the facets of the overgrown <00-1> domains. Some dark lines arising from the walls are also observed.

The CL spectra of both the layer and the substrate are also shown. Note the difference between both, the broad band of the substrate is due to doping, in particular, the substrate presents two main bands corresponding to an Si_{Ga}-V_{As} complex at 1.36 eV and a band at 1.47 eV due to an Si_{Ga}-Ga_{As} complex (L. Pavesi, N.H. Ky, J.D. Ganière, F.K. Reinhardt, N. Baba Ali, I.Harrison, B. Tuck, M. Henini; J.Appl. Phys. 71, 2225 (1992)). The narrow band of the epitaxial layers is consistent with a high quality layer and a very low free carrier concentration, however bands at 911 nm (1.36 eV) and 930 nm (1.325 eV) reveal the formation of native defects complexed with Si impurities (either Si_{As}-V_{As} or As_{Ga}-Si_{Ga}) Ga vacancies, $V_{Ga,}$ or Ga antisites (H.Birey, J. Sites; J. Appl. Phys. 51, 619 (1980)), which suggests that some residual Si couldd exist in the OP-GaAs layers.

Magnified images are shown in Figs. 2 and 3.
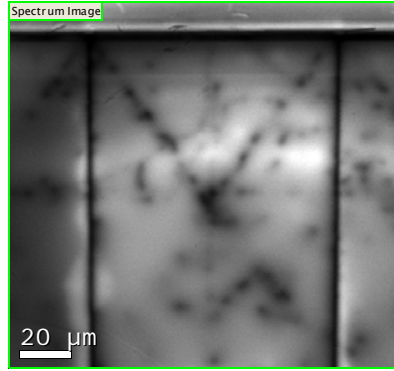
Panchromatic CL

Fig. 2. *Panchromatic image (a) showing the details of the domain walls and the dark lines and spots*
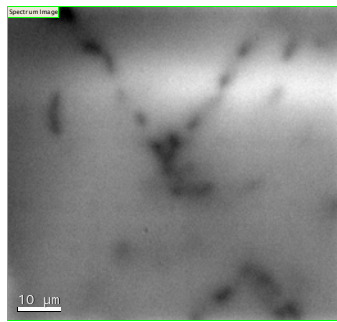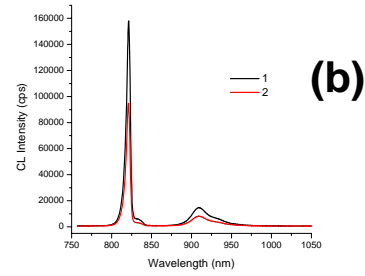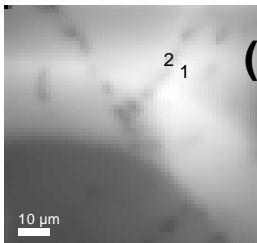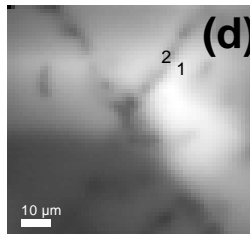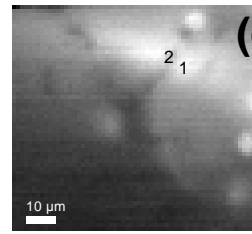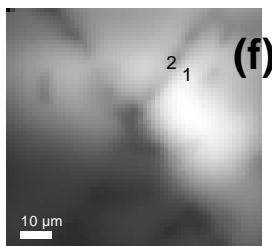
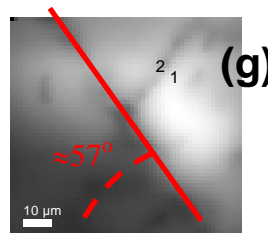**Fig.3.** *Panchromatic image of the dark lines (a), CL spetra inside and outside the dark lines, points 1 and 2 of the micrographs (b), monochromatic images, 820 nm (c), 835 nm (d), 865 nm (e), 910 nm (f) and 935 nm (g).*

The dark area in the lower left corner of the images is an artifact related to a luminosity lost caused by the collecting parabolic mirror reflection pattern and a slight misalignment of the optical beam.

The cross hatched dark lines are arrays of dislocations generated at the boundary between the GaAs and the Ge seeds, they form an angle ≈ 57°, with the substrate plane. This line is the intersection between the dislocation gliding planes (111) and the face plane (110), these dislocation lines are driven by stresses generated at the border between the two domain orientations; they seed at the triple boundary between the substrate and two adjacent domains. The CL spectrum in this region is similar to the spectrum in the dislocation free areas of the layer, the main difference concerns the intensity emission, the overall spectrum intensity is reduced, which is the consequence of the generation of deep levels around the domain walls and the dislocations. Note that the dislocation lines appear decorated by defects giving non radiative recombination. The defects are formed as a consequence of the interaction between the dislocation and the GaAs lattice. Arsenic antisites, As_{Ga} are the main candidates to act as non radiative recombination centers.
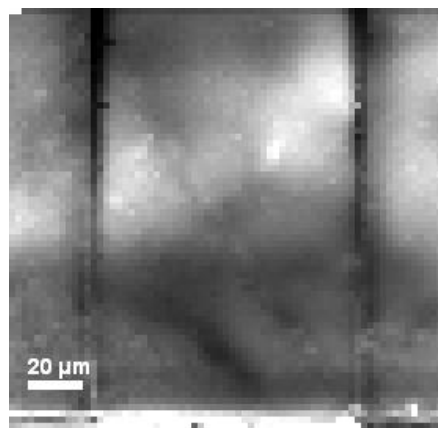
Fig.4. *Image of the relative intensity of the 910 nm band respect to the 820 nm band*

The defect related band at 910 nm is quenched at the walls, while the dislocation lines are very weakly contrasted, Fig.4, which suggests that the defects responsible for the defect related band are not sensitive to the interaction between the dislocations and the GaAs matrix. The defect related bands are highly probably related to Ga vacancy complexes (K.C.Shin, M.H.Kwaik, M.H.Oh, Y.B.Tak; J.Appl. Phys. 65, 736 (1989)) which suggests that the layers are slightly Ga deficient, which should explain the dominant role played by defects based on As excess. Antisite defects are typical products of the dislocation gliding (P.Martin, J. Jimenez, C. Frigeri, L. F. Sanz, J. Weyher;J. Materials Research 14, 1732 - 1743 (1999)).

.

4.3. Spectrum images

Spectra fittings permit mapping the different spectral parameters. The peak wavelength of the intrinsic CL band is imaged, This image can reveal the distribution of stresses. Stress is mostly concentrated around the domain walls and the dislocation lines.

4.3.1. Dislocation lines

The images corresponding to the spectral parameters of the band are shown in Fig.14 , where one represent also the profile values of the intensity, peak wavelength and full width at half maximum obtained along a scanning line.
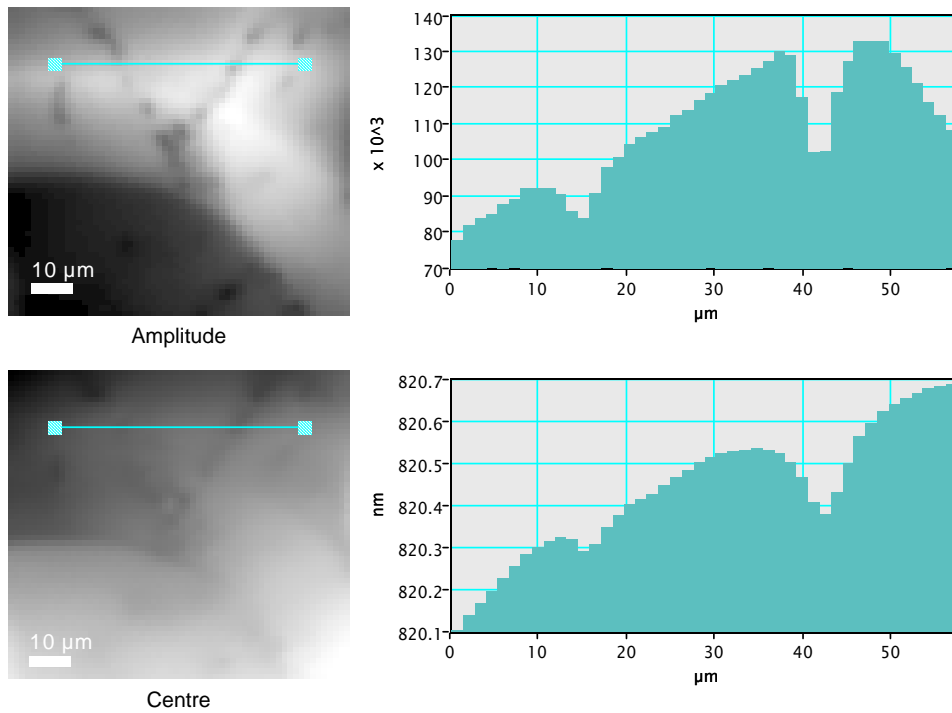
Fig.5. *Spectral images and scan profiles along the lines indicated in the figures. (a) intrinsic CL band amplitude, (b) peak wavelength*

One observes spatial correlation between the intensity and the peak wavelength, the areas surrounding the dislocation lines are compressed respect to the areas out of the dislocation strain field. The peak wavelength distribution can be converted to stress distribution taking into account that the pressure coefficient for the bandgap shift

induced by stress in GaAs is 11.527 eV/bar (Landolt Borstein, Numerical data and functional relationships in Science and Technology (Springer, Berlin 1986).

4.3.2.Domain Walls

A similar study was carried for domain walls, the results are shown in Fig. 6
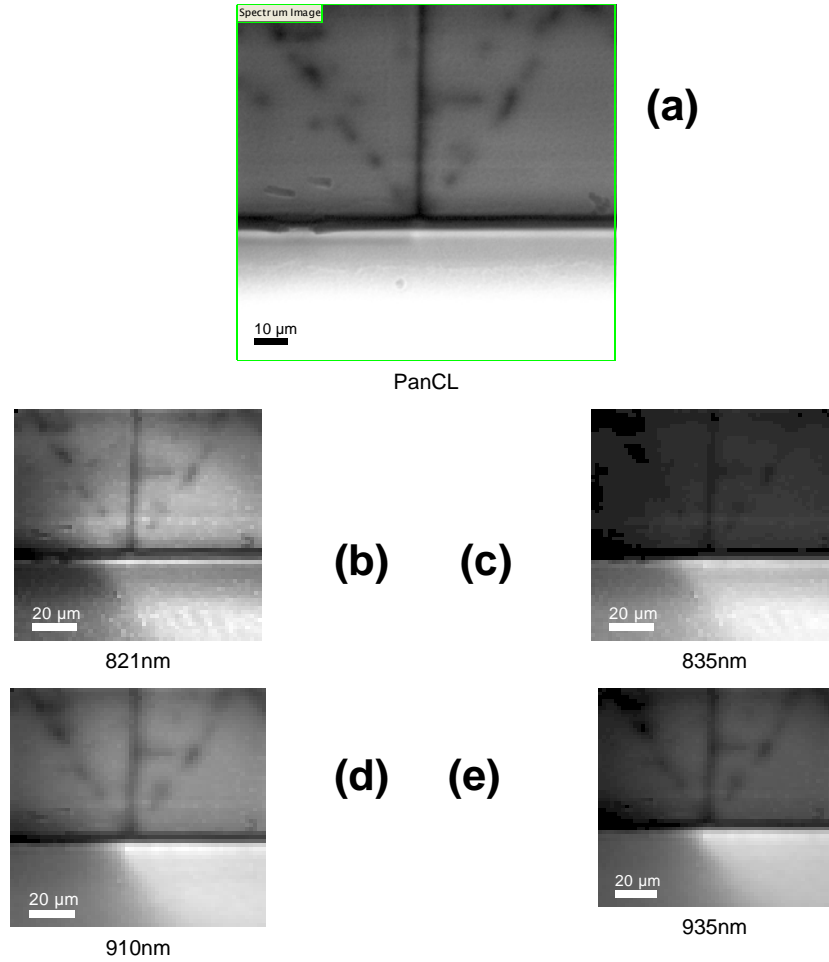
Fig. 6. panchromatic image (a), monochromatic images (b) 821 nm, (c) 835 nm, (d) 910 nm, (e) 935 nm

A region with the two phases and the substrate was selected, using a Gaussian fitting routine the spectral parameters were imaged.

We selected a smaller area to fit in order to minimize the mirror effect at the lower left corner of the image. The results are shown in Fig. 7.
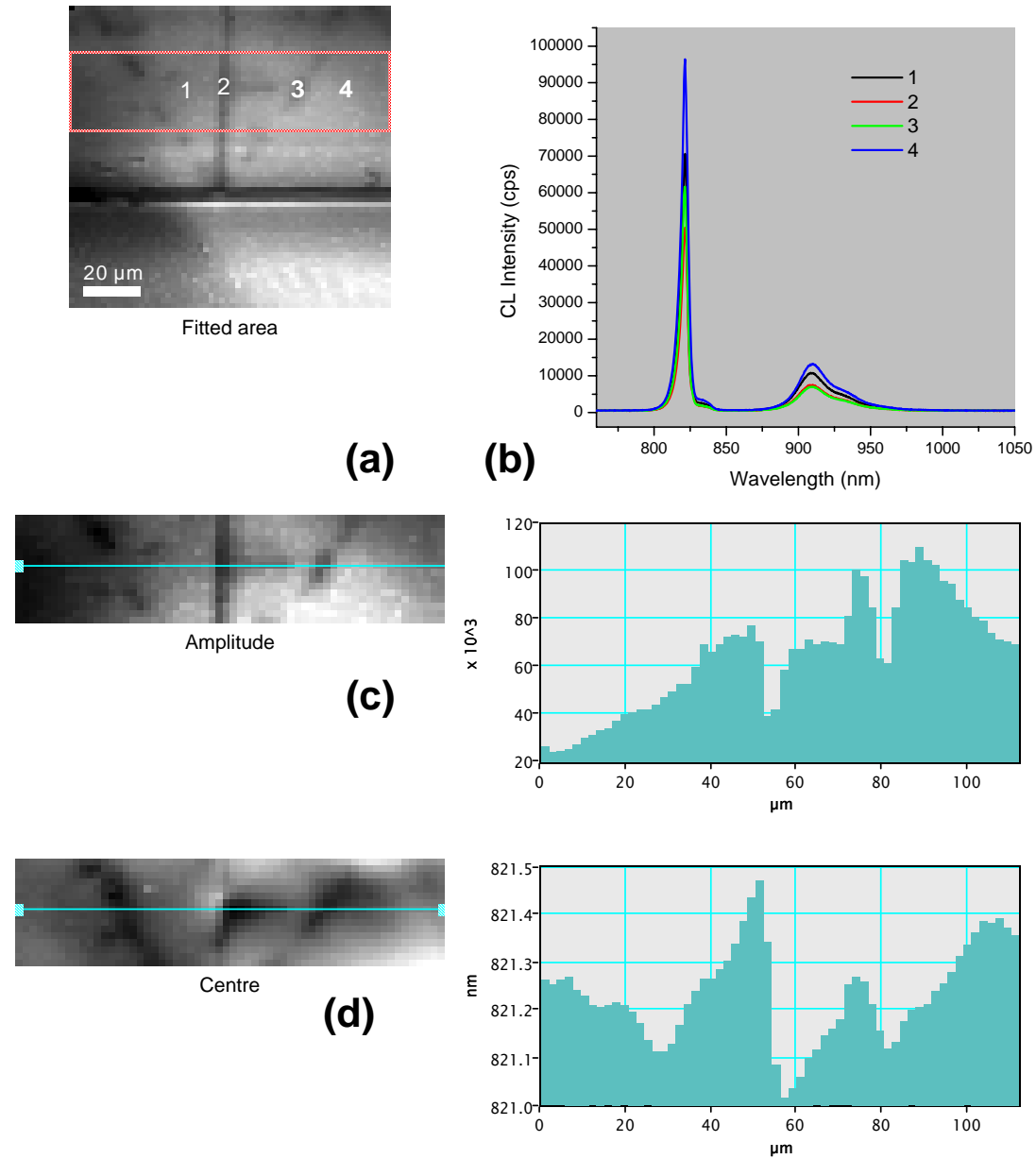
Fig.7. *Spectral image resulting from the fitting of the 820 nm band. a) panchromatic image, b) CL spectra, c) amplitude of the 820 nm ban, and amplitude profile across the horizontal line, d)peak wavelength and peak wavelength profile across the horizontal line*

The 820 nm luminescence response in the interface between the two domains shows a behaviour similar to that observed in the dislocation lines; with low emission intensity, which is governed by non-radiative recombination at the antibonds in the walls and the As_{Ga} like defects in the dislocation atmospheres. However, the stress presents opposite sign, the luminescence peak is shifted to the red, which corresponds to the existence of tensile stress around the domain walls, contrarily to the compressive strain observed

around the dislocations. One can argue that the atmospheres around the dislocations and the domain walls are different. In the image of the peak wavelengh the regions free of defects at the interface show a slight red shift in the boundary between the two domains, while a larger blue shift is observed in the neighbourhood of the dislocation lines.

4.3.3. Interface between the domain facets

This measurement was taken at the top edge of the layer, at the interface between the domains where the <00-1> domain overgrows the <001> domain, Fig. 17.
The reticular aspect of the panchromatic image arises from surface charging. It does not affect to the spectral response of the system.

Panchromatic CL

821nm   835nm

910nm   935nm
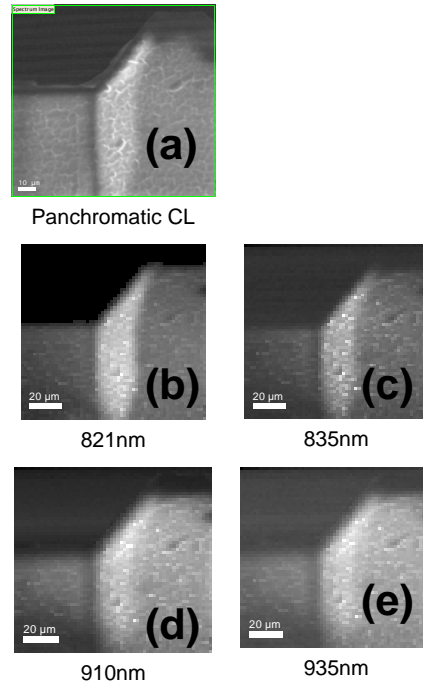
Fig.8 .*Panchromatic CL image (a), monochromatic images, 821 nm (a), 835 nm (b), 910 nm(c), 935 nm (d)*

The contrast associated with faceting is more pronounced for the band gap emission than for the extrinsic band, as deduced from the monochromatic images. The clear region in the <00-1> domain starts just at the interface region where the gliding dislocations intersect the domain wall. However, such an effect is not seen in the <001> domain. It seems related to a change in the growth kinetics responsible for the faceting observe in the top of this layer.

We selected a small area to fit the spectra in order to minimize the mirror effect at the lower left corner of the image. One observes red shift and broadening of the intrinsic luminescence peak, which fits the overall observation around the walls, Fig. 9. The enhanced luminescence seems to be associated with a reduced non radiative recombination efficiency, which can be related to the filtering of dislocations by the domain wall, which enhances the luminescence emission, but also the non incorporation of NRRCs..
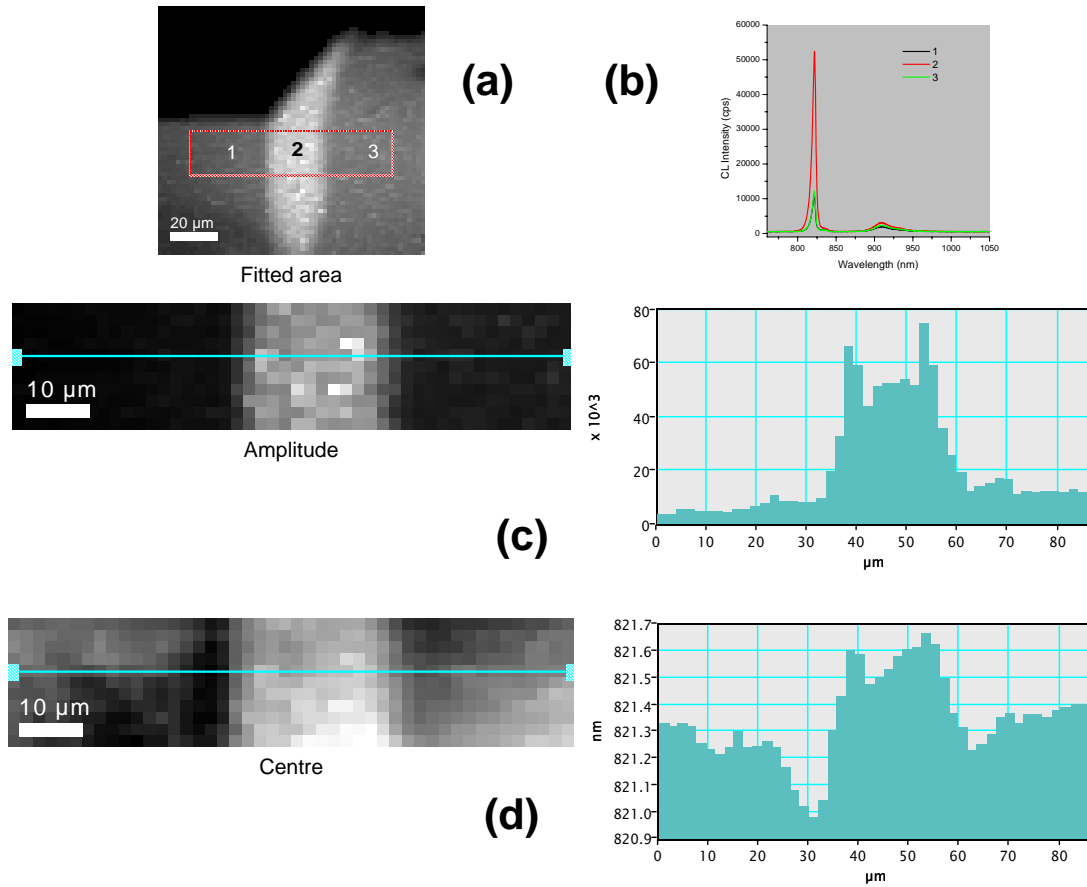

Fig. 9. *Panchromatic CL image (a), CL spectra at the points indicated in (a) (b), amplitude and profile along the scanning line (c), peak wavelength and profile along the scanning line (d).*

4.3.4. Domains grown in perpendicular cristal direction <1-10>

In the same wafer there was two pattern orientations, <1-10> and <110>. The panchromatic images of <1-10> patterned OP-crystal region reveal an irregular geometry of the domains with non vertical walls, Fig.10, contrarily to the very regular geometry of the <110> pattern oriented OP-crystals, previously studied. The differences

lies in the alignement of the substrate steps, since the layers are grown in vicinal substrates, in this case the OP axis is parallel to the terraces.

Panchromatic CL

822nm   835nm

910nm   935nm
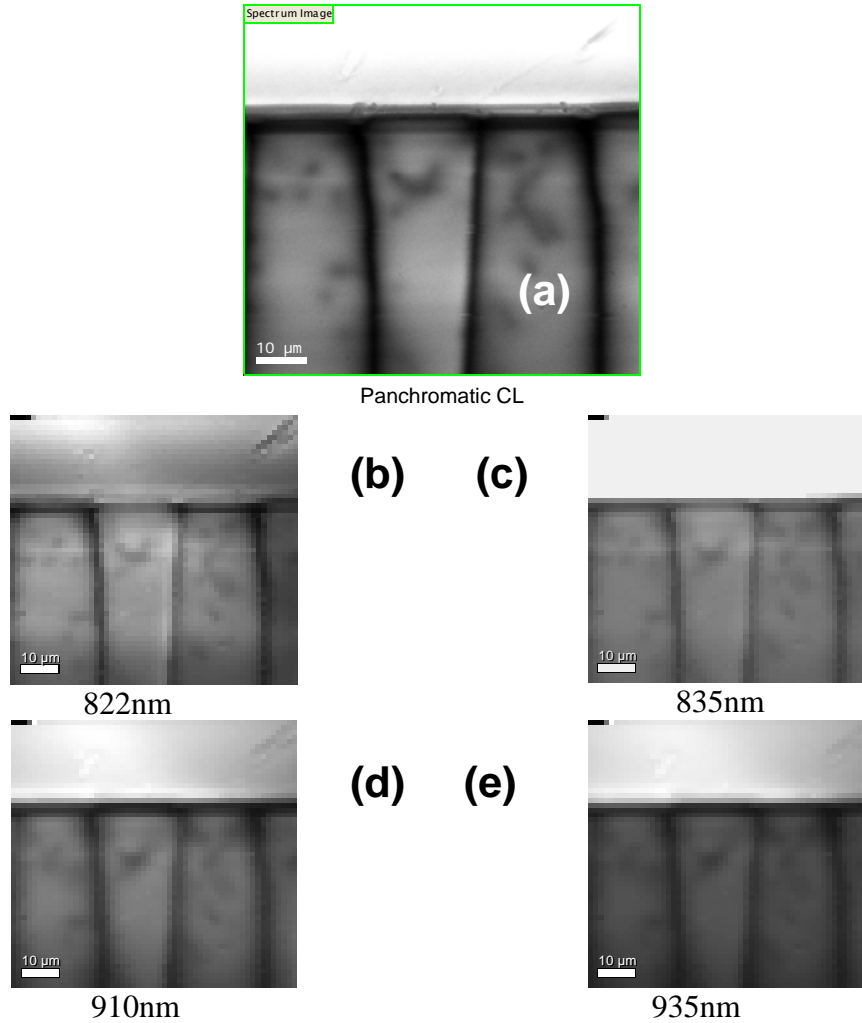
Fig.9. *Panchromatic image of <1-10> oriented OP crystal (a), monochromatic images (a), 822nm (b), 835 nm (c), 910 nm (d), 935 nm (e)*

4.4. *Stress*

Stress distribution was estimated from the shift of the intrinsic luminescence band. The spectral images were acquired at different regions of the crystals and then using Gaussian fitting routines we studied the main strain fields, which are imaged by means of the spectral parameter distributions. An image of the distribution of the peak wavelength is shown in Fig. 10. The stress is mainly concentrated around the domain walls and around the dislocation lines. One observes a good spatial correlation between peak wavelength and the FWHM, both of them being anticorrelated to the intensity emission.

The stress distribution is asymmetric around the domain walls, which suggests the existence of shear stresses between two adjacent domains. The areas surrounding the dislocation lines are compressed with respect to the areas out of the dislocation strain field.

According to the stress coefficients coefficient for the bandgap shift in GaAs, $11.5*10^{-9}$ eV/bar, stresses around 9 MPa can be estimated around the domain walls, though its distribution is very irregular, see Fig. 11, where one represents the peak wavelength and FWHM parallel to the domain wall at both sides of the wall. The stress around the dislocation lines is compressive, and its strain field is broader than the strain field of the antiphase walls, which might be due to the high concentration of point defects in the atmosphere of the dislocation. In the regions with stress gradients, domain walls and dislocation atmospheres, the FWHM is increased. Because the stress gradient is more abrupt around the domain walls the FWHM broadening is higher.
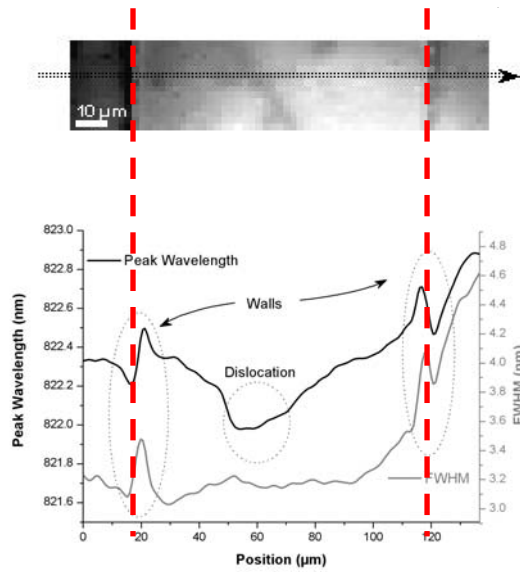
Figure 10. *a) peak wavelength distribution image, b)profiles of peak wavelength and FWHM along the line indicated in (a) showing the asymmetric stress distribution around the domain walls.*
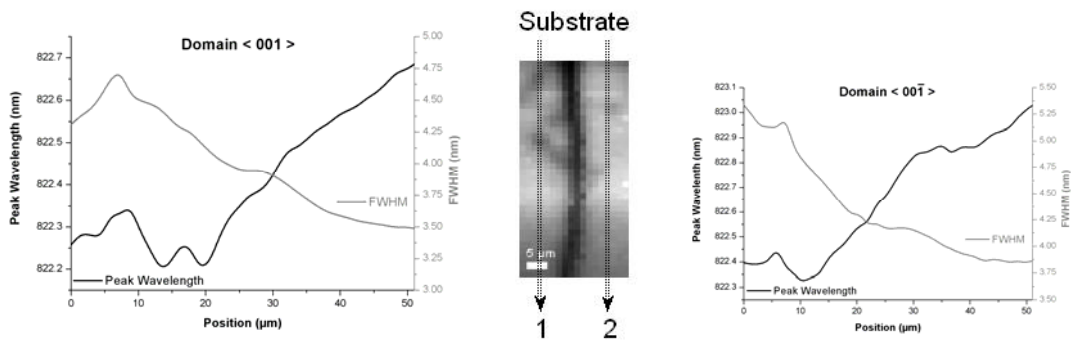
Figure 11. *CL image and corresponding peak wavelength and FWHM profiles along the vertical scanning lines of the CL image for the two domain orientations.*

One also imaged the stress induced by the substrate. The vertical profiles indicate a lower energy shift when moving away from the substrate, which corresponds to the progressive relaxation of the interface stress, Fig.11. The FWHM is larger in the regions under higher stress as expected from the stress gradient and the split of the valence band. Nevertheless, there is not a significant difference between the two domain orientations, which is expected from the very small lattice mismatch between Ge and GaAs. The highest stress is observed at the boundary between the two domains, where the glide dislocations were generated. This is probably due to the overgrowth in one of the domains, that induces shear stress above the threshold for plastic deformation, see Fig. 12
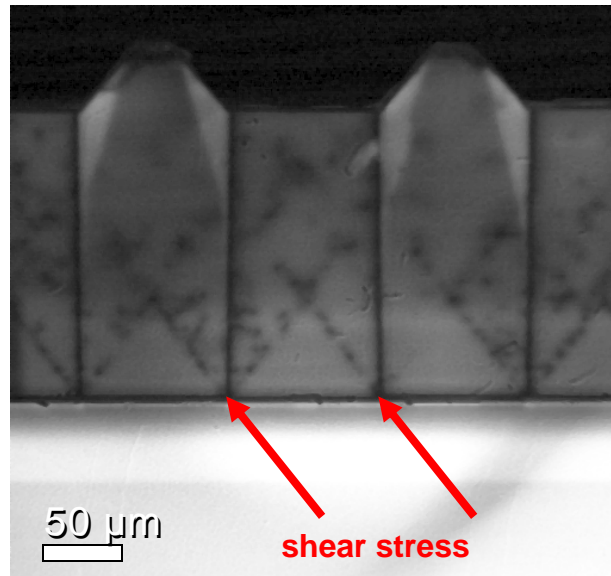
Fig.12.Panchromatic CL image, showing the corners between the two domain orientations, where dislocations are formed due to shear stress

4.5. *Influence of the growth conditions, residual free carrier concentration.*

Reference layers grown by HVPE (hydride vapor phase epitaxy) with different residual carrier concentrations were studied. The layers were grown using different HCl flows in the HVPE reactor. It is usually assumed that increasing the HCl flow inhibits the incorporation of Si from the walls of the reactor.

The sample properties, HCl flow, thickness and carrier concentration measured by Hall effect are presented in table I

sample	HCl (sccm)	Thickness (um)	type	Carrier conc (cm^{-3})
1/20/06	32	135	p	3.11E+13
3/3/06	38	135	p	1.14E+14
3/14/06	44	110	p	5.33E+14
3/17/06	0	112	n	6.13E+14

Table I. Properties of the different substrates used as probes for the influence of the chlorine flow on the luminescence spectrum.
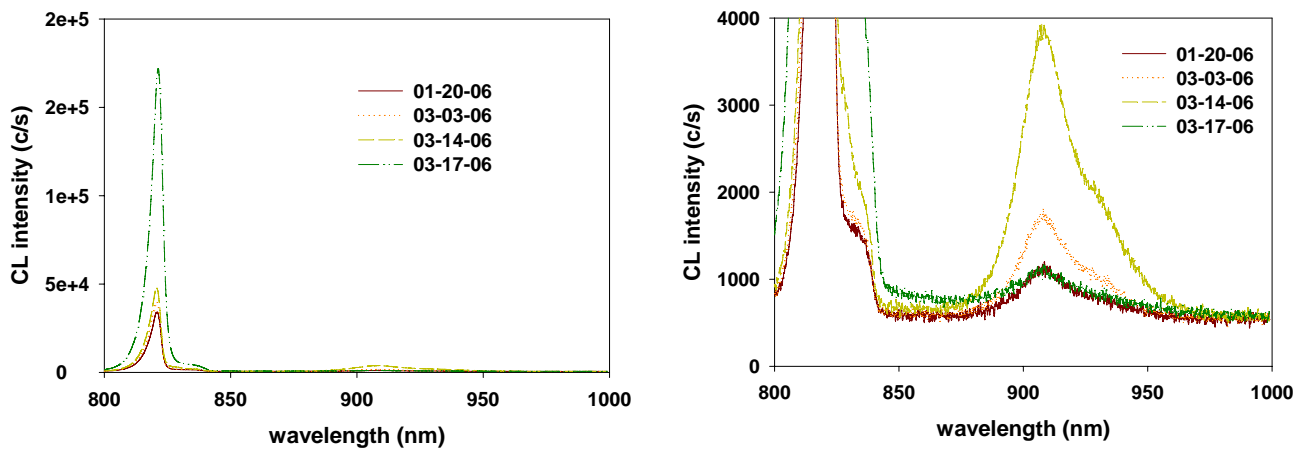

Fig.10.-*CL spectra of the reference samples described in table I*

The CL spectra of these samples are shown in Fig.10. There are two main spectral regions. The NBG (near band gap) region with the band to band trasition around 1.5 eV (820nm) and the extrinsic region, that presents two bands at 1.36 eV (910 nm) and 1.33 eV. These spectra are similar to those usually observed in the OP crystals. The defect related bands are usually related to complexes involving Ga vacancies.

The extrinsic bands are enhanced for increasing HCl flow; in particular, the intensity of the 1.36 eV increases with the hole concentration, see Fig. 11. These results suggest that the extrinsic bands are related to an acceptor level, in agreement with their relation to ga vacancy complexes. HCl is expected to inhibit the incorporation of Si, which should favor the formation of Ga vacancies; one could also assume that Si was incorporated in As position, however, this hypothesis is less reliable. Mobility measurements suggest that there is self-compensation, therefore, one can argue that Si_{As}-V_{As} are candidates to

be preferentially formed under increasing HCl flow. The role played by free carriers is very important since they are sources of light absorption, and therefore are detrimental to the light propagation in OPO crystals. These results show that the extrinsic band is a tester of the layer quality in terms of residual hole concentration.
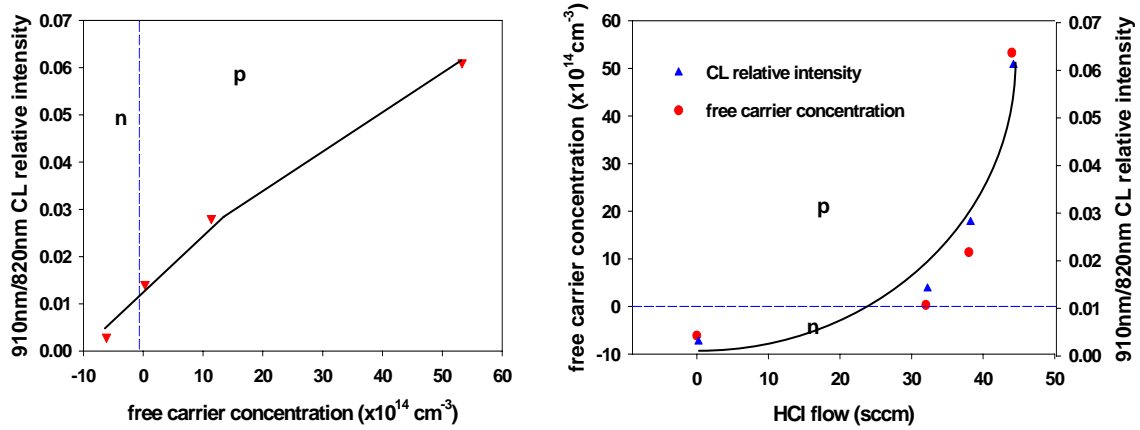
Fig.11. *a) Relative intensity of the extrinsic to the intrinsic bands vs the free carrier concentration. b) Free carrier concentration vs HCl flow and relative CL intensity of the extrinsic to the intrinsic bands vs the HCl flow. The lines are guides to the eye*

The OP crystals were studied by cathodoluminescence imaging. A CL image and the corresponding local spectra are shown in Fig.12. Clear differences related to the relative intensity of the extrinsic bands are observed among the different regions of the OP crystal. On the other hand, the extrinsic band is not equally distributed over the full OP crystal.

The two bottom interfaces are very similar, spectra 2 and 6. An additional band is observed around 1.39 eV, which the origin is, by instance, unknown; however, because it is observed at both interfaces one can rule out its relation with Ge impurities. This band is observed at the interfaces, and also at the growth interruption interfaces, which suggests that is introduced during the polishing step. Along the domain walls one observes dark contrast, due to the non-radiative recombination of the antibonds in GaAs. Also, some zones of the domain walls present an intense band peaking at 1.31-1.32 eV. This band is probably related to Ga antisites (P.W.Yu, D.W. Fischer, J. R Sizelove; Semicond. Sci.Technol. 7, 556 (1992)) which suggest Ga accumulation along

the domain walls; however, the non regular presence of this band along the domain walls requires additional studies.
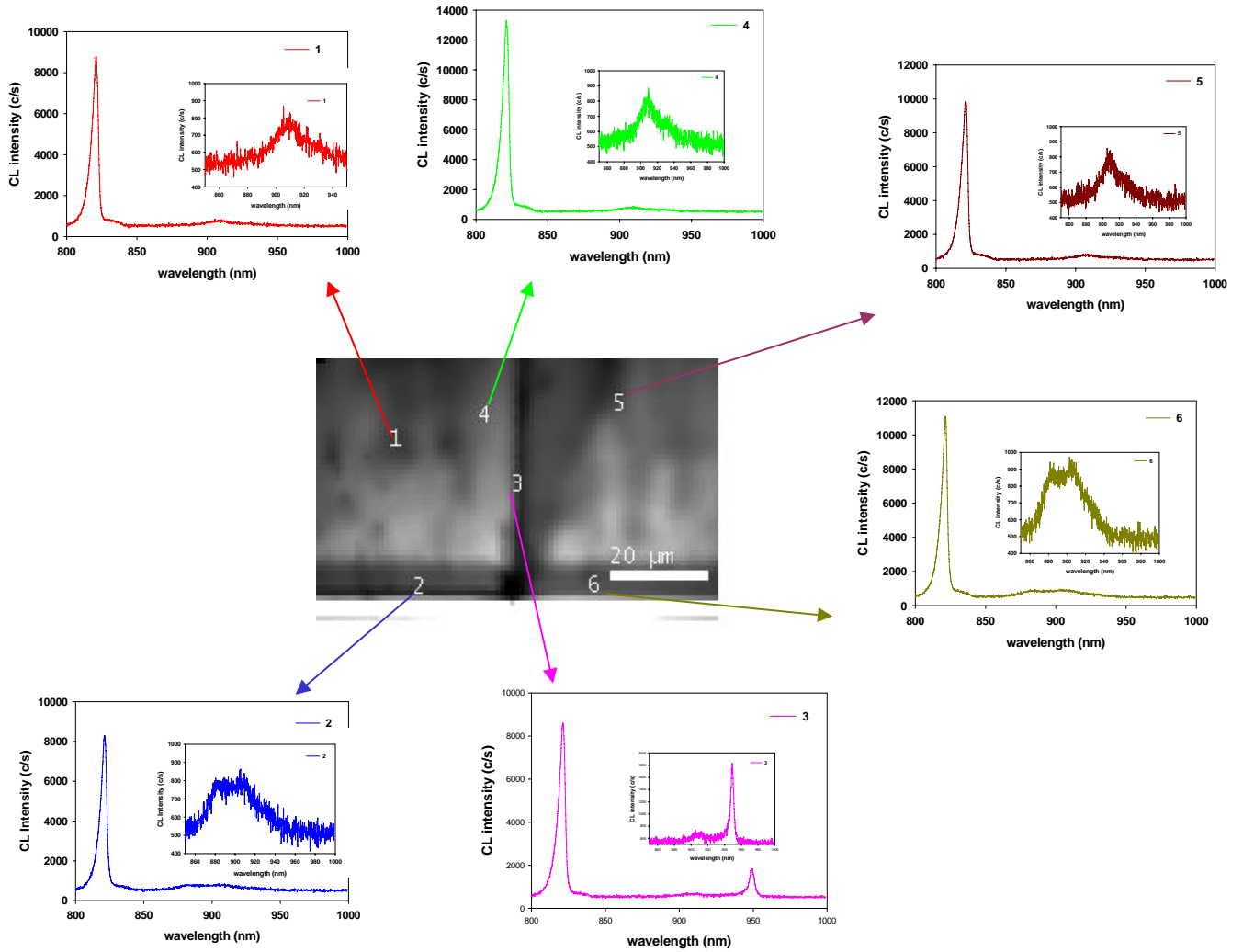

Fig.12. *CL image at the low part of the OP-crystal showing the different interfaces. Local spectra showing the main spectral features of the different regions are also shown*

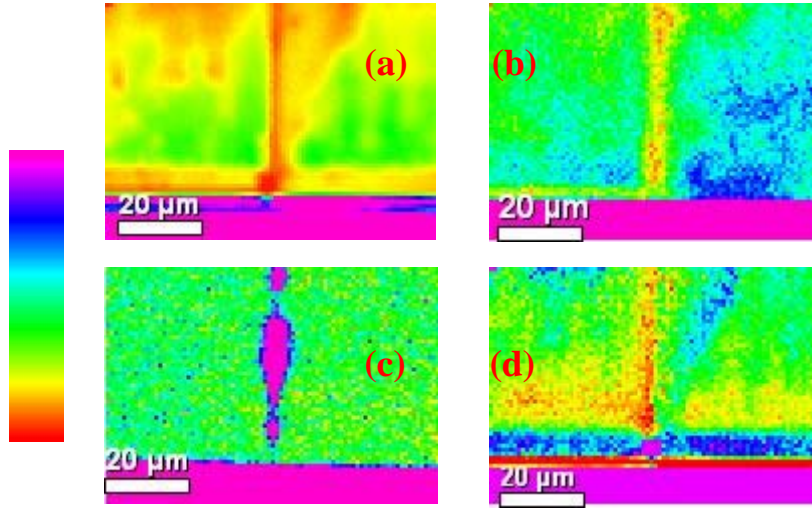Spectral images displaying the distribution of the different bands are shown in Fig.13.

Fig.13: *a) Monochromatic image (820 nm). b) Monochromatic image (910 nm), c) Monochromatic image (950 nm). d) Image displaying the relative intensity of the extrinsic band (910nm) respect to the intrinsic band (820 nm)*

One observes the non radiative activity of the domain walls and the lower interfaces in Fig. 13 a, the two domain orientations show a different incorporation of defects Fig.13d, giving different contrasts for the two domain orientations. The extrinsic band (910nm) is enhanced at the lower interfaces as revealed by Fig. 13d. However, this can be due to the presence of an additioanal band at 890 nm, which is observed at the interface with the substrate and also after growth interruptions. The 1.31 eV band is observed along the wall, Fig. 13c

Images of the full structure were also obtained. See the panchromatic image in Fig. 14a One appreciates the contrast between the two domains and the influence of the domain walls, which have a non radiative recombination activity. The defect related band (910 nm) band presents reversed contrast, respect to the 820nm band, see Fig. 14b. Also the dark area aroud the domain walls is broadened for the extrinsic band, which means that the domain walls are gathering the defects responsible of the 910 nm emission. The

relative intensity of the two bands along the two domain orientations is shown in Fig. 15. One observes the importance of the growth interruptions in the residual defects.
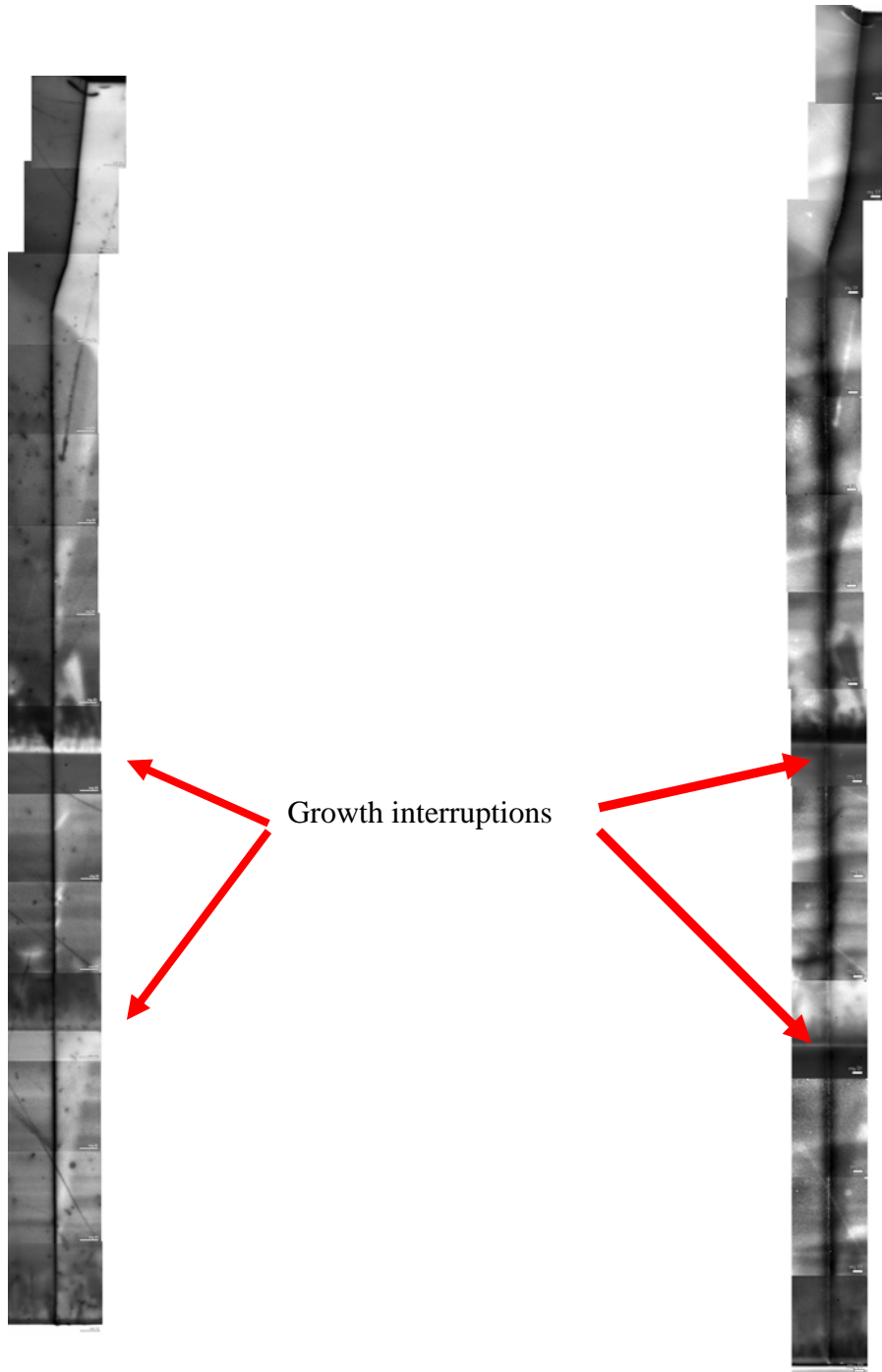

Growth interruptions

Fig.14. *a)Panchromatic CL image along the full thickness of theOP crystal, b) relative intensity of the extrinsic (910nm) to the intrinsic (820nm) band*
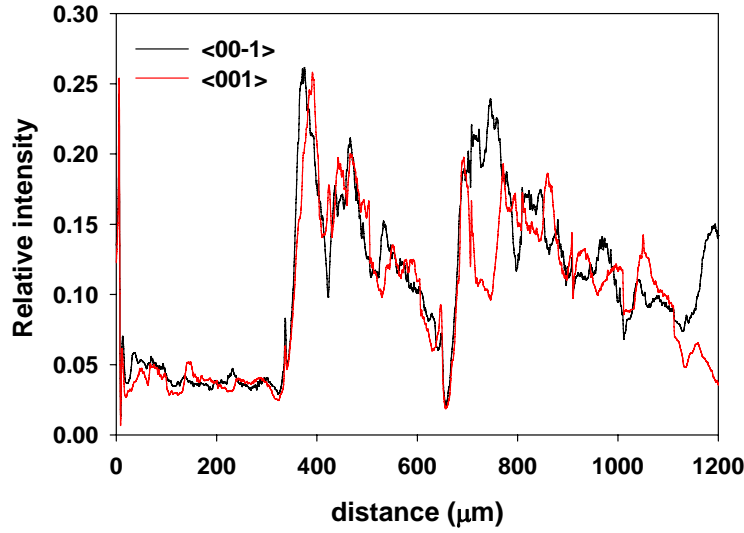
Fig.15. *Relative intensity of the extrinsic band (910 nm) respect the intrinsic band (820nm), along the two domain orientations. The two abrupt discontinuities correspond to the growth interruptions. The growth interruptions increase the presence of complex defects and then slowly decrease. The tendency is similar for the two domain orientations.*

4.6. *Domain walls*

The domain walls are dark for both monochromatic images (822 nm and 910 nm), this means that the CL contrast is governed by the non-radiative recombination activity of the domain walls. However, if one looks in detail the two images, one observes that the distribution around the domain wall is not equivalent for the two images. In fact, the dark area around the walls is more expanded for the 910 nm emission. The monochromatic images, the relative intensity image and the peak wavelength images are shown in Fig.16.

See the transverse profiles of Fig. 17. The intensities of the two bands show different distribution around the wall, while the distribution out of the wall zone is similar for both domains, suggesting that the luminescence intensity in both domains is mostly determined by the incorporation of non-radiative recombination centers. Around the walls the region depleted is broadened for the defect related band (910nm), respect to the intrinsic emission (822 nm). This is better observed in the images corresponding to the relative intensity of the two emissions. In these images there are two important observations; first, there is a relative intensity increase of the 910 nm band along the wall, which suggests that there is a capture of the defects responsible for this band at the domain wall; therefore, the surrounding area appears depleted of these defects, which confirms the attraction of the defects by the compressive strain field around the domain
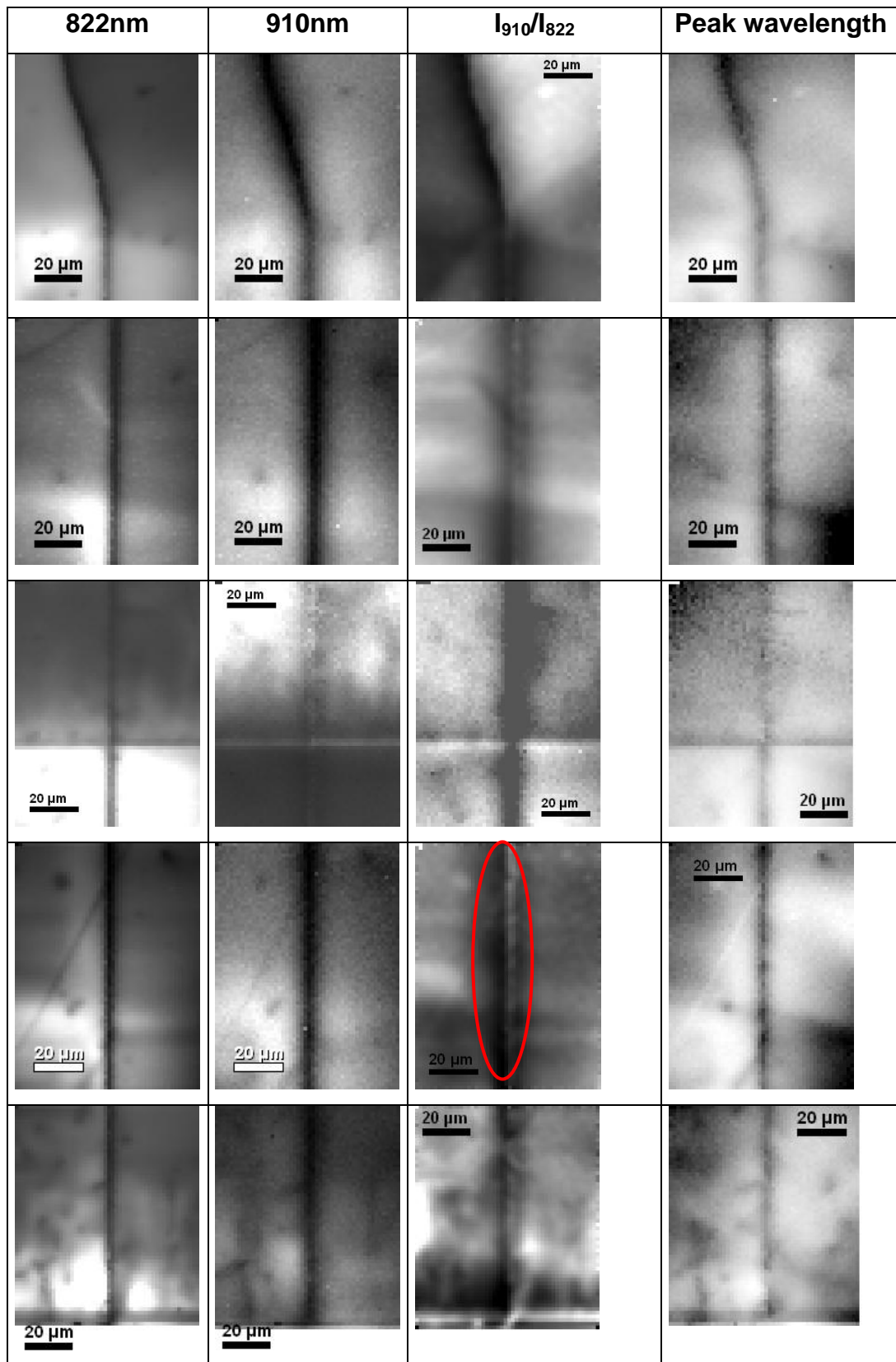
Fig16 . *Monochromatic images at 822 nm and 910 nm respectively. Relative intensity of the 910 nm band to the 822 nm band. Distribution of the peak wavelength of the 822 nm band, which can be related to strain distribution*

wall, see also the corresponding profile in Fig.17, where one observes the enhancement of the relative intensity of the 910 nm band localized along the domain wall. The strain distribution is observed in the peak wavelength images; along the domain wall there is a shift to the low wavelength, which accounts for a compressive stress; see the profile in Fig. 17. Note that in this sample the wall strain is compressive, contrarily to the tensile strain of the sample of Figs, 6 and 7.

In fig.18 the profiles of Fig.17, are compared, the monochromatic CL intensity, both 822nm and 910nm, and their relative intensity are compared with the stress distribution (peak wavelength). One observes a good agreement between the distribution of the 910 nm band and the strain field, which suggests that the distribution of acceptor like defect complexes is governed by the strain field of the domain wall; furthermore, see the coincidence between the small peak in the relative intensity profile and the dip in the peak wavelength distribution, the accumulation of the complex defects is mostly
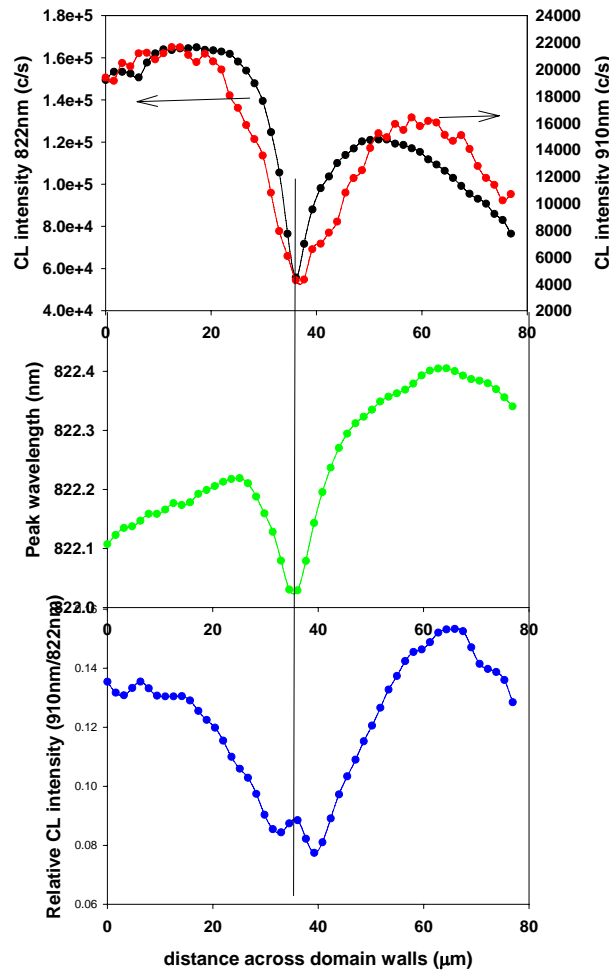
Fig.17. *Profiles obtained along lines crossing the domain wall of the 822 nm and 910 nm band intensities, the relative intensity of both bands and the peak wavelength*

achieved for the maximum stress, see the encircled region in the lower profile of Fig.18
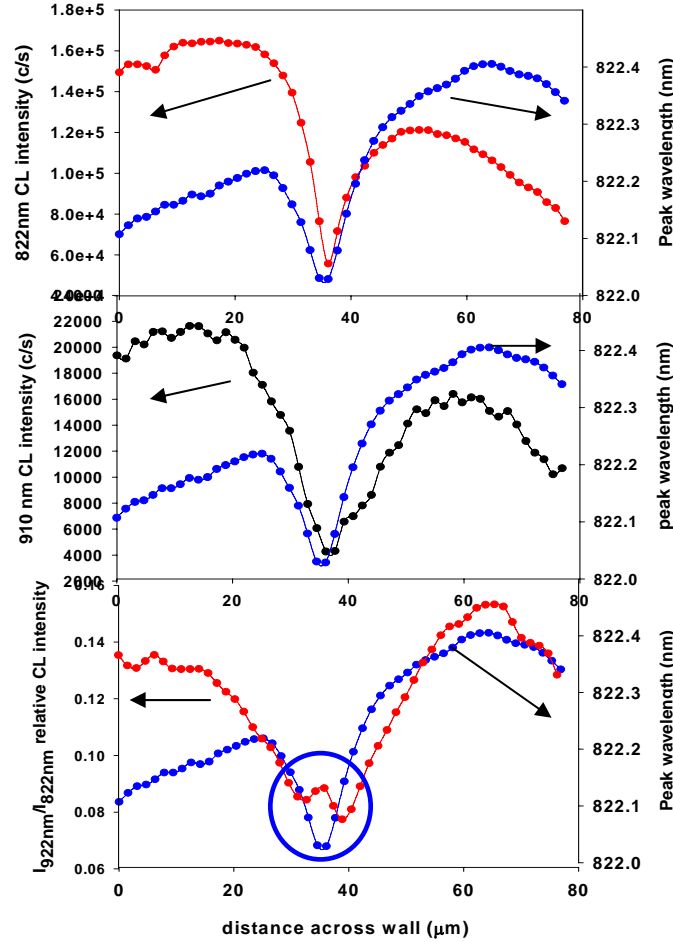

Fig.18. *Comparative profiles of the 822 nm and 910 nm band intensities, the relative intensity of both bands with the peak wavelength (stress)*

One of the main issues concerns the non uniformity of the CL signal along the domain walls. The relative intensity and peak wavelength distributions along the domain wall are shown in Fig.19. One observes that the relative intensity of the two bands and the peak wavelength are roughly anticorrelated, revealing a higher presence of complex defects responsible for the 910 nm band in the regions where the compression is higher. This suggests that the higher the compression the higher the gathering of defects, or that the inhomogeneous stress distribution along the domain wall can be determined by the the defect clustering.
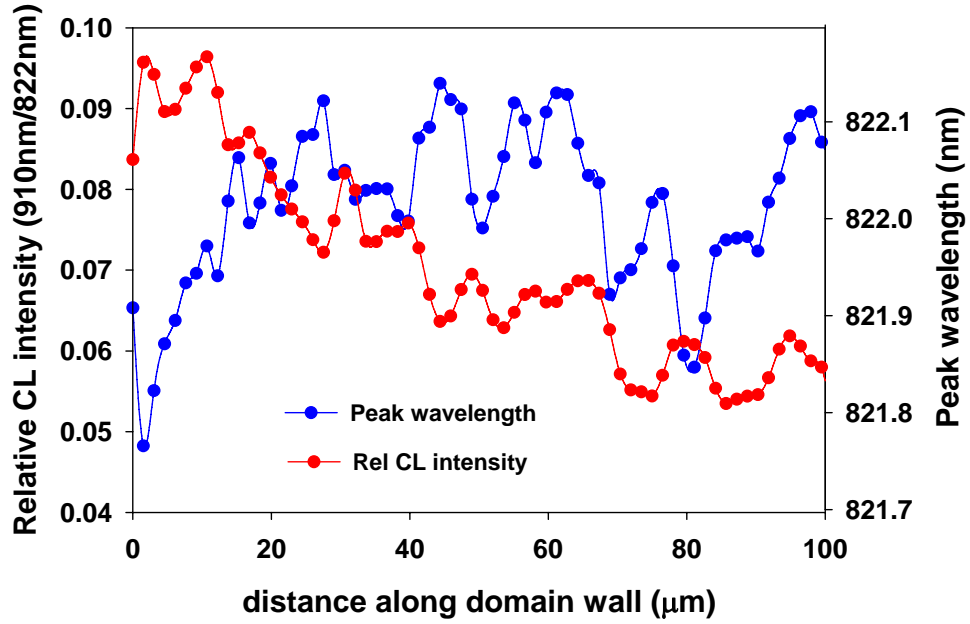
Fig.19. *Profiles along the domain wall of the relative intensity of the 910 nm band and the peak wavelength of the 820 nm band*

Finally, clear contrast between the two domain orientations is observed at the end of the OP crystal where the walls bend, see Figure 16, top images. One observes that the (00-1) domain (right domain) is darker and that the relative intensity of the 910nm band to the 822 nm band is increased. These images suggest that defects, both Ga vacancies related complexes and non radiative defects (usually As_{Ga} related) are formed in a higher amount in the (00-1), which is accentuated in this part of the crystal, it shows a tendency to increase along the domains. This accumulation of defects could account for the non conservation of the domain geometry for long growth times.

A tentative scenario of the domain walls is shown in Fig.20. The green dots are the complex defects responsible for the 910 nm emission, under the strain field of the domain wall, they are gathered, leaving a depleted area at both sides of the domain wall, this depletion is responsible for the profile of the 910 nm emission, which is highlighted using its relative intensity respect to the 822 nm band, its distribution is represented by the red curve and fits reasonably the strain distribution represented by the peak wavelength distribution, blue line. The distribution of the 822 nm emission, green line, is determined by the non radiative recombination, which mostly occurs at the domain walls, therefore, this profile does not fit the strain field.
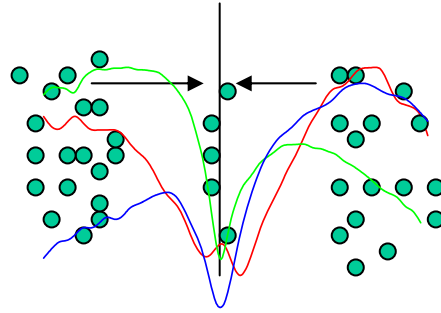
Fig.20. *Scheme of the structure of the domain wall and surrounding areas*

4.7. CL study of annealed OP-GaAs crystals

First, one should discuss the main aspects of the CL spectra of these structures. The spectra recorded are typical of undoped GaAs, with a near band gap (NBG) emission consisting of an excitonic transition (821 nm) and a band to band recombination emission (818nm). An additional shoulder at 836 nm is also observed, this band has been associated with an e-A° transition, with C_{As} as the acceptor; also this band was associated with As vacancies (APL 19, 143 (1971)). Another band is observed at 908 nm with a shoulder at 928 nm. This band has been largely reported in the literature, being only observed in undoped GaAs, and associated with Ga vacancies (K.C. Shin et al; J. Appl. Phys.65, 736 (1989)). The low energy band at 928 nm could be a phonon replica of the 907 nm band, since its intensity ratio remains almost constant and the energy separation between both bands is around 33 meV, which is very close to the 36 meV of the LO phonon in GaAs. Finally, a band peaking at 950 nm is discontinuosly observed at the domain walls, generally, in the regions close to the seeds. This band can be associated with Ga_{As} point defects (S.G.Bishop; J.Appl. Phys. 56, 1785 (1984)), which are double acceptors, in particular, this emission should correspond to the e-Ga_{As}^{0}/Ga_{As}^{-} transition, the e-Ga_{As}^{0}/Ga_{As}^{-} emission is not observable at 80 K. These samples present a very low intensity 910 nm band, respect to other samples previously studied.

The CL image contrast is mainly controlled by the distribution of the deep levels. The domain walls give a dark contrast; however, the luminescence is not fully quenched, which suggests that the As-As and Ga-Ga antibonds are partially inhibited, since they are recognized as active non radiative recombination centers; as an example the luminescence intensity in GaAs layers grown on Ge with antiphase boundaries (APBs) is quenched by almost 4 orders of magnitude, respect to the corresponding emission in samples without APBs (G. Brammertz; J. Appl. Phys. 99, 093514 (2006)). This suggests that the domain walls are not true APBs, probably, with defects inhibiting the antibonds. The gettering of defects by the domain walls supports this idea. In particular, either Ga_{As} or V_{Ga} defects are found to getter around the domain walls in selected regions.

The OP-GaAs layers must be thick, (>500µm), which demands long growth runs, with the result that their composition in terms of the CL signature evolves along the growth run, showing non homogeneous distribution along the growth axis. This is due to the effective change of the growth parameters during the growth run, because of the parasitic nucleation. This non-homogeneity, makes difficult the comparison between different crystals. See the low resolution panchromatic CL images of the as-grown and annealed samples, Figs. 21-22
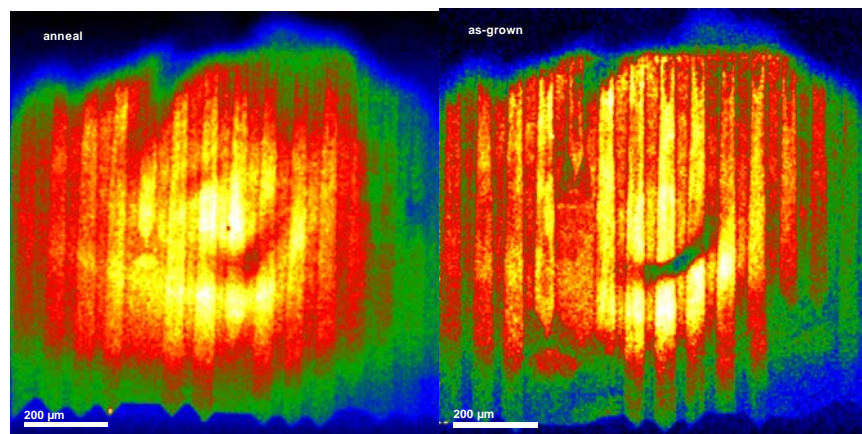
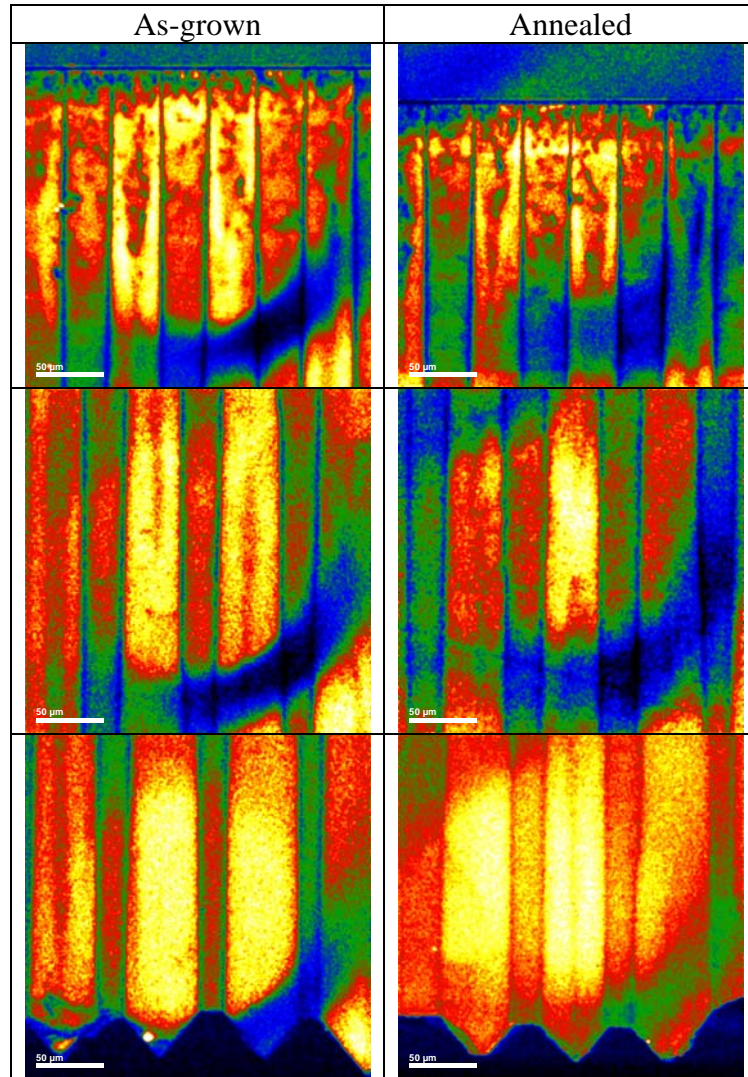*Fig.21. Low resolution panchromatic CL images*

Fig.22. Panchromatic CL images of the three sectors, lower, mid and upper (from top to bottom)

Here, we present a study of as-grown and annealed OP-GaAs crystals. One can find in the literature of undoped GaAs a number of annealing studies. The luminescence emission depends on the annealing conditions; in particular, it is determined by the temperature, atmosphere, and the capping layer, which does not concern this study. Depending on the annealing conditions the changes affect in a different way the two sublattices. Also one should expect differences in the annealing result for different regions of the crystals depending on the background defect content of the as-grown samples; which is not homogeneous along the growth axis because of the reasons exposed above.

In the case of OP-crystals, one should also study the role of the domain walls, in the redistribution/ formation of point defects, in fact one could a priori expect that the

domain walls are sinks for out-diffusing defects . Hall measurements evidenced a net increase of p-type carriers, after annealing. In the case of p-type layers there was an increase of the free hole concentration, and in the n-type layers a conversion from n to p was recorded. This behaviour points either, to shallow acceptor generation, or donor annealing; both effects would balance the compensation ratio towards the p-type. Another interesting observation is the decrease of the mobility, which points to an increase of scattering centers, which in principle should point to the generation of acceptors.

The CL study of the annealed samples should provide some insight about these points. We have studied different regions of the two samples. We have selected three regions, lower, close to the seed, mid and upper, close to the end of the OP-GaAs laye, see Fig.22. We will try to compare the results obtained in the three regions indicated in Fig. 22. for as-grown and annealed samples. As mentioned above this comparison is not easy because of the lack of homogeneity; nevertheless we will establish some remarkable differences between the two samples.

First, panchromatic CL images were acquired, Figs.21-22. They show the typical contrast between the two domain orientations, which reveals the distribution of the deep levels, which are incorporated in a higher concentration in the <001> domains. Possible candidates for those deep levels are As antisites, As_{Ga}, and/or residual oxygen impurities; both are deep donors, acting as compensators of the shallow acceptors:

$N_{DD}+N_D > N_A+N_{DA}$ n-type

$N_{DD}+N_D < N_A+N_{DA}$ p-type

One should note that the Hall data after annealing point to a situation where N_A/N_D ratio increases. First we will present the results for the different regions.

Lower region, close to the seed
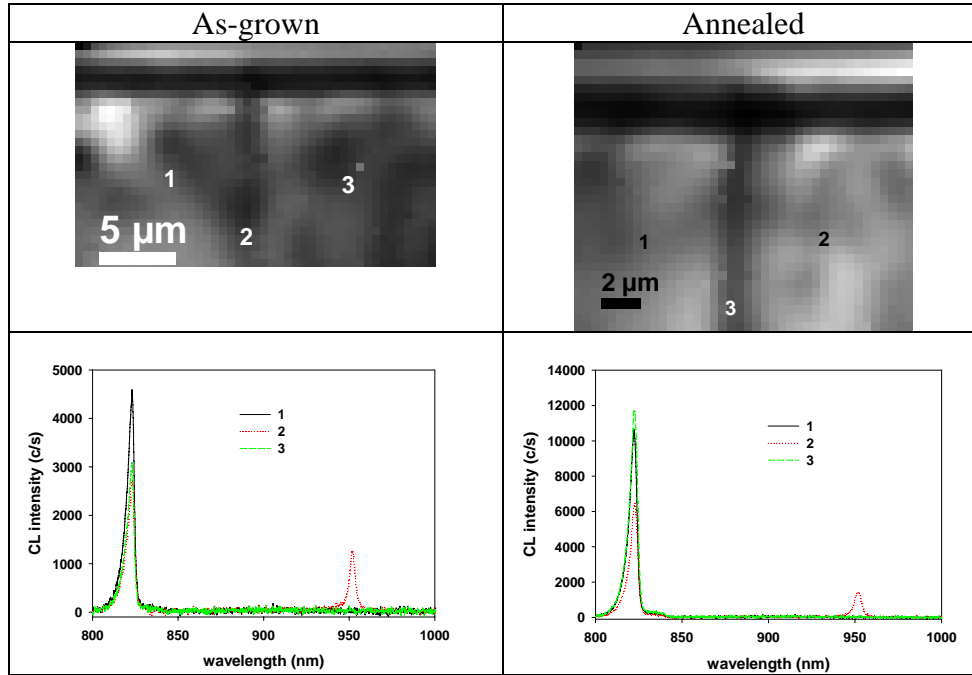

As-grown	Annealed

Fig.23. CL images of the lower regions ofas-grown and annealed samples. Also the corresponfing CL spectra at different points (1:(001), 2:(00-1) and 3: wall)

The difference observed in the incorporation of defects between the two domains, is probably associated with the different growth planes for the two crystal orientations. Normally one observes a darker contrast for the (001) domains, which points to a higher incorporation rate of deep levels in this orientation. If one admits that the main deep levels are As_{Ga} related defects one can deduce that the incorporation rate of As is higher in (001) domains.

The contrast of the CL images, and, therefore, the concentration of deep levels, evolves along the domains, as a consequence of the effective change in the growth gas flows due to the influence of the parasitic nucleation inside the reactor. This variation is not only monitored by the contrast, but also by the different emission bands present in the spectrum at different zones of the OP-GaAs layer.

In the lower region, close to the seed the CL spectrum presents the near band edge (NBE) emission in both domain orientations, and the defect related band peaking at 950 nm, discontinuously observed along the domain wall. On the other hand, the V_{Ga} related bands, 908 nm and 927 nm, are not observed in this region independently of the

domain orientation. This together with the observation of the 950 nm band, points to a relatively high incorporation of Ga along the domain walls.. The CL images reveal the presence of "dark" clusters, see Fig.23 , which seem to correspond to decorated extended defects. Due to the presence of these defects is difficult to establish significant differences between the two domain orientations in this region as compared to the results that will be presented for the other regions of the OP. crystal.

The peak wavelength is roughly correlated to the NBE emission distribution. Roughly, these images reproduce the role of the interface and the extended defects in the distribution of the point defects; this is well observed in the 3-D plots of Fig.24. After annealing, one observes an increase of the CL intensity, while the V_{Ga} related band still remains absent. On the other hand the CL parameters after annealing present a smoother distribution. See the images in Fig.24, where the 3D images are shown for the two samples, as-grown and annealed, in the same expansion scale, for both the intensity and the peak wavelength.

The peak wavelength shifts to the low energy, which is opposite to the behaviour observed in the other regions of the OP-crystal.

As-grown	Annealed	
		Amplitude NBE
		Peak wavelength NBE
		Amplitude band 950 nm

		Amplitude NBE
		Peak wavelength NBE
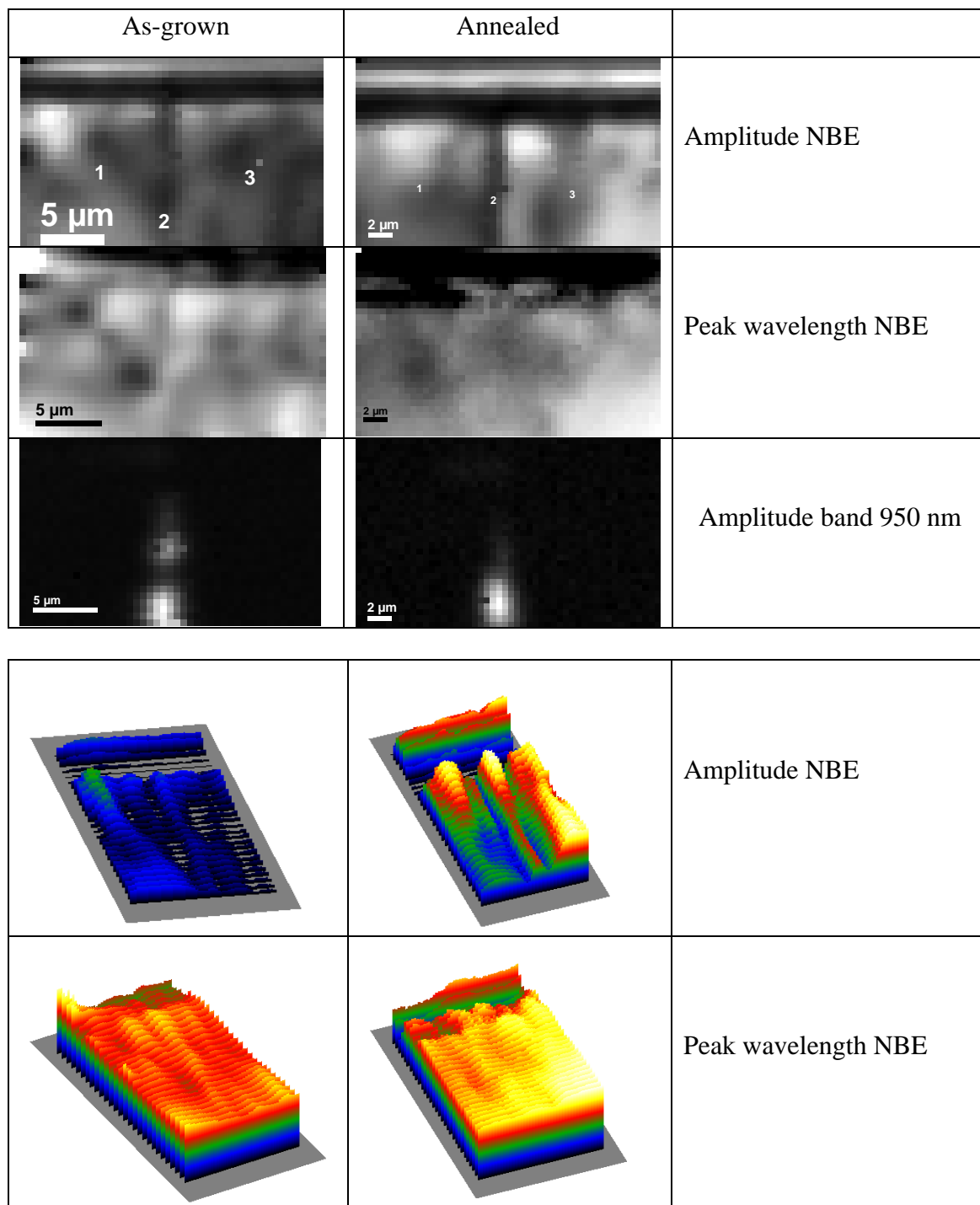
Fig.24. Images of the different spectral parameters of the lower rgion of the two samples. The 3-D plots are reported to the same scale expansion for both crystals, showing the higher CL intensity after annealing and the peak wavelength shift to the low enrgy.

Mid and upper regions

The results obtained in mid and upper regions of the crystals present differences with the lower region, which was strongly influenced by the existence of the extended defects, which are not present in the other regions. In these regions the two domains appear homogeneous, free of extended defects. Fig. 25.
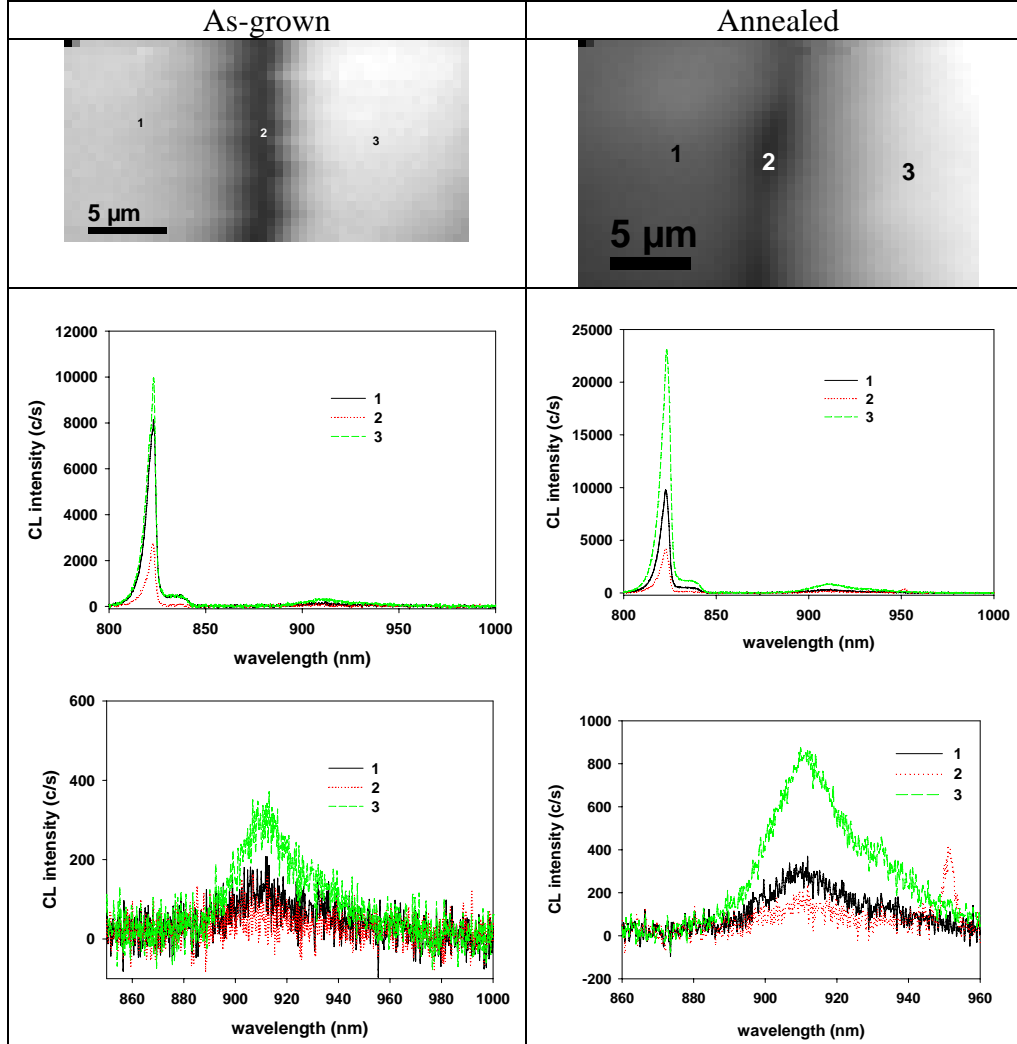
Fig.25: CL images of the as-grown and annealed mid regions. The spectra obtained at the two domains and the wall are also shown

In the mid region of the crystal, the as-grown sample does not exhibit the 950 nm band along the domain wall. On the other hand, the 910 nm band is practically absent in the (001) domain and peaks up in the (00-1) domains. This change evidences the evolution of the layers during the growth run. The relative intensity (I_{910}/I_{820}) image shows a partial increase of the 910 nm band along the domain wall. On the other hand, the stress distribution, proportional to the peak wavelength shift of the NBE band, corresponds to the compression around the domain walls, usually observed in the

different samples studied, Fig.26. The clustering distribution observed close to the seeds in the lower region is anymore observed.
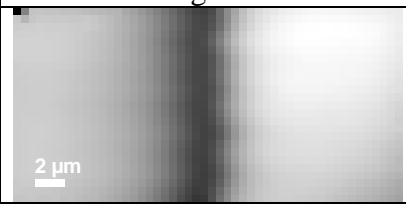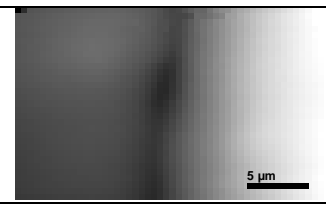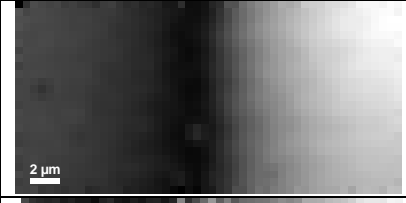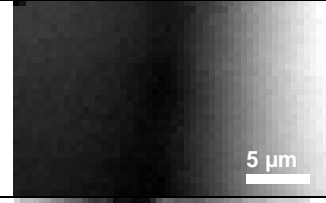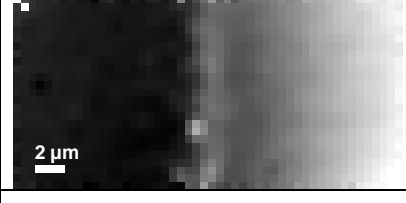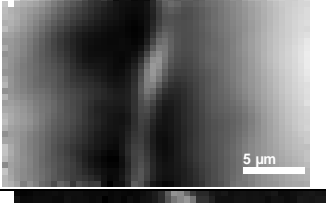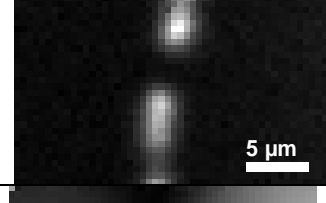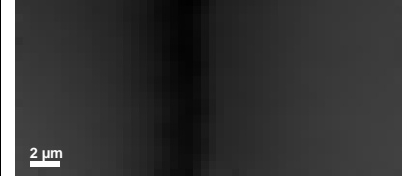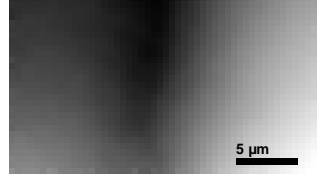
As-grown	Annealed	
		Amplitude NBE
		Amplitude 910 nm
		Relative amplitude 910/NBE
No 950 nm band		Amplitude 950 nm
		Peak wavelength

Fig.26. Images of the different spectral parameters in the as-grown and the annealed samples in the mid region.

The annealing has several consequences. The NBE luminescence is enhanced, specially, in the (00-1) domains. The annealing does not introduce new luminescence bands, which means that no new defects are generated, and, in particular, the hypothesis of new shallow acceptor levels is not supported. Therefore, the main effect of the annealing seems to be the removal of deep levels, which results in the overall increase of the luminescence emission.

The 950 nm is observed in the annealed sample along the domain wall, revealing anticorrelation with the 910 nm band; see the relative amplitude 910/NBE, and the amplitude 950 nm, images in Fig.26, note the anticorrelation along the domain wall among the two bands. This anticorrelation is consistent with the opposed nature of the

defects responsible for these emissions, V_{Ga} for 910 nm band, and Ga_{As} for the 950 nm band, showing the stoichiometry conflict.

The 910nm band follows similar trends to the NBE, which suggests that the main evolution during annealing concerns the deep levels. It should be noted that the main changes occur in the (00-1) domain, where the concentration of V_{Ga} related defects seems to be higher. The diffusion of As_{Ga} antisite defects, deep donor levels, needs V_{Ga}, according to this, one should expect a higher luminescence increase in the regions with higher content of V_{Ga}, as apparently occurs.

Another interesting point concerns the peak wavelength of the NBE emission. This wavelength shifts to the short wavelengths in annealed samples. If one considers that the As_{Ga} defects expand the GaAs lattice, the annealing of those defects should shift the NBE band towards the short wavelength. However, the difference between the two domain orientations, with a larger shift to the blue for the (001) domain is contradictory with the hypothesis of a shorter lattice parameter in annealed samples because of the annealing of the As_{Ga} defects. Though a reduction of the As_{Ga} defects can contribute to the blue shift of the luminescence peak, other factors must also influence the blue shift.

Horizontal profiles across the images are shown in Fig.27, in these profiles one can appreciate the magnitude of the different spectral variations.
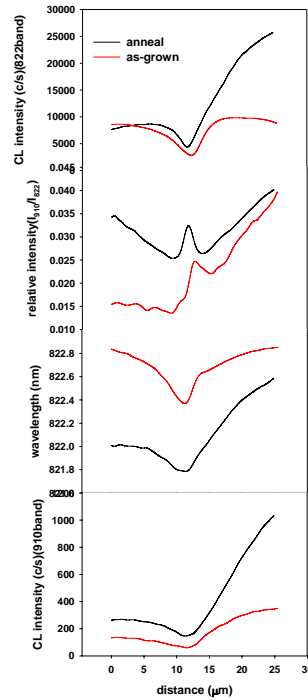

Fig.27. Profiles along a line crossing transversally the images of Fig. 26

The behaviour is very similar in the upper region of the OP-GaAs layer, see Fig.28. The comments made for the mid region could apply for the upper region. The only difference is the absence of the 950 nm band in the annealed sample, all the other observations are very similar and confirm the results of the mid region
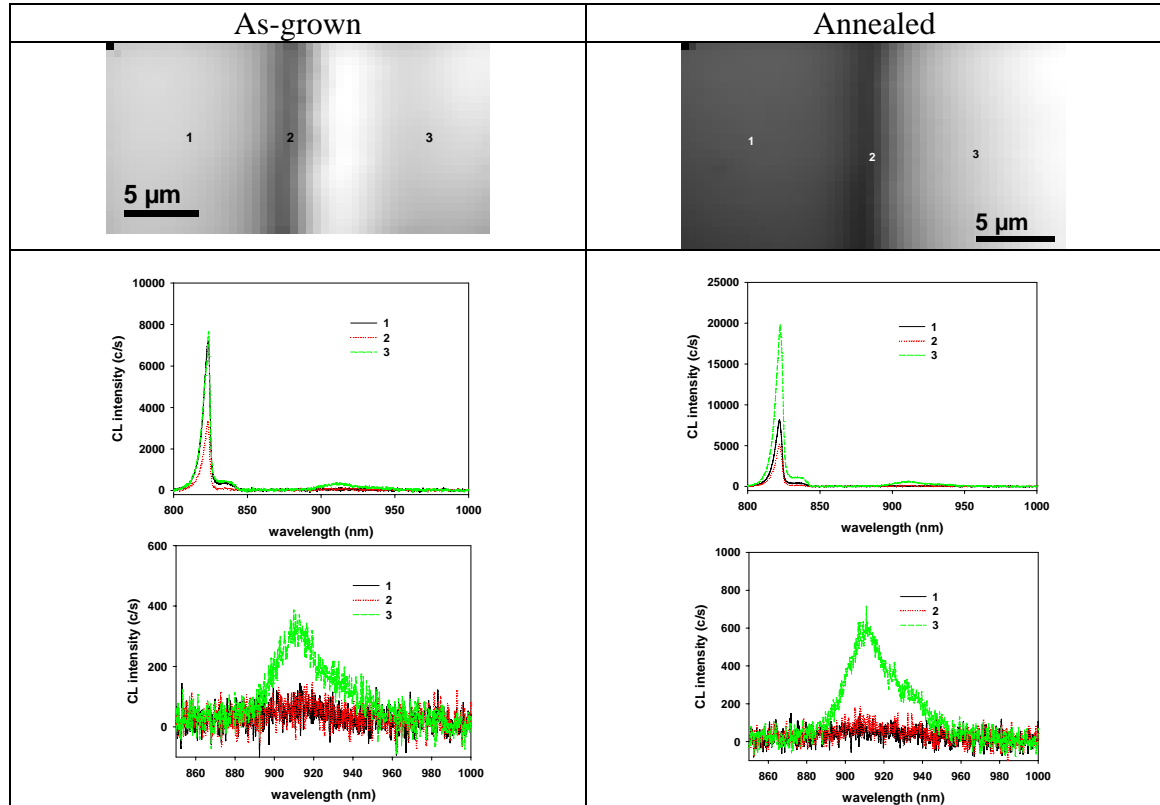

Fig.28: CL images of the as-grown and annealed upper region. The spectra obtained at the two domains and the wall are also shown

The spectral images representing the distribution of the main spectral parameters are shown in Fig.29. There one can appreciate that the results are basically the same as those obtained in the mid region; in particular, the annealed samples respect to the as-grown samples present the following features:

Increase of the luminescence efficiency, specially in the (00-1) domain.

Increase of the 910 nm band.

Accumulation of V_{Ga} defects at the domain wall

Blueshift of the peak wavelength

Smoothing of the compressive stress at the domain wall

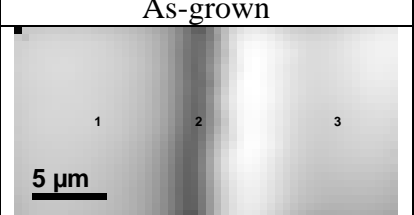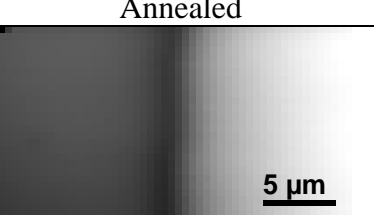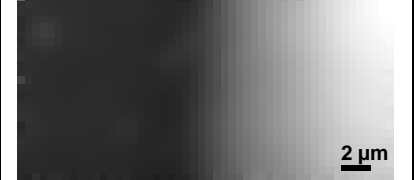These results are summarized in Figs.29 and 30.
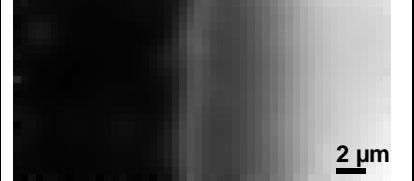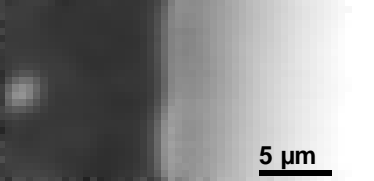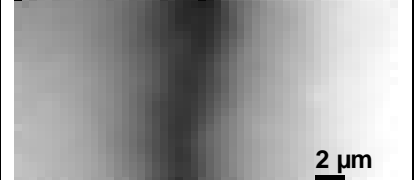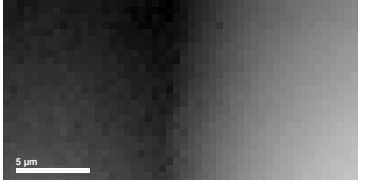
As-grown	Annealed	
		Amplitude NBE
		Amplitude 910 nm
		Relative amplitude 910/NBE
		Peak wavelength

Fig.29. . *Images of the different spectral parameters in the as-grown and the annealed samples in the upper region.*
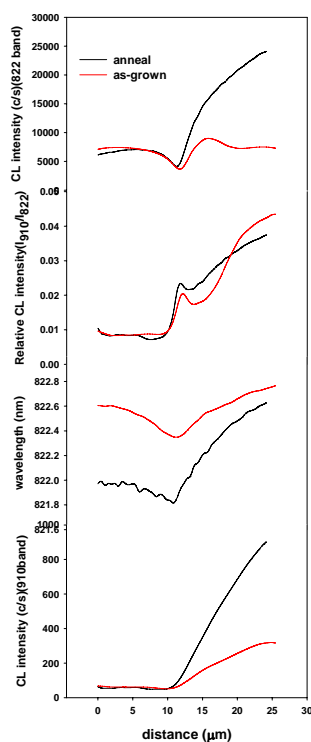

Fig.30. *Profiles along a line crossing transversally the images of Fig. 29*

The effect of the annealing consist of the removal of deep levels, this effect seem to demand a higher presence of V_{Ga} defects. The candidates for deep levels are As_{Ga}-type defects, which are deep donors balancing the compensation ratio towards the p-type. The decrease of the mobility observed in Hall measurements of annealed samples respect to the as-grown samples, suggest the formation of scattering centers, which could be associated with the increase of V_{Ga} defects. Also the decrease of the lattice parameter could account for such a decrease. Further studies are necessary, anneals in different atmospheres, and the use of dielectric cappings could help to understand the role of the different native defects in the properties of the OP-GaAs crystal.

5. Cathodoluminescence of Ti-sapphire samples

The CL spectra of the two samples present two main bands in coincidence with the literature. These bands are a blue band (BB) and a red band (RB). They are presumably composed of more than one transition, which should explain the broad lineshape, and the relative shifts of the peaks depending on the samples and the part of the sample studied. In general the luminescence intensity is weak.

The two samples, labelled 6.3 and 7.4, present differences between them concerning the intensity of their emissions, but also the spectral shape.

Sample 7.4 presents a significantly stronger emission than sample 6.3.

This can be due to two possible causes, differences in the concentration of Ti or more concentration of Fe in sample 6.3, since Fe^{2+} ions are assumed to be non radiative
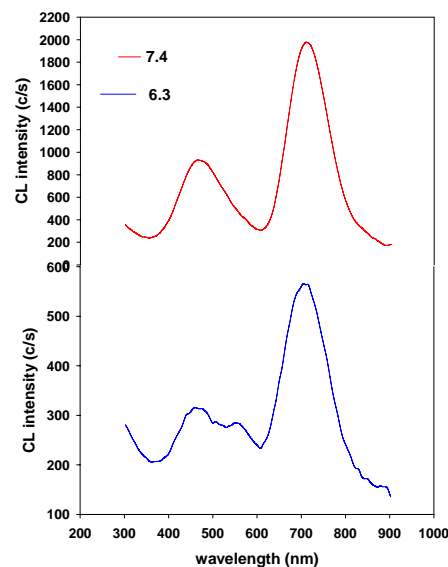

Fig.1. Low temperature CL spectra

recombination centers.Typical spectra of the two samples are shown in Fig.1. A table with the main spectral parameters is also supplied.

Sample 6.3 exhibits a band in the low energy tail of the BB, this band is centered around 560 nm, and we label it the green band, GB. GB is not resolved in sample 7.4, but it is probably masked by the BB band, because one observes an incipient shoulder in the 7.4 spectrum, which suggests that it is due to a point defect present in both samples, but in a higher amount in samples 6.3. The GB has been associated also with oxygen Ti complexes quite similar to those reported for the BB.

sample7.4	band	peak wavelength (nm)	FWHM (nm)	Integrated intensity
	UVB	300.2	46.2	4362
	BB	470	102.8	66375
	RB	715.6	93.3	140748

sample6.3	band	peak wavelength (nm)	FWHM (nm)	Integrated intensity
	UVB	297	65.5	1255
	BB	467.2	85.6	7620
	GB	560.7	54.2	3443
	RB	703.4	90.9	20867
	RB2	752.4	116	5129

TableI

Both the BB and the RB are associated with internal transitions of Ti.
The blue band has been associated with a charge transfer transition involving the Ti(IV) ion of the $[Ti(IV)O_6]^{8-}$ complex. The RB has been associated with the $^2E \rightarrow {}^2T_2$ of Ti^{3+} ions. Nevertheless, several levels could contribute to the RB. See the RB spectra obtained at different regions of the samples, showing evident spectral changes for the
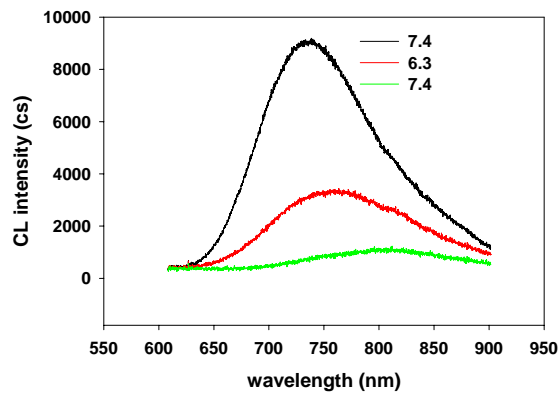

Fig.2. RB spectra showing its complex behaviour

RB, which suggests the existence of at least two transitions, which the balance determines the peak wavelength and the lineshape of the broad RB, Fig.2.

It should be mentioned that the narrow band peaking at 694 nm, usually observed in sapphire is not resolved in these samples. This band has been related to the $^2E \rightarrow {}^4A_2$ transitions of Cr^{3+} ions. This suggests that these samples have a low content of Cr

Finally, an additional band is observed in the UV spectral range, peaking around 300 nm. I have not found references for this band, Fig.3.
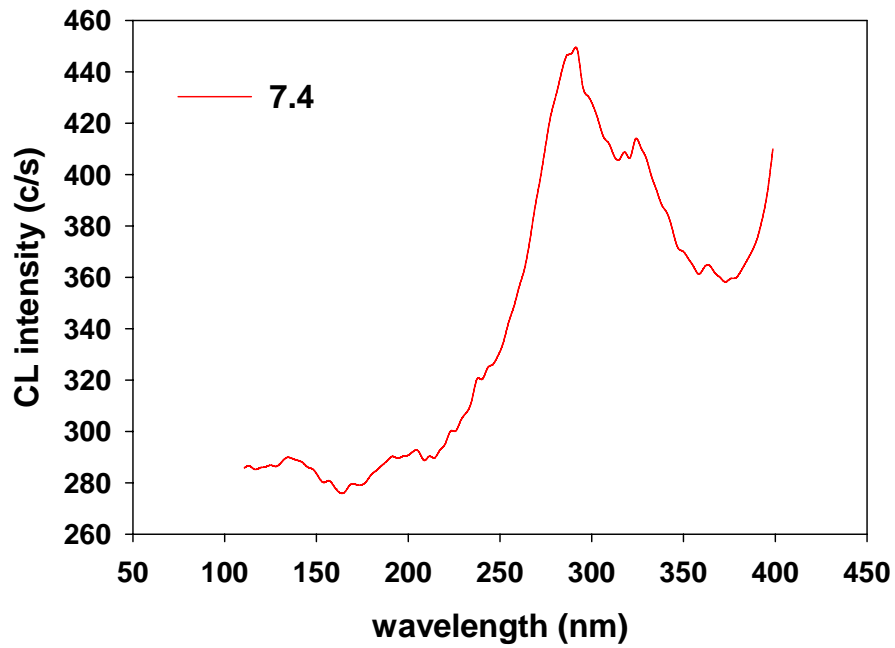

Fig.3. UV-band

Depth analysis.

The spectra were acquired with different acceleration voltages of the e-beam. The penetration depth of the e-beam probe depends on the acceleration voltage according to the empiric relation:

$$R = (0.052/\rho)\, E_{beam}^{1.75} \qquad\qquad (1)$$

Where R is the primary electron range in μm, r is the material density (g/cm^3) and E $_{beam}$ Is the electron energy in keV.

The primary electron range is taken in a first approach as the probe depth.

The panchromatic CL images of the regions where the two samples were studied are shown in Fig4. There are two regions with different contrast, the spectra were acquired in the green framed region. The e-beam energy was varied from 5 keV to 20 keV, which according to (1) correspond to probe depths ranging from 0.16 to 1.89 µm. Which are relevant to the SIMS profiles. The main CL bands are the blue band (BB), the green band (GB) and the red band (RB)
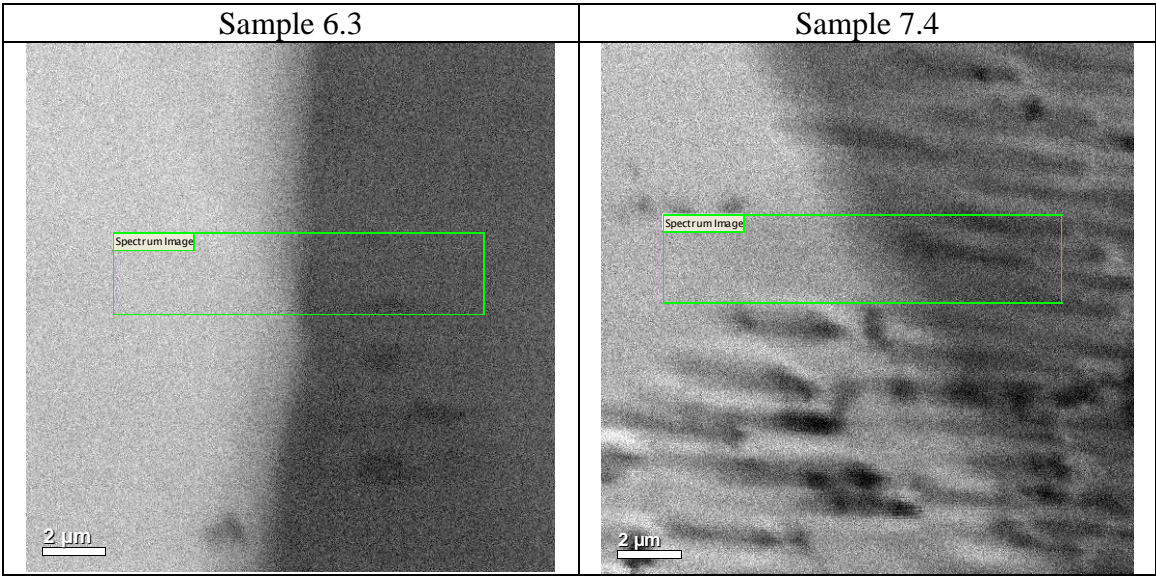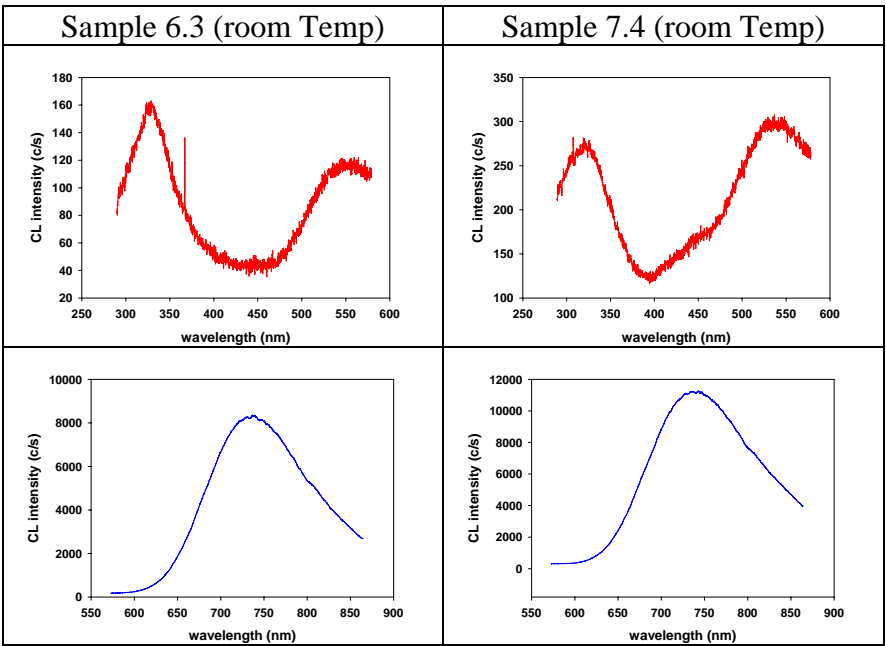

Fig. 4. PanCL images

Fig.5. CL spectra of the two samples at room temperature

Typical spectra are shown in Fig. 5. Note that in these spectra the UV band peaks up, and the BB is better observed in the 7.4 sample. The green band is shifted respect to the previous measurements, which were done with the photomultiplier (PMT).

The intensities of the RB for the two samples as a function of the probe depth are represented in Fig.6

Fig.6.Depth profiles of the RB in the two samples and the two sectors measured
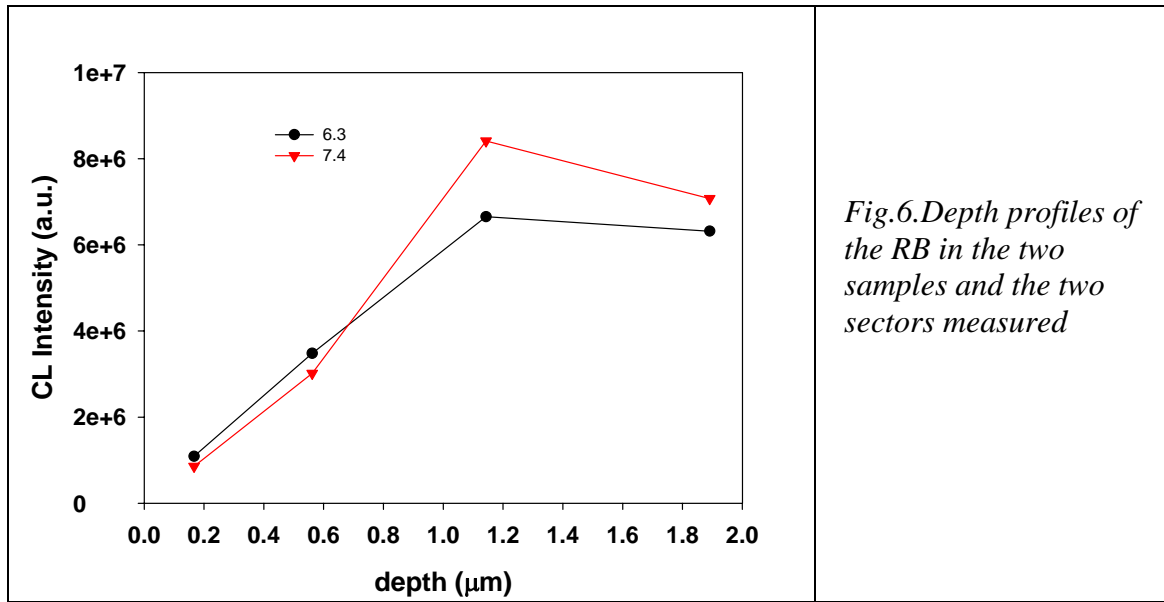
These results fit the SIMS data. Note that for a depth below 1 µm the intensity is increasing because of the decrease of [Fe] concentration, which is a non radiative recombination center. In the case of sample 7.4, the [Fe] decreases very sharply. Beyond 1µm, the effect of the [Fe] decrease is not more relevant; then, one observes a slight decrease of the intensity of the RB, because of the progressive decrease of the [Ti] concentration, see Fig. 7.

In the case of sample 6.3, the intensity close to the surface is higher than for sample 7.4, because the [Fe] concentration is smaller, then, the intensity decreases below the intensity of the sample 7.4, because the decrease of the [Fe] concentration is more gradual, and extends beyond the probe depth of the e-beam. Simultaneously the [Ti] concentration increases, which gives an almost constant emission beyond 1 µm.
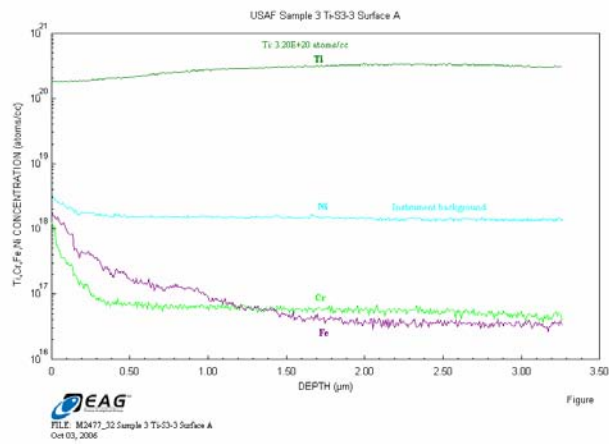
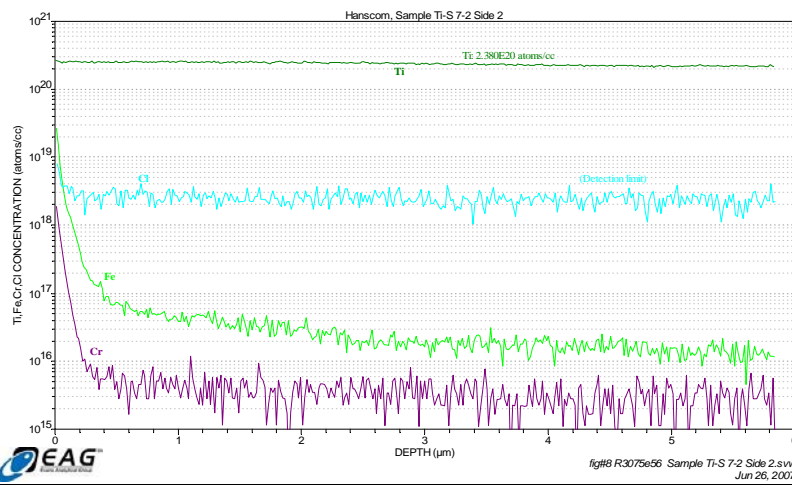|	
	Sample 6.3
	Sample 7.4

Fig.7, SIMS profiles

List of publications:

1) Spectrally resolved cathodoluminescence (SRCL) of Hydrothermal ZnO crystals; J. Mass, M. Avella, J. Jiménez,. M. Callahan, E. Grant, K. Rakes, D. Bliss;. Buguo Wang Mater. Res. Symp. Proc. 878, Y171 (2005)

2) Cathodoluminescence characterization of hydrothermal ZnO crystals; J. Mass, M. Avella, J. Jiménez,. M. Callahan, E. Grant, K. Rakes, D. Bliss;. Buguo Wang; Superlatt. and Microstruct. 38, 223-230 (2005)

3) Cathdoluminescence study of indented ZnO crystals MRS Sym. Proc. 0957-K06-03 (2007) Julio Mass, Manuel Avella, Juan Jiménez, Tomás Rodríguez, Michael Callahan, E. Grant, K. Rakes, David Bliss, Buguo Wang

4) Study of the temperature dependence of E2 and A1(LO) modes in ZnO MRS Symp. Proc. 0957-K07-11(2007) Esther Alarcon-Llado, Ramon Cusco, Jordi Ibanez, Luis Artus, Juan Jimenez, Buguo Wang, Michael Callahan

5) Raman scattering characterization of implanted Zn MRS Symp. Proc. O0957-K07-24 (2007) Esther Alarcon-Llado, Ramon Cusco, Luis Artus, German Gonzalez-Diaz, Ignacio Martil, Juan Jimenez, Buguo Wang, Michael Callahan

6) Cathodoluminescence study of Hydrothermal Zn1-xMgxO alloy crystals MRS Symp. Proc. 0957-K07-36 (2007) Julio Mass, Manuel Avella, Juan Jiménez, Michael Callahan, E. Grant, K. Rakes, David Bliss, Buguo Wang

7) Temperature dependence of Raman scattering of ZnO; R.Cuscó, E.Alarcón, L.Artús, J. Ibáñez, J. Jimenez, M. Callahan, B. Wang; Phys. Rev.B 75, 165202 (2007)

8) Cathodoluminescence study of visible luminescence in hydrothermal ZnO crystalsJ. Mass, M. Avella, J. Jiménez, M. Callahan, E. Grant, K. Rakes, and D. Bliss, B. Wang; Appl. Phys.A 88, 95 (2007)

9) Cathodoluminescence study of extended defects in hydrothermal ZnO crystals; J. Mass, M. Avella, J. Jiménez , M. Callahan, E. Grant, K. Rakes, D. Bliss, B. Wang; Superlattices and microstructures 42, 306 (2007)

10) Isotopic study of the nitrogen related modes in N+ implanted ZnO. L.Artús, R.Cuscó, E.Alarcón-Lladó, G.González-Díaz, I. Mártil, J. Jiménez, B. Wang, M.Callahan; Appl. Phys. Lett. 90, 181911 (2007)

11) Cathodoluminescence study of ZnO wafers cut from hydrothermal crystals; J. Mass, M. Avella, J. Jiménez, A. Rodríguez, T. Rodríguez, M. Callahan, D. Bliss, Buguo Wang ; J. Cryst. Growth 310, 1000 (2008)

12) Cathodoluminescence study of defects created by Vickers indentation in hydrothermal ZnO crystals; J. Mass, M. Avella, J. Jiménez, M. Callahan, D. Bliss;. Buguo Wang; J. Mater. Res. 22, 3526 (2007)

13) Properties of orientation-patterned GaAs crystals studied by cathodoluminescence spectroscopy; O. Martínez, M. Avella, H. Angulo, J. Jiménez, C. Lynch, D. Bliss; submitted

BOOK CHAPTERS

Visible luminescence in ZnO in New materials and Processes for incoming semiconductor technologies; Ed. by S. Dueñas.
 Transworld Research Network (Kerala, India) ,p113

Articles and Conferences

Conferences
*MRS Spring Meeting 2005
Spectrally resolved cathodoluminescence (SRCL) of Hydrothermal ZnO crystals; J. Mass, M. Avella, J. Jiménez,. M. Callahan, E. Grant, K. Rakes, D. Bliss;. Buguo Wang

*Sossex (Semiconductor oxides for UV optoelectronics, surface acoustics and spintronics) Workshop. Gallipoli (Italy) September 2005

Cathodoluminescence study of visible luminescence in hydrothermal ZnO crystals

J. Mass, M. Avella, and J. Jiménez ˙ M. Callahan, E. Grant, K. Rakes, and D. Bliss, B. Wang

*MRS Fall meeting, Boston November 2005.

Cathodoluminescence study of orientation patterned GaAs films for non linear optics
C. Lynch, D. Bliss, T. Zens, D. Weyburne, J. Jimenez, M. Avella
European MRS meeting, Nice, France, 28 May-2 June 2006

Cathodoluminescence study of extended defects in hydrothermal ZnO crystals

J. Mass, M. Avella, and J. Jiménez ˙ M. Callahan, E. Grant, K. Rakes, and D. Bliss, B. Wang

*IPRM (Indium Phosphide and Related Materials) 2006, Princeton, 8-11 May, Princeton, New Jersey

Characterization of HVPE-Grown Thick GaAs Structures for IR and THz Generation
C. Lynch, D. Bliss, T. Zens, D. Weyburne, J. Jimenez, M. Avella

[*]MRS Fall meeting 2006, 26 November –1 December 2006

Cathodoluminescence study of hydrothermal $Zn_{1-x}Mg_xO$ alloy crystals (poster presentation)

J. Mass, M. Avella, J. Jiménez, M. Callahan, E. Grant, K. Rakes, D. Bliss;. Buguo Wang

*MRS Fall meeting 2006, 26 November –1 December 2006

Cathodoluminescence study of indented ZnO crystals

J. Mass, M. Avella, J. Jiménez,.T.Rodríguez, M. Callahan, E. Grant, K. Rakes, D. Bliss;. Buguo Wang

*E-MRS (Strasbourg, France 2007)

 Cathodoluminescence study of ZnO wafers cut from hydrothermal crystals

J. Mass, M. Avella, J. Jiménez, A. Rodríguez, T. Rodríguez, M. Callahan, D. Bliss, Buguo Wang

Articles.

14) *Spectrally resolved cathodoluminescence (SRCL) of Hydrothermal ZnO crystals*; J. Mass, M. Avella, J. Jiménez,. M. Callahan, E. Grant, K. Rakes, D. Bliss;. Buguo Wang Mater. Res. Symp. Proc. 878, Y171 (2005)

15) *Cathodoluminescence characterization of hydrothermal ZnO crystal*s; J. Mass, M. Avella, J. Jiménez,. M. Callahan, E. Grant, K. Rakes, D. Bliss;. Buguo Wang; Superlatt. and Microstruct. 38, 223-230 (2005)

16) *Cathodoluminescence study of visible luminescence in hydrothermal ZnO crystals;* J. Mass, M. Avella, J. Jiménez,. M. Callahan, E. Grant, K. Rakes, D. Bliss;. Buguo Wang; Appl. Phys. A 88, 95 (2007)

17) *Visible luminescence in ZnO;* J. Mass, M. Avella, J. Jiménez,. M. Callahan, E. Grant, K. Rakes, D. Bliss;. Buguo Wang; New materials and Processes for incoming semiconductor technologies Ed. by S. Dueñas. Transworld Research Network (Kerala 2006, India) ,p113

18) *Cathodoluminescence study of orientation patterned GaAs films for non linear optics* M.Avella, J. Jiménez, D.Bliss, C. Lynch, D Weyburne, Mater. Res. Soc. Symp. Proc.891, 0891, EE03-20.1 2006

19) *Cathodoluminescence study of extended defects in hydrothermal ZnO crystals* Superlattices and Microstructures 42, 306 (2007)

20) *Characterization of HVPE-Grown Thick GaAs Structures for IR and THz Generation*; C. Lynch, D. Bliss, T. Zens, D. Weyburne, J. Jimenez, M. Avella; IEEE catalog number 06CH37737C. p. 151-156, (2006)

21) *Temperature dependence of Raman scattering of ZnO*; R.Cusco, E.Alarcón, L. Artús, J. Ibáñez, . Jiménez, M.C allahan, BuGuo Wang; *Phys.Rev.B* 75, 165202 (2007)

22) Isotopic study of the nitrogen related modes in N+ implanted ZnO. L.Artús, R.Cuscó, E.Alarcón-Lladó, G.González-Díaz, I. Mártil, J. Jiménez, B. Wang, M.Callahan; Appl. Phys. Lett. 90, 181911 (2007)

23) *Cathodoluminescence study of ZnO wafers cut from hydrothermal crystals*; J. Mass, M. Avella, J. Jiménez, A. Rodríguez, T. Rodríguez, M. Callahan, D. Bliss, Buguo Wang ; J. Cryst. Growth (in the press)

24) *Cathodoluminescence study of defects created by Vickers indentation in hydrothermal* ZnO crystals; J. Mass, M. Avella, J. Jiménez, M. Callahan, D. Bliss;. Buguo Wang; J. Mater. Res. (in the press)